DETECTION OF IMATINIB AND DOXORUBICIN RESISTANCE IN K562 LEUKEMIA CELLS BY 3D-ELECTRODE CONTACTLESS DIELECTROPHORESIS

A THESIS SUBMITTED TO
THE GRADUATE SCHOOL OF NATURAL AND APPLIED SCIENCES
OF
MIDDLE EAST TECHNICAL UNIVERSITY

BY

YAĞMUR DEMİRCAN

IN PARTIAL FULFILLMENT OF THE REQUIREMENTS
FOR
THE DEGREE OF MASTER OF SCIENCE
IN
ELECTRICAL AND ELECTRONICS ENGINEERING

JUNE 2013

Approval of the thesis:

DETECTION OF IMATINIB AND DOXORUBICIN RESISTANCE IN K562 LEUKEMIA CELLS BY 3D-ELECTRODE CONTACTLESS DIELECTROPHORESIS

submitted by **YAĞMUR DEMİRCAN** in partial fulfillment of the requirements for the degree of **Master of Science in Electrical and Electronics Engineering Department, Middle East Technical University** by,

Prof. Dr. Canan Özgen
Dean, Graduate School of **Natural and Applied Sciences** _____

Prof. Dr. Gönül Turhan Sayan
Head of Department, **Electrical and Electronics Engineering** _____

Assoc. Prof. Dr. Haluk Külah
Supervisor, **Electrical and Electronics Eng. Dept., METU** _____

Examining Committee Members:

Prof. Dr. Tayfun Akın
Electrical and Electronics Engineering Dept., METU _____

Assoc. Prof. Dr. Haluk Külah
Electrical and Electronics Engineering Dept., METU _____

Prof. Dr. Ufuk Gündüz
Biology Dept., METU _____

Prof. Dr. Nevzat Güneri Gencer
Electrical and Electronics Engineering Dept., METU _____

Assoc. Prof. Dr. Barış Bayram
Electrical and Electronics Engineering Dept., METU _____

Date: **13.06.2013**

I hereby declare that all information in this document has been obtained and presented in accordance with academic rules and ethical conduct. I also declare that, as required by these rules and conduct, I have fully cited and referenced all material and results that are not original to this work.

Name, Lastname: Yağmur Demircan

Signature:

ABSTRACT

DETECTION OF IMATINIB AND DOXORUBICIN RESISTANCE IN K562 LEUKEMIA CELLS BY 3D-ELECTRODE CONTACTLESS DIELECTROPHORESIS

Demircan, Yağmur
M. Sc., Department of Electrical and Electronics Engineering
Supervisor: Assoc. Prof. Dr. Haluk Külah

June 2013, 98 pages

Dielectrophoresis (DEP) is a MEMS-enabled technique defined as the relative movement of particles and medium under nonuniform electric field. DEP can be utilized for biomedical applications manipulating biological particles based on their dielectric properties and sizes. For example, cancer cells are different than normal tissue cells in terms of both their sizes and dielectric properties, leading to the potential use of DEP in early cancer detection. DEP can provide even the separation of cells with similar size, based only on the differences dielectric properties such as, multidrug resistant (MDR) cancer cells. MDR is a condition enabling a cancer cell to resist distinct drugs or chemicals of a wide variety of structure or function targeted at eradicating the cell. In this case, patients do not respond the chemotherapy. Therefore, MDR detection in early stages is crucial to choose the most proper treatment and to accelerate the recovery period. This thesis presents the detection of imatinib and doxorubicin resistance in K562 leukemia cells by 3D-electrode contactless dielectrophoresis (DEP). The main objective of the thesis is to detect MDR in cancer cells based on their dielectric properties with continuous flow DEP in label free manner.

For the proof of cell manipulation by DEP based only on dielectric properties, the 1st generation devices' design was achieved with the iterations in finite element (FEM) simulations in COMSOL. In this design, 3D-electrodes were used in the form of reciprocal short and long electrodes to provide nonuniform electric field in channel length and width. Fabrication flow for this design was developed and fabrication of these devices was performed. Very thin (~0.3 μm) parylene layer was coated on electrodes to prevent Joule heating and cell damaging. Testing of the 1st generation devices was carried out with the viable and nonviable yeast cells. Therefore, triple shell cell modeling of them was carried out through MATLAB before testing. It was reported that viable yeast cells were trapped with a purity of 96.8 % at the crossover frequency of nonviable yeast cells (1.45 MHz), at which nonviable yeast cells carried away with the capillary flow inside microchannel. Considering the problems associated with the fabrication and experimental setup of the 1st generation devices, a 2nd generation DEP device was designed for the detection of MDR in K562 cells.

In the 2nd generation design, 5 V-shaped parylene obstacles were utilized to direct the cells into DEP area hydrodynamically eliminating the usage of the external pressure actuation devices, utilized in the 1st generation. Moreover, 3D separated electrodes, which provide

uniform DEP force through the channel depth, were utilized in side walls along the channel length to increase the efficiency of DEP device. A thin parylene coating (~0.3 μm) on the electrodes provided the insulation of electrodes as in the 1st generation devices. Due to very thin parylene coating, the necessary voltage (minimum 5 V_{pp}) for DEP operation is considerably lower than the voltage of other contactless DEP devices reported in the literature. Before testing of this device, dielectric modeling of imatinib and doxorubicin resistant, and sensitive K562 cells were achieved by double shell cell modeling through MATLAB. While the trapping of doxorubicin and imatinib resistant K562 cells was observed at the crossover frequency (48.64 MHz) of sensitive K562 cells, sensitive K562 cells were not trapped under the same experimental conditions. This result shows that the separation of imatinib and doxorubicin resistant K562 cells can be achieved with this design. Moreover, performance tests of the 2nd generation devices are made with changing the key parameters of design: the flow rate, voltage magnitude and cell concentration. Device has a trapping ability at minimum 5 V_{pp} voltage and 20 μl/ min flow rate when cell concentration is 625000 cells/ml. Finally, the effect of drug (doxorubicin) resistance level on the DEP response of K562 cells was examined. The trapping characteristics of cells which have different degree of drug resistance were differentiable according to the preliminary test results. It is worthy to note that all test results are consistent with theoretical expectations and numerical solutions in finite element simulations.

In conclusion, the proof of DEP concept based only on dielectric properties was achieved. Two different DEP device design were utilized to improve the quality of fabrication and test results. The detection of imatinib and doxorubicin resistance in K562 cells were achieved with different performance parameters, including voltage magnitude, flow rate and cell concentration. The degree of drug resistance in cancer cells was examined for the first time in the literature in electrical manner. With the further improvements in design, the detection of MDR in real patient blood is the ultimate goal.

Keywords: Contactless dielectrophoresis (DEP), 3D-electrode, cell detection, multidrug resistance (MDR), the degree of drug resistance.

ÖZ

IMATINIB VE DOXORUBICIN DİRENCİ GELİŞTİRMİŞ K562 LÖSEMİ HÜCRELERİNİN 3 BOYUTLU ELEKTROT KULLANILARAK TEMASSIZ DİELEKTROFOREZ İLE TESPİTİ

Demircan, Yağmur
Yüksek Lisans, Elektrik ve Elektronik Mühendisliği Bölümü
Tez Yöneticisi: Doç. Dr. Haluk Külah

Haziran 2013, 98 sayfa

Dielektroforez (DEF) MEMS teknolojisi sayesinde uygulanabilir olan ve homojen olmayan elektrik alanın varlığında, sıvı içerisinde bulunan bir parçağın sıvıya göre hareketi şeklinde tanımlanan bir tekniktir. Dielektroforez biyolojik parçacıkların dielektrik özelliklerine veya boyutlarına göre manipule edilmesini sağlayabildiği için biyomedikal uygulamalarda kullanılmaktadır. Örneğin, kanser hücreleri yapı ve büyüklükleri itibariyle normal doku hücrelerinden farklı olduklarından DEF sistemleri kanserin erken teshisinde etkin bir çözüm yolu olma potansiyeline sahiptir. DEF yöntemi kanser hücrelerinin normal hücrelerden ayrıştırılmasında kullanılabileceği gibi, boyutları birbirine çok yakın olan çoklu ilaç direnci (ÇİD) geliştirmiş kanser hücrelerinin ayrıştırılmasında da kullanılabilir. ÇİD bir tümörün bir ilaca karşı direnç geliştirmesinin ardından, o ilaçla aynı yapısal ve fonksiyonel özelliklere sahip olmayan başka ilaçlara karşı da çapraz direnç geliştirmesi olarak tanımlanır. Bu tip vakalarda hastalar kemoterapiye cevap vermemektedir. Bu sebeple kanser hücrelerinin içinde ÇİD geliştirenlerin tespit edilebilmesi kullanılacak tedavi yöntemini belirlemek ve tedavi sürecini hızlandırmak açısından önemlidir. Bu tez, imatinib ve doxorubicin direnci geliştirmiş K562 lösemi hücrelerinin 3 boyutlu elektrot kullanılarak temassız dielektroforez (DEF) ile tespitini anlatmaktadır.Tezin temel amacı ilaç direnci geliştirmiş lösemi hücrelerinin sürekli sıvı akışı olan kanallar içerisinde hücre boyaması (hücre işaretleme) yapılmadan tamamen dielektrik özellik farklarına dayanarak tespit edilmesidir.

DEF ile sadece dielektrik özellik farkına dayalı biyolojik hücre manipulasyonunun yapılabileceğinin kanıtlanması için, 1. Jenerasyon DEF çiplerinin dizaynı sonlu element modellemeleri ile yapılan simülasyonlarla iterasyonlar sayesinde yapılmıştır. Bu dizaynda hem kanal genişliği hem uzunluğu boyunca homojen olmayan elektrik alan sağlamak için 3 boyutlu, kanal içerisine karşılıklı duvarlara yerleştirilmiş kısa ve uzun elektrotlar kullanılmıştır. Bu dizayn için üretim akışı geliştirilerek bu çiplerin üretimi yapılmıştır. Yaklaşık 0.3 μm inceliğinde olacak şekilde bir parilen tabakası elektrotlar üzerine kaplanarak "*Joule heating*" ve hücrelerin zarar görmesi engellenmiştir. Bu çiplerin test edilmesi için canlı ve ölü maya hücreleri kullanılacağından bu hücrelerin dielektriksel modellemesi (*triple shell cell modeling*) MATLAB kullanılarak gerçeklenmiştir. Test sonuçlarına göre canlı maya hücreleri elektrotlar üzerine % 96.8 saflık oranı ile tutundurulurken ölü maya hücreleri kapiler akış ile kanal çıkışına doğru yönlenmiştir çünkü bu testler ölü maya hücrelerinin sıfır DEF kuvveti (f_{cross}) gördüğü 1.45 MHz'te

gerçeklenmiştir. 1. Jenerasyon çiplerindeki üretimsel ve deneysel sorunlar göz önünde bulundurularak 2. Jenerasyon çipleri dizayn edilmiştir.

2. Jenerasyon çiplerinde hücreleri pasif olarak DEF alanlarına yönlendirmek amacıyla kanal içerisinde 5 adet V şekilli parylene engel kullanılmış ve bu şekilde 1. Jenerasyonda kullanılan basınç kontrollü olarak hücreleri DEF alanına yönlendirebilen aktif basınç tahrik cihazlarının kullanımı saf dışı bırakılmıştır. Ayrıca kanal boyunca 3 boyutlu elektrot dizileri kullanılarak hem kanal derinliği boyunca homojen bir DEF kuvveti sağlanmış hem de DEF çiplerinin verimliliği arttırılmıştır. 1. Jenerasyon çiplerinde olduğu gibi yaklaşık 0.3 μm inceliğinde olacak şekilde bir parilen tabakası elektrotlar üzerine kaplanmıştır. Parilen kaplamasının inceliği sebebi ile bu çiplerde DEF operasyonu için gerekli minimum voltaj (5 V_{pp}) literatürdeki diğer temassız DEF çipi örneklerinden önemli ölçüde düşüktür. Bu çiplerin test edilmesi için kullanılacak imatinib ve doxorubicin dirençli ve dirençsiz K562 lösemi hücrelerinin dielektriksel modellemeleri (*double shell cell modeling*) MATLAB kullanılarak gerçeklenmiştir. İlaç dirençliliği olmayan K562 hücrelerinin sıfır DEF kuvveti görerek sürekli akış ile kanal çıkışına yönlendiği 48.64 MHz frekansta, imatinib ve doxorubin dirençli K562 hücreleri elektrotlar üzerinde tutunmuştur (diğer deney koşulları bu iki test için de sabit tutulmuştur). Bu sonuç dirençli ve dirençsiz K562 hücrelerinin bu dizayn ile ayrıştırılabileceğini göstermektedir. Ayrıca, 2. Jenerasyon DEF çiplerinin performans analizleri de dizaynda kullanılan anahtar parametrelerin (akış hızı, voltaj büyüklüğü, hücre konsantrasyonu) değiştirilmesi ile gerçeklenmiştir. Bu analizlere göre 2. Jenerasyon çipleri minimum 5 V_{pp} voltajda 20 μl/dk akış hızı ile 625000 hücre/ml konsantrasyonlu, dirençli K562 hücrelerini elektrot üzerinde hapsedebilme yeteneğine sahiptir. Son olarak ilaç dirençliliği derecesinin K562 hücrelerinin DEF kuvvetine verdiği tepkiye olan etkisi incelenmiştir. İlk sonuçlara göre farklı derecede ilaç dirençliliği gösteren K562 hücrelerinin DEF karakteristiği de farklı olmuştur. Tüm tez boyunca yapılan çalışmalar teorik beklentilerle ve numerik simülasyonlarla tutarlı olarak gerçeklenmiştir.

Sonuç olarak bu tezde sadece dielektrik özellik fark kullanılarak DEF konseptinin gerçeklenebildiği gösterilmiştir. Üretim ve test sonuçlarının kalitesinin arttırılması adına 2 farklı DEF çipi dizayn edilmiştir. İmatinib ve doxorubicin dirençliliği geliştrilmiş K562 hücrelerinin teşhisi farklı performans parametreleri (akış hızı, voltaj büyüklüğü, hücre konsantrasyonu) ile gerçeklenmiştir. Literatürde ilk olarak, ilaç dirençlilği derecesi farklı olan K562 hücreleri elektriksel karakteristikleri açısından incelenmiştir. Dizaynın geliştirilmesi ile gerçek bir hastanın kanı kullanılarak ÇİD teşhisinin başarılabilmesi en üst düzey amaç olarak belirlenmiştir.

Anahtar Kelimeler: Temassız dielektroforez (DEF), 3 boyutlu elektrot, , hücre tespiti, çoklu ilaç direnci (ÇİD), ilaç dirençliliği derecesi etkisi.

To my mother, father, grandmother and "zuzu"

ACKNOWLEDGEMENTS

When I was 12-14 years old, the word “chip” is a dream for me. To touch my dream, I would like to thank Prof. Dr. Tayfun Akın and Assoc. Prof. Dr. Haluk Külah. I would also like to express my deep thanks to my thesis advisor, Assoc. Prof. Dr. Haluk Külah for believing and supporting me during my undergraduate and graduate studies. I am also thankful to Prof. Dr. Ufuk Gündüz to collaborate us with providing biological laboratory and cancer cell lines.

I would like to thank The Scientific and Technological Research Council of Turkey (TUBITAK) for the scholarship support for me.

I am particularly thankful to my old colleague Gürkan Yılmaz for his guidance and patience for my endless questions. Many thanks to Dr. Ebru Özgür for her helps in test procedures with biological cells, sharing new point of views in integration of biology and electronics, and priceless academic writing skills development effort on me. I would also thank to Dr. Yekbun Adıgüzel for her helps in my thesis preparation.

I would like to thank Aziz Koyuncuoğlu for developing my fabrication procedure and helping me for fabrication of my devices. Moreover, I am also grateful to him for his endless patience and indulgence. Before meeting with him, I was a singleton but now I have a brother. I would also like to thank Murat Erdem for providing me cancer cells whenever I want and his friendship.

Many thanks to Hasan Uluşan to simplify my life and with Taylan Töral and Mustafa Kangül to create a very enjoyable work environment for me. Above all, I am very thankful to them for being good friends. Moreover, I am particularly thankful to Taylan Töral for all contributions to my fabrication.

I would also like to thank all METU-MEMS Center staff for their kind helps in cleanroom. Many thanks particularly to Orhan Akar for sharing his deep knowledge on microfabrication and for his helps in the cleanroom.

I am especially thankful to all my lab friends in the BioMEMS and PowerMEMS groups: Dr. Hatice Ceylan Koydemir, Garsha Bahrieh, Rui Çolaço, Kaveh Gharebaghi, Parisa Naghinejad, Salar Chamanian, Levent Beker and Dr. Özge Zorlu for being good friends and creating a peaceful work environment. I would also like to thank the former and present members of the METU MEMS-VLSI and RF-MEMS groups for their friendship and kind helps.

I would like to express my deepest thankfulness to my mother, Günay Kahraman, my father, Rahmi Demircan, and my grandmother, Kübra Kahraman, for their endless, priceless and ineffable patience and support. Moreover, I am thankful to them to give me the freedom for achieving all my dreams.

Finally, I would like to thank to Hüseyin Yalçın for his patience, support, love, and never leave me alone. Thanks to him, all question marks are deleted from my life.

TABLE OF CONTENTS

ABSTRACT v
ÖZ vii
ACKNOWLEDGEMENTS x
TABLE OF CONTENTS xi
LIST OF TABLES xiii
LIST OF FIGURES xiv
CHAPTERS
1. INTRODUCTION 1
1.1. Particle Manipulation Techniques in LOC Systems 4
1.1.1. Mechanical Manipulation 4
1.1.2. Magnetic Manipulation 6
1.1.3. Optical Manipulation 8
1.1.4. Acoustic Manipulation 9
1.2. Electrical Manipulation and Literature Review about DEP in LOC 11
1.2.1. Electrophoresis 11
1.2.2. Dielectrophoresis 11
1.2.3. Multi Drug Resistance (MDR) Detection in Cancer Cells 17
1.3. Research Objectives and Thesis Organization 19
2. THEORY OF DIELECTROPHORESIS 21
2.1. Dipole Moment 21
2.2. Dielectrophoresis 22
2.4. Microelectrode Configurations in DEP Devices 26
2.5. Operating Strategies in DEP 27
3. DIELECTRIC MODELING OF CELLS 31
3.1. The Analogy between Biological Cells and Electrical Circuit Elements 31
3.2. Cell Dielectric Modeling Techniques 33
3.3. Dielectric Modeling of Yeast Cells 34
3.4. Dielectric Modeling of K562 (Human Chronic Myeloid Leukemia (CML)) cancer cells 35
4. DESIGN AND SIMULATION 39
4.1. Design of the DEP Devices 39
4.1.1. The Design of 1st Generation DEP Devices 39
4.1.2. The Design of 2nd Generation DEP Devices 41

4.2. Simulation Method 44
4.2.1. Simulations of 1st Generation DEP Devices 47
4.2.2. Simulations of 2nd Generation DEP Devices 49
5. FABRICATION 51
5.1. Fabrication of the 1st Generation Devices 51
5.2. Fabrication of the 2nd Generation Devices 55
6. RESULTS AND DISCUSSION 61
6.1. Proof of DEP Concept with 1st Generation Devices 61
6.1.1. Preparation of Yeast Cells 61
6.1.2. Test Procedure, Test Results and Discussions 62
6.2. Imatinib and Doxorubicin Resistance Detection in K562 Cells 64
6.2.1. Cell Preparation 64
6.2.2. Experimental Setup 65
6.2.3. Test Results and Discussions 65
6.3.1. Cell Preparation 69
6.3.2. DEP Trapping Test and Cell Counting 71
6.3.3. Test Results 74
7. CONCLUSION AND FUTURE WORK 75
REFERENCES 79
APPENDICES
A: MATLAB CODES FOR CELL MODELING 89
B: SIMULATIONS IN MATLAB 91
C: PROCESS FLOW 93

LIST OF TABLES

TABLES

Table 1.1: Literature review of DEP for clinical applications [5]…….15

Table 3.1: The dielectric properties of viable and nonviable yeast cells [114]…….34

Table 3.2: Dielectric properties of K562 and K562/100dox [97]. * is used to mark average values. 36

Table 4.1: Design parameters utilized for the 1st generation devices.....41

Table 4.2: Design parameters utilized for the 2nd generation device……43

Table 6.1: Perfomance test results of the 2nd generation devices for different voltages at 10 µl/min flow rate and 625000 cells/ml cell concentration.…….67

Table 6.2: Perfomance test results of the 2nd generation devices for different flow rates and cell concentrations (voltage=15V_{pp})……..68

Table 6.3: The principles of cell counting utilizing light intensities. "X" means not considerable……...72

LIST OF FIGURES

FIGURES

Figure 1.1: BioMEMS as a high level interdisciplinary research area. 2

Figure 1.2: The comparison of dimensions in microsystems and biological agents. 2

Figure 1.3: The schematic view of a typical LOC system [12]. 3

Figure 1.4: Size dependent particle separator. (A) The principle of separator with its top and cross sectional view, (B) Separation of 3 different size (20, 50, and 70 μm) polystyrene particles [15]. 5

Figure 1.5: A mechanical particle manipulation system. (A) The working principle of the manipulator with symmetric and asymmetric channel structures, (B) Focusing of 10 μm polystyrene particles with different densities, (C) Alignment of RBCs at the center of the microchannel [16]. 5

Figure 1.6: A size based blood filtration device. (A) The working principle of the filtration system composed of focusing, expansion and collection units, (B) Separation of *E.coli* from RBCs [17]. 6

Figure 1.7: MAP and DEP based continuous flow microseparator. (A) Working principles focusing on electric and magnetic field distribution in the microchannel and MAP and DEP force directions, (B) The separation of RBCs and WBCs with only DEP effect (i) and with the utilization of MAP with DEP (ii) [20]. 7

Figure 1.8: A magnetic cell sorting system. Tests results obtained with HeLa cells are presented without magnetic field applied (A) and sorting of the cells under the effect of magnet (B) [21]. 7

Figure 1.9: Optically trapping and alignment of RBC at different angles: (A) 180°, (B) 45°, and (C) 90° [29] 8

Figure 1.10: Optically induced flow cytometry micro particle manipulator. (A) Experimental setup, (B) Device structure, Sorting of larger particles(C) to lower outlet and smaller particles(D) to upper outlet [32]. 9

Figure 1.11: Acoustic radiation force based micro particle manipulator. (A) Device principles. RBCs are focused at the middle of the channel and lipid particles are pushed towards external channel walls at both sides. (B) Experimental results [35]. 10

Figure 1.12: Acoustophoretic size and density based separation system. (A) Operational principles of device, (B) Experimental results for 3 different size particles (3, 7 and 10 μm) when ultrasound (US) is OFF (left) and ON (right) [34]. 10

Figure 1.13: Differential analysis based EP chip. (A) Device structure, (B) Band formation and histogram: (1) The same base pairs in wild and mutant DNA, (2) Polymorphism, (3) Gel interface [38]. 11

Figure 1.14: A real blood cell and plasma separation system. Blood stream flow is shown in the different parts of the DEP area: (A) Entrance region, (B) Middle region, and (C) Ending region. (D) The separation of plasma and blood cells at the end of the channel [58]. 12

Figure 1.15: *E.coli* separation from blood cells. (A) Device structure with the dimensions of channel and insulators, (B) Electric field simulation of device, (C) *E.coli* and blood cell separation results, (D) Close-up view of the trapped *E.coli* between the tips of insulators [63]. 13

Figure 1.16: Salmonella typhimurium detection based on DEP. (A) Device structure, (B) Trapping of Salmonella typhimurium at a frequency of (i) 10 kHz, (ii) 100 kHz, (iii) 300 kHz [43]. 13

Figure 1.17: Isolation of cancer cells from blood. (A) Separation of metastatic human breast cancer cells from dilute blood utilizing castellated electrode structures. (i) Initial condition, (ii) Starting of trapping of cancer cells, (iii) Trapped cancer cells at the tip of electrodes, (iv) The alignment of blood cells between electrodes [75], (B) Isolation of HeLa (green arrow) cells from RBCs (red arrow). (i) Device structure, (ii) Initial condition (loading of cells), (iii) Starting of DEP operation and cell alignment between spiral electrodes, (iv) Collection of HeLa cells at the center before RBCs [80]..... 14

Figure 1.18: DEP research in stem cell therapy. (A) DEP trapping analysis of NSPCs, neurons and astrocytes [83], (B) Aggregation of stem cells at (i) 0 h, (ii) 24 h, (iii) 48h, even in the presence of some inhibitory factors [85]. 15

Figure 1.19: Multi drug resistance mechanism in tumor cells. (A) Drug (Cy) efflux through ATP binding cell membrane proteins (P-gp and MRP), (B) Drug intake by means of modulator (M) treatment [100]. 18

Figure 1.20: DEP collection spectrum of (A) K562 (drug sensitive leukemia) and (B) K562AR (drug resistant leukemia) cells. Collection starts to decrease at 3MHz for sensitive cells while it starts to decrease at 8MHz for resistant ones [97]. 19

Figure 2.1: Positive and negative DEP force. If $\varepsilon p * > \varepsilon m *$, particles are pulled into the stronger electric field region by positive DEP (pDEP) force. If $\varepsilon p * < \varepsilon m *$, particles are pushed into weaker electric field region by negative DEP (nDEP) force [3]……..….23

Figure 2.2: $Re(F_{CM})$ vs frequency graph of three particles with different conductivities: $\sigma_{P1}=4x10^{-3}$ S/m, $\sigma_{P2}=4x10^{-4}$ S/m, $\sigma_{P3}=8x10^{-4}$ S/m. Conductivity of the medium is taken as 10^{-4} S/m for this illustration [105]..... 23

Figure 2.3: Crossover frequency coefficient distribution of different tumor cell lines and normal blood cells. Courtesy of Gascoyne et al. [67], [3]. 24

Figure 2.4: Forces acting on a particle inside microchannel..... 25

Figure 2.5: The electric field simulations of different electrode configurations utilized in DEP, castellated (A), ratchet (B), and quadrupole (C), and insulating DEP (iDEP). 27

Figure 2.6: The principles of DEP-FFF (Adapted from [67])..... 28

Figure 2.7: The structure and working principle of different operating strategies utilized in DEP: Multi-step (A), Travelling-wave (B), Multiple-frequency (C), Medium conductivity gradient (D), and Immuno-asisted (E) [111]..... 29

Figure 3.1: Charged or polarizable molecules exchange from cell membrane [112]……...31

Figure 3.2: Biological cell membrane structure (Encyclopedia Britannica, Inc., 2007)..... 32

Figure 3.3: The analogy between biological cell and suspending medium, and electrical circuit [12]..... 33

Figure 3.4: $Re(F_{CM})$ vs. frequency graphs of viable and nonviable yeast cells in a medium with 2.5 mS/m conductivity and 78 permittivity coefficient [115]..... 35

Figure 3.5: $Re(F_{CM})$ vs. frequency graphs of K562 & K562/dox 100 cells in a medium with 2.5 mS/m conductivity and 78 permittivity coefficient [105]..... 37

Figure 4.1: The illustration of the 1st generation DEP devices, with an enlarged view of DEP area……40
Figure 4.2: Illustration of the 2nd generation device structure. 42
Figure 4.3: The dimensions of V-shaped obstacles. 43
Figure 4.4: 3D simulation of the gradient of electric field square. 44
Figure 4.5: Key paramters in time dependent simulations of COMSOL 45
Figure 4.6: Key parameters for particle tracing simulatins in COMSOL 46
Figure 4.7: The gradient of electric field square for 1st generation design. 47
Figure 4.8: Yeast cells path in 1st generation devices. In the left figure, voltage is not enough to trap the cell on electrode but it still affects the cell by pulling it to short electrode. In the right figure, voltage is high enough to trap the cell. 48
Figure 4.9: Electric field line simulations in DEP area of 1st generation dev ices. 49
Figure 4.10: The gradient of electric field square for 2nd generation design. 49
Figure 4.11: The path of K562 sensitive (A) and resistant (B) cells under DEP effect in 2nd generation devices (*flow rate=10 µl/min, voltage=20 V_{pp}*)..... 50
Figure 5.1: The fabrication flow of 1st generation devices……51
Figure 5.2: Mask 1 of the 1st generation devices. This mask is used for the patterning of seed layer..... 52
Figure 5.3: The image of seed layer after wet metal etching step. 52
Figure 5.4: Mask 2 of the 1st generation devices. This mask is utilized for the determination of electroplating area. 53
Figure 5.5: Channel structure after the AZ9260 photoresist photolithography step. 54
Figure 5.6: Device structure with 3D-electrodes after electroplating step. 54
Figure 5.7: Mask 3 of the 1st generation devices. This mask is used for the determination of inlet and outlet reservoirs places. 55
Figure 5.8: Fabricated device for the 1st generation. 55
Figure 5.9: Fabrication flow of the 2nd generation devices. 56
Figure 5.10: Mask 1 for seed layer paterning in the 2nd generation devices. 56
Figure 5.11: Seed layer in the 2nd generation devices. 57
Figure 5.12: Mask 2 as dark field for the determination of electrode places in the 2nd generation devices. 57
Figure 5.13: 3D-electrode structure in 2nd generation devices. 58
Figure 5.14: Mask 3 for the formation of channels in 2nd generation devices..... 58
Figure 5.15: Mask 4 for the determination of inlet and outlet reservoirs in the 2nd generation devices. 59
Figure 5.16: Fabricated device. 59
Figure 5.17: The dimensions of nanoports used for the fluidic connections [119]. 60
Figure 6.1: Yeast cell preparation for testing of the 1st generation devices……..62
Figure 6.2:.Viable yeast cells' trapping, forming pearl chain structure on electric field lines, in DEP area [115]. 63

Figure 6.3: Viable yeast cells manipulation with the 1st generation devices. At t=0s, by means of DEP force, 4 viable yeast cells formed a pearl chain structure. Next, at t=2s, power was turned off and 2 of them flowed with the capillary flow. At t=7s, power was turned on again. At t=8s, 2 viable yeast cells were trapped at a different place on long electrode [115]. 63

Figure 6.4: Cancer cell preparation for testing of the 2nd generation devices. 64

Figure 6.5: Experimental test setup for the 2nd generation devices. 65

Figure 6.6: The trapping of imatinib (A) and doxorubicin (B) resistant K562 cells with the 2nd generation devices (flow rate = 10 µl/min, voltage = 9 V_{pp}, frequency = 48.64MHz) [105]. 66

Figure 6.7: The pathway of sensitive K562 cells while they flow through the microchannel in the 2nd generation devices (flow rate = 10 µl/min, voltage = 9 V_{pp}, frequency = 48.64 MHz) [105]. 67

Figure 6.8: Sample images of trapped imatinib resistant K562 cells under different voltages. 68

Figure 6.9: XTT results for the determination of IC_{50} values of 100 nM doxorubicin resistant K562 cells. 69

Figure 6.10: XTT results for the determination of IC_{50} values of 300 nM doxorubicin resistant K562 cells. 70

Figure 6.11: XTT results for the determination of IC_{50} values of 500 nM doxorubicin resistant K562 cells. 70

Figure 6.12: Example images used in cell counting with ligth intensity analysis in *Image J*. In top image only one cell is trapped. In bottom image, 4 more cells are trapped. 72

Figure 6.13: Due to sharp arms of V-shaped obstacles, air bubble forms and damages the trapped cells in microchannels. 73

Figure 6.14: Intensity change in whole image because of waste fluid in outlet resorvoir although there is not trapped cell. 73

Figure 6.15: Trapped cell number belongs to the different degree of doxorubicin resistant K562 cells (100, 300 & 500 nM). Comparing the hypothetical P-gp expression, the increase in the trapping cell number is in saturation trend. 74

CHAPTER 1

INTRODUCTION

In World Health Statistics 2012 [1], specific causes of deaths are examined under three main categories: injuries, communicable diseases and noncommunicable diseases. The most common communicable diseases are AIDS, malaria, influenza, cholera, and hepatitis. The last data of World Health Organization (WHO) show 34 million people live with Human Immunodeficiency Virus (HIV) and 1.8 million died because of AIDS related illnesses worldwide in 2010. 1.2 million of these deaths were in Africa, a low-income continent. Cardiovascular and chronic respiratory diseases, cancer, and diabetes are the most widespread types of noncommunicable diseases. In 2008, these diseases caused 36 million of 57 million deaths. Due to unsatisfactory medical conditions, a significantly higher percentage (80%) of these deaths occurs in low and middle-income countries. One of the most important reasons is the unavailability of medical instruments. According to WHO (2010), while computed tomography was accessible for one per 64 900 people in high-income countries; this value is one per 3.5 million people in low-income countries, on average. Besides, inadequate number of medical instruments, lack of trained people and inappropriate hygiene conditions for safe treatment, such as injections, results in high death rate in these countries. Re-usage of syringes and needles causes the spread of infection of blood-borne viruses. 160 000 HIV, 4.7 million hepatitis C and 16 million hepatitis B infections in each year are attributable to these re-usages [2].

The last century has witnessed the elevated efforts for realization of affordable technologies and healthcare strategies to allocate the welfare all over the world, even in low-income countries. Advances in the biomedical microelectromechanical systems (BioMEMS) technology within the field of microelectromechanical systems (MEMS) and nanotechnology addresses the listed problems above, including scarcity of medical instruments, lack of trained personnel and risk-bearing unhygienic conditions, as a high level interdisciplinary technology in the healthcare area (Fig. 1.1).

BioMEMS technology enables the production of faster, more sensitive, disposable, and easy usage medical instruments with reduced energy, cost and size. In addition, several techniques like dielectrophoresis and capillary electrophoresis, which cannot be done with macro systems, has been made possible by BioMEMS technology. Due to the comparable dimensions of MEMS systems with biological systems, single cell or particle analyses have been conceivable (Fig. 1.2).

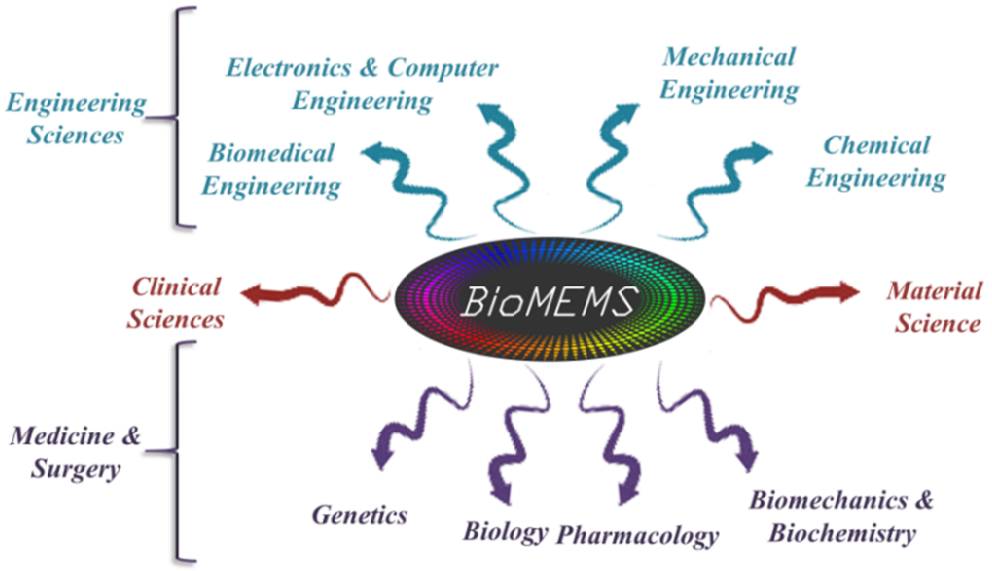


Figure 1.1: BioMEMS as a high level interdisciplinary research area.

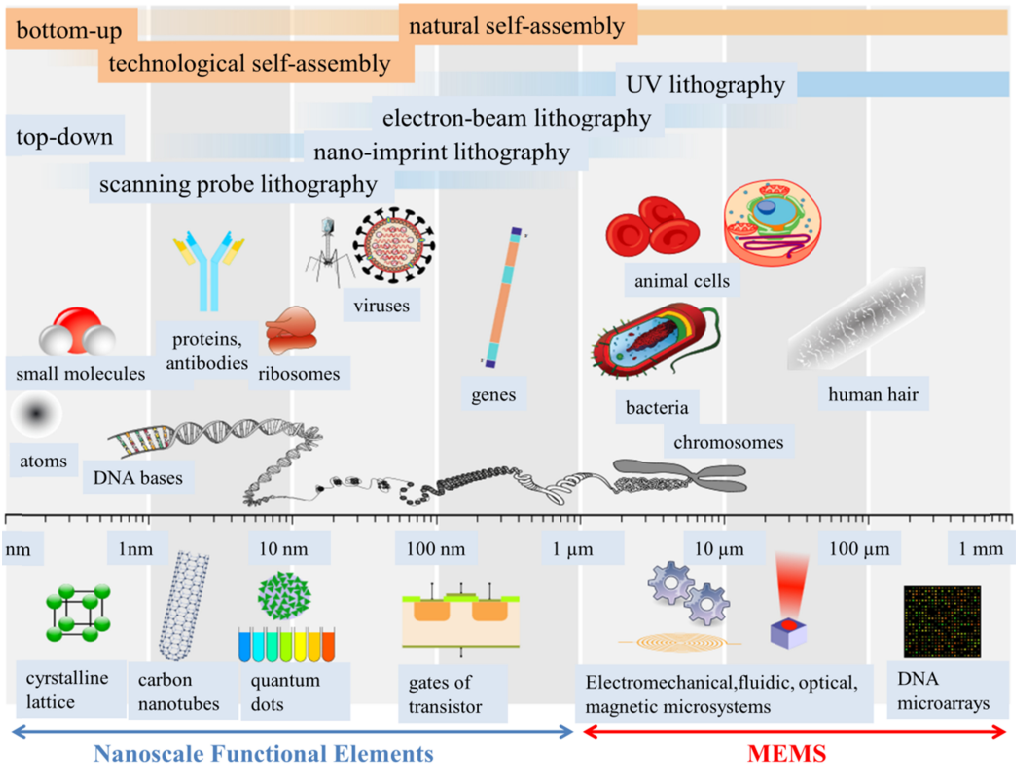


Figure 1.2: The comparison of dimensions in microsystems and biological agents.

Besides medical area, BioMEMS technology based devices have found important applications in many areas, such as environmental monitoring, homeland security, and food

and defense industry, besides medical area. This is for the sake of the following favorable properties of this technology [3].

- Reduced cost and analysis time,
- Rendering portability, providing the bed site diagnosis and point-of-care (POC) analysis,
- Disposability, preventing the cross contamination,
- Diminished need for the trained personnel for the use of equipment,
- Reduced reagent consumption, preventing redundant blood losses,
- Reduced invasiveness of sample drawing procedure due to simplified sample preparation processes,
- Enhanced sensitivity,
- Promoting new methods that are rendered possible only by the micro systems.

Diagnosis and therapy of diseases are two main research areas in BioMEMS [4]. Diagnostic systems mainly focus on the analyses of clinically significant analytes in physiological fluids [5], [6], [7]. Therapeutic systems cover implantable devices, such as drug delivery systems [8], [9], and injection instruments, such as microneedles [10], [11]. The focus of the BioMEMS application described in this thesis is a diagnostic system.

Lab-on-a-chip (LOC) system is the ultimate goal of BioMEMS. As its name suggests, the aim of LOC systems is to make possible all laboratory analysis on a single chip to decrease the operational complexity and cost, to provide the disposability, and to reach wider populations especially for those living in low or middle-income countries. Figure 1.3 shows a typical LOC system schematic view. The main subparts of LOC systems, such as sample pretreatment, fluid control, thermal reaction, mixing and signal detection, have already been studied in detail. However, the main problem of LOC systems is to combine these subparts on a single platform.

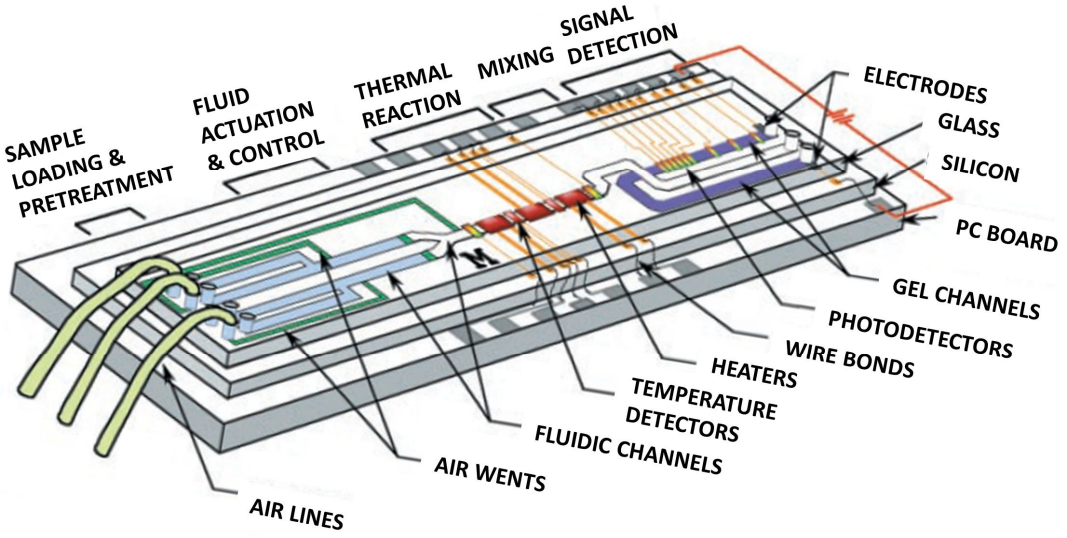


Figure 1.3: The schematic view of a typical LOC system [12].

Particle manipulation is one of the most important applications of LOC systems. It can be achieved with different methods (mechanical, magnetical, optical, acoustical, and electrical) according to target particle properties [5].

This thesis reports the detection of imatinib and doxorubicin resistance in K562 leukemia cells by 3D-electrode contactless dielectrophoresis (DEP). Proof of DEP concept is also presented with yeast cells. In addition, device performance tests are carried out by changing experimental parameters, such as flow rate. Finally, the effect of degree of drug (doxorubicin) resistance on DEP response of K562 cells is examined.

In this chapter, different particle manipulation techniques in LOC systems are discussed with a literature survey and necessary background information about DEP technique is given. In Section 1.1, different manipulation techniques, presented in the literature, are described along with a discussion about their advantages and drawbacks. Section 1.2 presents the fundamentals of electrical manipulation techniques with focusing on DEP technique and utilization of DEP for multidrug resistance (MDR) in cancer cells. Finally, research objectives and thesis organization are given at the conclusion of this chapter.

1.1. Particle Manipulation Techniques in LOC Systems

Particle manipulation (separation, trapping, detection or enrichment) is defined as any interactions with a particle that causes a variation on its normal behavior [13]. Particle manipulation techniques in LOC systems can be separated into five main classes based on their sensing mechanisms: Mechanical, magnetic, optical, acoustic and electrical manipulation. They are described with their advantages and drawbacks in the following sections [14].

1.1.1. Mechanical Manipulation

Mechanical manipulation techniques are based on the mechanical properties of particles, including shape, size, density, elasticity, and stiffness. Common approach in this technique is to utilize the size and shape differences of particles. Using different size microchannels or obstacles provide a kind of filtration. These techniques do not necessitate exerting destructive forces on the particles, which would especially be critical for the biological media [15]. Figure 1.4 (A) shows a size based particle manipulation system which has three spiral microchannels on a microchamber and mechanical obstacles between channels. Due to centrifugal force, all particles are pushed towards out of the center of microchamber and by means of mechanical obstacles; larger particles cannot pass into outer spiral microchannels while smaller ones can pass. Maruyama et al. [15] reported the manipulation of three different size polystyrene particles (20 μm, 50 μm and 70 μm) with using this system (Fig 1.4 (B)). To improve the system efficiency, channel lengths can be increased but it extends the operation time.

Carlo et al. [16] presented a mechanical particle manipulation system, utilizing symmetric and asymmetric microchannels (Fig. 1.5 (A)). They utilize levitation forces and laminar flow inside microchannels. Manipulation of particles is achieved with focusing them at the center of the channel. System efficiency depends on the ratio of particle size to microchannel size and flow characteristics. Figure 1.5 (B) shows focusing of 10 μm polystyrene particles even when they have different densities. Rotational alignment of red blood cells (RBCs) at the center of the channel was also achieved with this system (Fig. 1.5 (C)). The possible bottleneck of this system is the need of a delicate flow control through implementing precise flow rates.

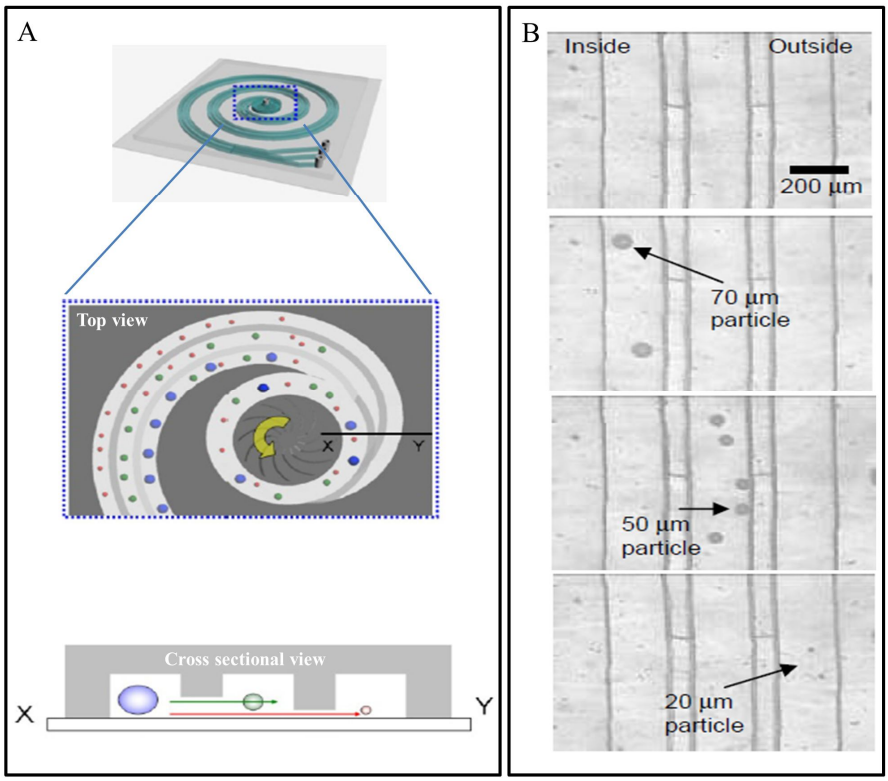


Figure 1.4: Size dependent particle separator. (A) The principle of separator with its top and cross sectional view, (B) Separation of 3 different size (20, 50, and 70 µm) polystyrene particles [15].

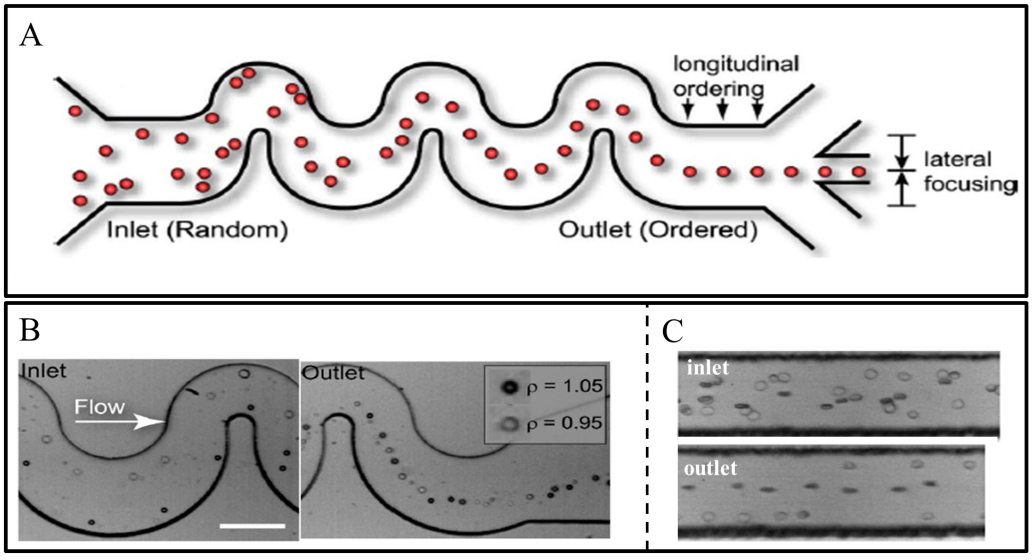


Figure 1.5: A mechanical particle manipulation system. (A) The working principle of the manipulator with symmetric and asymmetric channel structures, (B) Focusing of 10 µm polystyrene particles with different densities, (C) Alignment of RBCs at the center of the microchannel [16].

Mach et al. [17] demonstrated a size based blood filtration microdevice (Fig. 1.6 (A)) which accomplished the separation of bacterial cells from whole blood with >80 % efficiency. Different aspect ratios along microchannel, levitation forces and parabolic flow profile were utilized in this device to focus larger cells (blood cells) near the channel walls. Figure 1.6 (B) shows test results with *E.coli* infected blood.

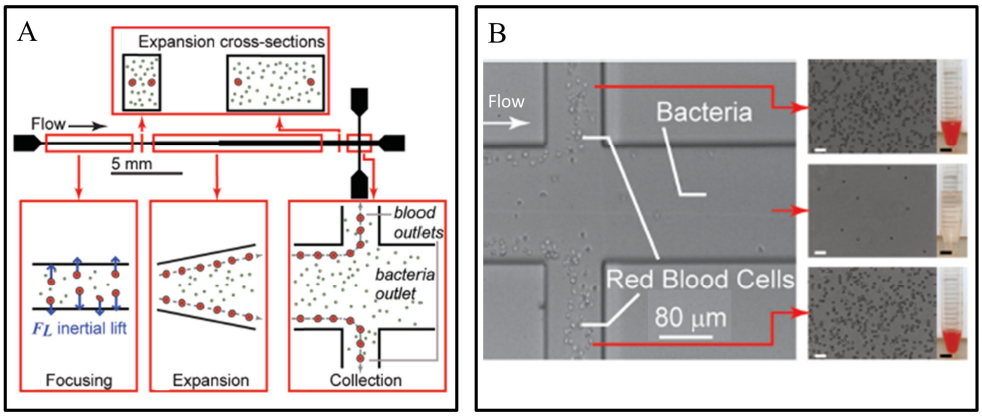


Figure 1.6: A size based blood filtration device. (A) The working principle of the filtration system composed of focusing, expansion and collection units, (B) Separation of *E.coli* from RBCs [17].

Mechanical techniques provide label free, harmless, and robust particle manipulation for LOC systems. However, their sensitivities are strongly dependent to precise flow controls. Moreover, biological cells, which have similar sizes, shapes and densities, cannot be effectively manipulated with these techniques. For example, carcinogenic cells have nearly the same size and shapes with the normal tissue cell at the early stages of cancer. Therefore, these techniques are not eligible for early diagnosis of cancer.

1.1.2. Magnetic Manipulation

Particle magnetic manipulation is achieved in nonuniform magnetic field by means of different magnetic susceptibilities of particles, such as paramagnetic, diamagnetic and nonmagnetic. In this technique, two methods can be applicable: 1) Using particles' native magnetic properties, 2) Tagging particles, magnetically. RBCs magnetic manipulation is an example to method 1 since RBCs have hemoglobin, which has ferrous (Fe) atoms in their structure [18], [19], [20]. Zborowski et al. [18] reported that the migration velocity of oxyhemoglobin RBCs (diamagnetic) and methemoglobin (paramagnetic) RBCs are different inside external magnetic field. They also showed that cells remain viable under magnetic field. Jung et al. [20] presented a continuous flow microdevice for label free separation of RBCs and white blood cells (WBC) with using magnetophoresis (MAP). To increase the efficiency of device, DEP was used together with MAP. This device utilizes the natural magnetic and electrical properties of blood cells. RBCs are pulled by magnetic force while WBCs are repelled by magnetic force and pulled by electric forces at the same time. Figure 1.7 shows devices structure (A) and tests results (B) of this device. In method 2, particles are tagged with either attachment of magnetic particles on their surface or introducing magnetic particles into them [21], [22], [23], [24]. Pamme et al. [21] exploited

the latter tagging approach in developing a magnetic cell sorting system. Without magnet, human ovarian cancer cells (HeLa) flowed straight through microchannel by means of laminar flow. On the other hand, when magnetic field is applied, magnetically tagged HeLa cells were sorted through magnetic field according to their magnetic susceptibility (Fig. 1.8).

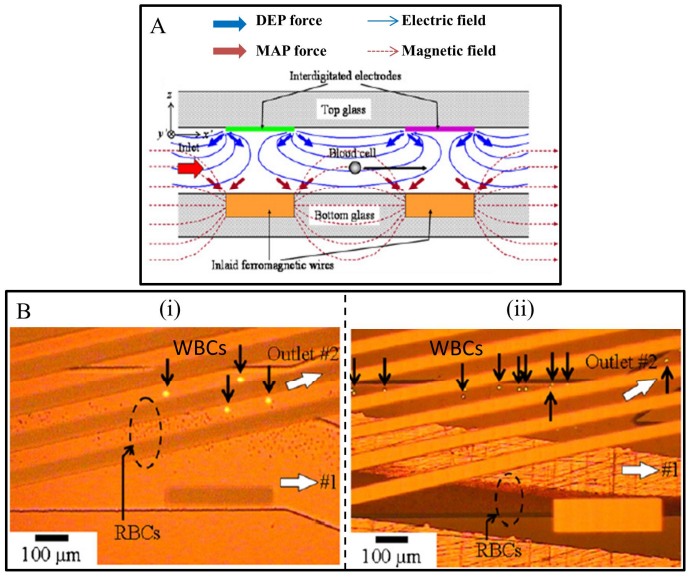


Figure 1.7: MAP and DEP based continuous flow microseparator. (A) Working principles focusing on electric and magnetic field distribution in the microchannel and MAP and DEP force directions, (B) The separation of RBCs and WBCs with only DEP effect (i) and with the utilization of MAP with DEP (ii) [20].

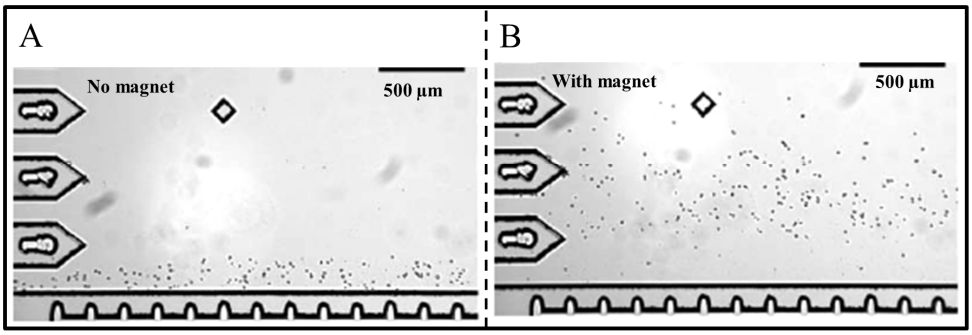


Figure 1.8: A magnetic cell sorting system. Tests results obtained with HeLa cells are presented without magnetic field applied (A) and sorting of the cells under the effect of magnet (B) [21].

Lee et al. [22] utilized both approaches for tagging budding yeasts (former approach) and bovine capillary endothelial (BCE) cells (latter approach) to manipulate them with a

magnetic sorter, which is an IC/microfluidic integrated system. They produced magnetic coil arrays with a microfluidic channel on IC. By controlling magnetic coils (magnetic field), they achieved the spatial manipulation of yeasts and BCE cells. Robert et al. [23] reported a cell sorting system for separating cells into subpopulations according to their endocytotic capacity. Iron was introduced into cells for magnetic tagging. Based on endocytotic capacity, iron concentration in each cell became different so their reaction to magnetic field changed and sorting into different subpopulations of them was achieved.

Magnetic manipulation can be achieved by utilizing natural magnetic properties of particles even they have similar sizes. However, the efficiency of the systems is usually not enough because most of the particles, such as biological cells, are nonmagnetic or they have weak magnetic properties. Therefore, some magnetic tagging approaches should be used. Even though tagging particles is biocompatible [23] and magnetic field is not harmful for biological cells [18]; this method causes the loss of label free property. Besides, labeling of the particles should be made by a trained person or a tagging part should be integrated into LOC system. However, this integration cannot be successful since magnetic tagging requires sensitive procedure, such as sensitive incubation time.

1.1.3. Optical Manipulation

Optical properties of the particles, such as refractive index, light transparency and light scattering, are utilized for the optical manipulation of them [25], [26], [27], [28]. Sato et al. [29] reported a single laser beam optical trapping device, achieving the RBCs trapping and rotation (Fig. 1.9). This contactless and harmless method utilizes transported photon momentum from laser beam to trapped particle by means of the refraction and reflection of the laser beam on the surface of particle. Although there exist other successful studies about laser beam optical trapping of particles [30], [31], this method is expensive and complex for LOC systems.

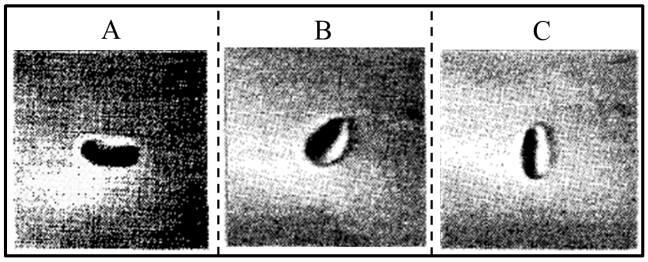


Figure 1.9: Optically trapping and alignment of RBC at different angles: (A) 180°, (B) 45°, and (C) 90° [29].

Lin et al. [32] developed an optically induced flow cytometry micro particle manipulator, utilizing optical fibers and optically induced dynamic switches. Figure 1.10 (A) & (B) show the experimental setup and device structure, respectively. For dynamic switching and DEP focusing of particles indium thin oxide (ITO) electrodes, which are induced with illumination, were used. Manipulation mechanism is based on size difference between particles since as the particle becomes larger; light is blocked more completely. Thanks to avalanche photodiode sensor module, reflected light amount was determined and dynamic switches were induced to sort the particle into accurate outlet. While larger particles are

directed to the lower outlet (Fig. 1.10 (C)), smaller ones go to the upper outlet (Fig. 1.10 (D)). As particle size decreases, scattered light becomes smaller. Therefore, optically induced DEP force drops and dynamic switching for sorting of particle cannot be made, efficiently. Decreasing the flow rate can solve this problem but it increases the analysis time.

Although optical manipulation techniques are label free, nondestructive, and contactless, complex and expensive systems are required for their usage. Therefore, they are not preferable for LOC systems.

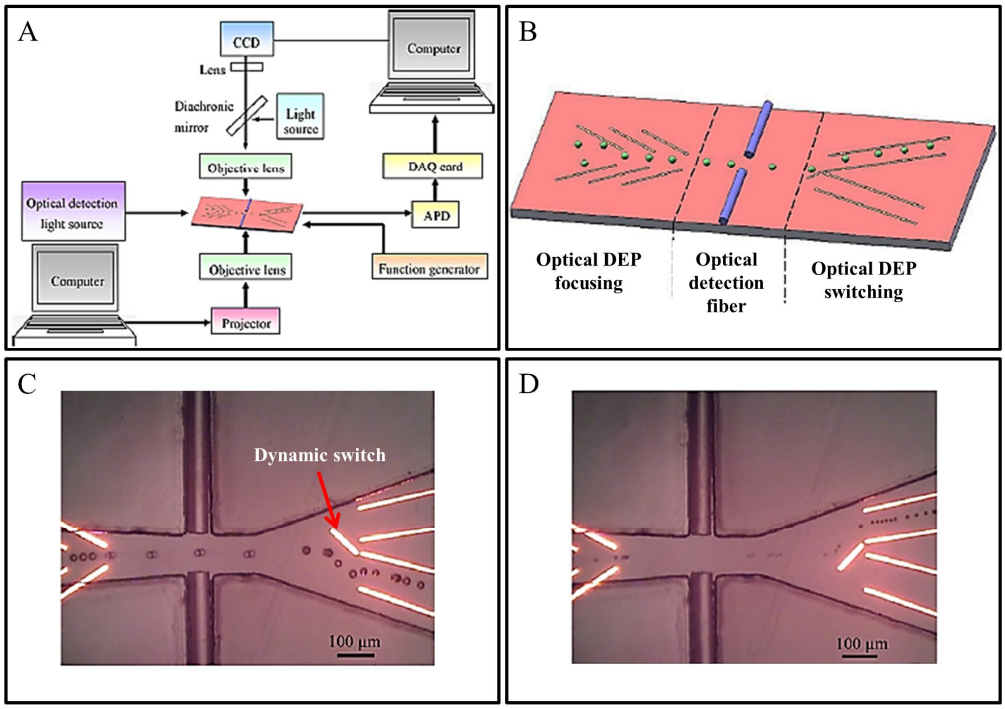


Figure 1.10: Optically induced flow cytometry micro particle manipulator. (A) Experimental setup, (B) Device structure, Sorting of larger particles(C) to lower outlet and smaller particles(D) to upper outlet [32].

1.1.4. Acoustic Manipulation

In this technique, particles are manipulated with acoustic radiation forces, utilizing ultrasonic standing wave field. Particles move to pressure nodes or antinodes based on their compressibility and density [14], [33], [34], [35]. Hawkes et al. [33] presented a continuous flow acoustic particle filtering device. By means of acoustic force pressure, particles are focused on the center of the microchannel. Utilizing laminar flow in microchannel, particles, focused at the center of microchannel, are driven to center outlet and obtained medium was purified. Petersson et al. [35] showed that RBCs, exposed to acoustic radiation force, are driven to pressure nodes and lipid particles are moved to antinodes (Fig. 1.11 (A)). Utilizing this property and laminar flow in microchannel, they separated lipid particles and RBCs (Fig. 1.11 (B)). Petersson et al. [34] also reported an

acoustophoretic size and density based separation system, utilizing multiple outlet fractions (Fig. 1.12 (A)). Figure 1.12 (B) shows the separation of 3, 7 and 10 µm particles with this system.

Sized based manipulation of the particles is achieved with the acoustic manipulation. Besides size, density can also be manipulated in this technique. Moreover, acoustic forces are not destructive for biological particles, and high throughput and low cost analyses are possible with these systems for LOC applications.

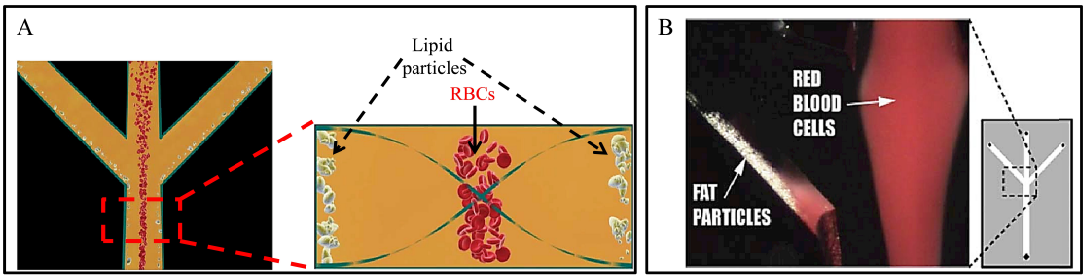


Figure 1.11: Acoustic radiation force based micro particle manipulator. (A) Device principles. RBCs are focused at the middle of the channel and lipid particles are pushed towards external channel walls at both sides. (B) Experimental results [35].

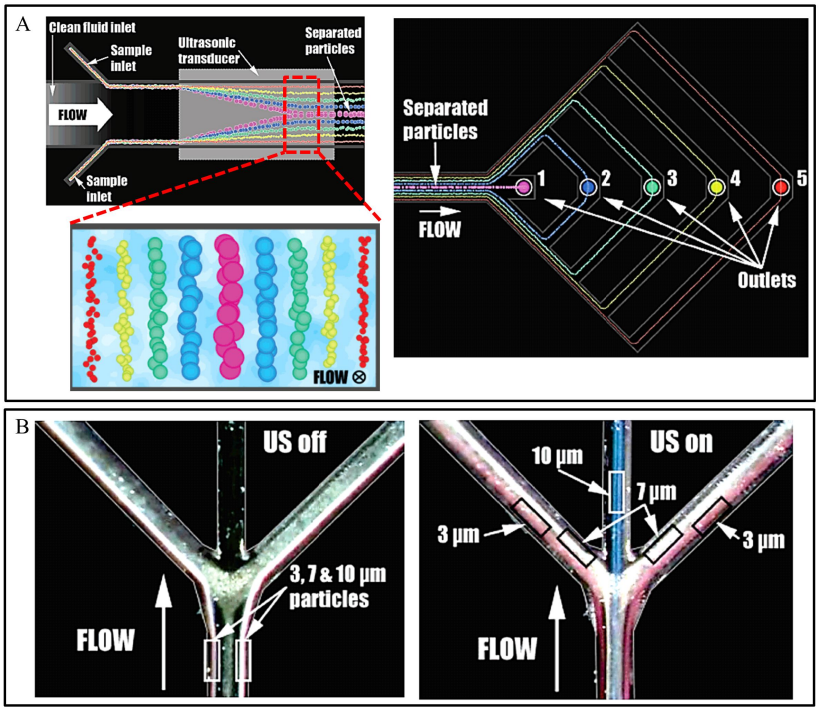


Figure 1.12: Acoustophoretic size and density based separation system. (A) Operational principles of device, (B) Experimental results for 3 different size particles (3, 7 and 10 µm) when ultrasound (US) is OFF (left) and ON (right) [34].

1.2. Electrical Manipulation and Literature Review about DEP in LOC

Particle electrical properties are more distinctive than their mechanical properties, such as shape and size, and label free analysis can be utilized with electrical manipulation techniques. Therefore, these techniques are significantly eligible for LOC systems, utilizing two main phenomena: electrophoresis (EP) and dielectrophoresis (DEP). Manipulation of charged particles (e.g. DNA and proteins) is achieved with EP while DEP manipulates both charged and dielectric particles (e.g. biological cells). The main properties of EP and DEP are described in this part. In addition, a detailed literature review about DEP in LOC applications is presented focusing on MDR detection in cancer cells.

1.2.1. Electrophoresis

EP is defined as the manipulation of charged particles under uniform electric field. The magnitude and direction of the EP force is proportional to the charge of the particles. Electrophoretic manipulation of the particles (e.g. DNA and proteins) can be utilized for different clinical applications, including single nucleotide polymorphism detection [36] and meningitis diagnosis [37]. As a negatively charged particle, DNA electrophoresis is one of the most common electrophoretic manipulation applications. The electrophoretic mobility of DNA fragments is proportional with the mass to charge ratio of them. Therefore, their displacement becomes the same and they are not separated with EP. To deal with this problem, sieving matrix is utilized with EP, forming different resistances for different length fragments.

EP has been achieved in macro scale systems for years. However, micro scale EP brings more advantages, including faster and multiple processing in a much smaller area, and low reagent consumption [3].

Figure 1.13 (A) shows a microscale EP device which was fabricated in BioMEMS research group of METU [38]. Polymorphism detection in nucleotides of wild and mutant DNA was reported by using double channel structure for making differential analysis between wild type and mutant DNA samples, simultaneously (Fig. 1.13 (B)).

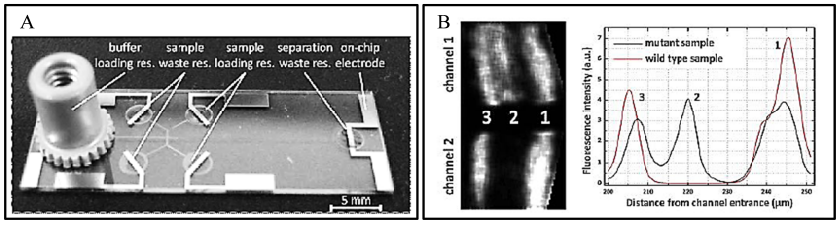


Figure 1.13: Differential analysis based EP chip. (A) Device structure, (B) Band formation and histogram: (1) The same base pairs in wild and mutant DNA, (2) Polymorphism, (3) Gel interface [38].

1.2.2. Dielectrophoresis

DEP is a MEMS-enabled method and defined as the relative motion of suspensoid and medium by means of electric field gradient, firstly by Pohl in 1951 [39]. Pohl utilized DEP

to cope with the problem of removing carbon-black filler from polyvinyl chloride samples. He also focused on the utilization of DEP in bioparticle characterization and he published the first DEP book, named as Dielectrophoresis, in 1978. Since 1966, around 2900 publications about DEP were come out (the database of Web of Knowledge, Jan, 2013). The focus of these publications moved from theory to application. This tendency shows that the theory of DEP matured and present studies are over applying DEP to solve unsatisfactory practical needs in clinical analysis [40]. Being label free, rapid, sensitive, and no need for trained people, biomedical applications of DEP have a great interest in last decades, including manipulation (trapping [41], [19]; [42]; [43], detection [44], separation [45], [46], [47],[48], focusing [49], [50], etc.) and dielectric characterization [51], [52] of biological particles, such as DNA and cells.

Clinical applications of DEP can be examined under the following subcategories:

1.2.2.1. Analysis of Blood

Blood is composed of plasma (~%60 v/v) and cells (~%40 v/v), such as RBCs and WBCs. The separation of blood cells from plasma and differentiation of blood cells have considerable importance in the diagnosis of many diseases, including leukemia, AIDS, and hepatitis. Separation of plasma and cells has been achieved with conventional centrifugal methods. However, centrifugal forces cause the damage and loss of blood cells. Utilization of DEP in these applications prevents loss of cells and provides more sensitive analysis with decreasing analysis time [5]. Continuous separation RBCs and WBCs [53], and platelets [54], [55], and differentiation of all blood cell types based on their sizes [56] have been reported up to now. Moreover, Nakashima et al. presented a microfluidic plasma separator from whole blood to achieve downstream clinical analyses [57]. While diluted blood was used in all these studies, Wang et al. achieved the separation of plasma from real blood sample, recently [58]. Figure 1.14 presents the experimental verification of their system. Due to differences in their antigenic markers, RBCs have different dielectric properties and ABO blood type analysis could be achieved with DEP [59]. Noninvasive separation of fetal cells from maternal blood was also realized by means of DEP. This will prevent the fetal losses due to amniocentesis or fetal blood sampling [60].

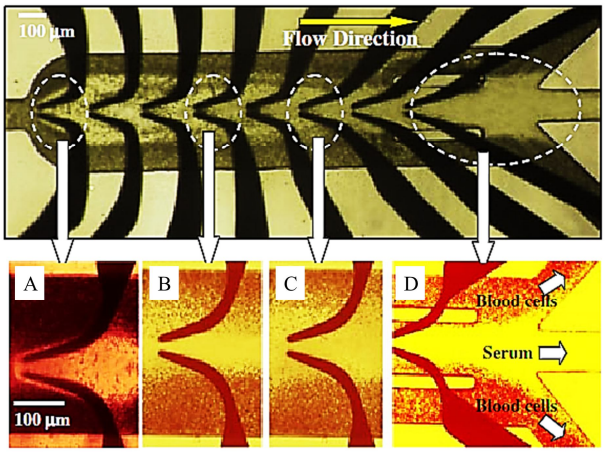


Figure 1.14: A real blood cell and plasma separation system. Blood stream flow is shown in the different parts of the DEP area: (A) Entrance region, (B) Middle region, and (C) Ending region. (D) The separation of plasma and blood cells at the end of the channel [58].

1.2.2.2. Infectious Diseases Diagnosis

To enrich the microorganisms to a detectable value, cell culturing is utilized in conventional analyses, which is an expensive, time consuming and labor-intensive method. As a very low concentration of pathogens can become fatal, a rapid and sensitive pathogen detection is necessary. DEP based detection systems denote sensitive and rapid diagnosis of infectious diseases [5]. Markx et al. showed that some bacterial cells, even if they are all gram (+), could be separated by DEP, including *Bacillus subtilis*, *Bacillus megaterium* and *Enterococcus faecalis* [61]. Zhou et al. reported a DEP based bacteria analysis system, utilizing single-wall carbon nanotubes (SWNTs). By means of SWNTs, DEP effect on bacterial cells was increased and 10^4 bacteria /ml was trapped in 5 minutes [62]. Chou and coworkers reported a DEP-based bacterial cell detection system from blood, and achieved separation of *E.coli* from blood cells [63]. Figure 1.15 shows their device structure, electric field analysis and the result of biological tests.

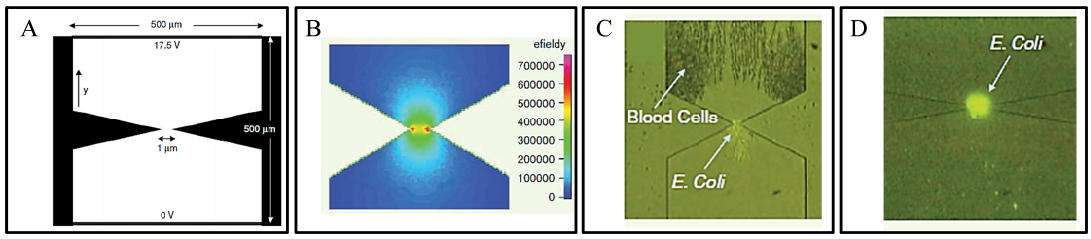


Figure 1.15: *E.coli* separation from blood cells. (A) Device structure with the dimensions of channel and insulators, (B) Electric field simulation of device, (C) *E.coli* and blood cell separation results, (D) Close-up view of the trapped *E.coli* between the tips of insulators [63].

Salmonella typhimurium, a waterborne pathogen, detection was also realized by Zellner and coworkers, utilizing a continuous flow and high throughput DEP based system [43]. Device structure and trapping of *S. typhimurium* with DEP at different frequencies are shown in Figure 1.16. Besides bacterial detection analysis, DEP can be utilized to diagnose virus based diseases [64], [65], [66].

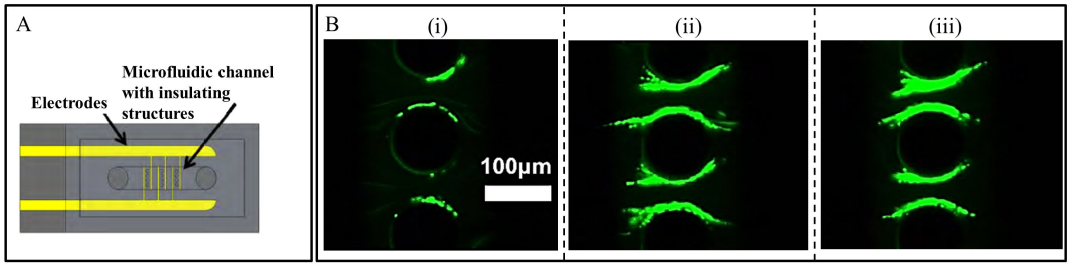


Figure 1.16: Salmonella typhimurium detection based on DEP. (A) Device structure, (B) Trapping of Salmonella typhimurium at a frequency of (i) 10 kHz, (ii) 100 kHz, (iii) 300 kHz [43].

1.2.2.3. Cancer Diagnosis

Early and precise diagnosis has a crucial role in the treatment of cancer. DEP is a highly sensitive technique for early diagnosis of cancer in LOC systems. However, it is still inadequate for early diagnosis of cancer, even its efficiency is relatively high (one cancer cell per 10^5 peripheral blood cell) [67]. DEP has been utilized in the diagnosis studies of lots of cancer types, including skin [68], [69], blood [70], [71], [72], [73], oral [74], breast [67], [75], [76], [77], [9], colorectal [45], lung [78], ovarian [79], cervical [80], prostate [81], and pancreatic [82]. Becker et al. [75] reported the separation of metastatic human breast cancer cells from diluted blood (Fig. 1.17 (A)). Figure 1.17 (B) shows the isolation of HeLa (human cervical cancer cells) from RBCs [80].

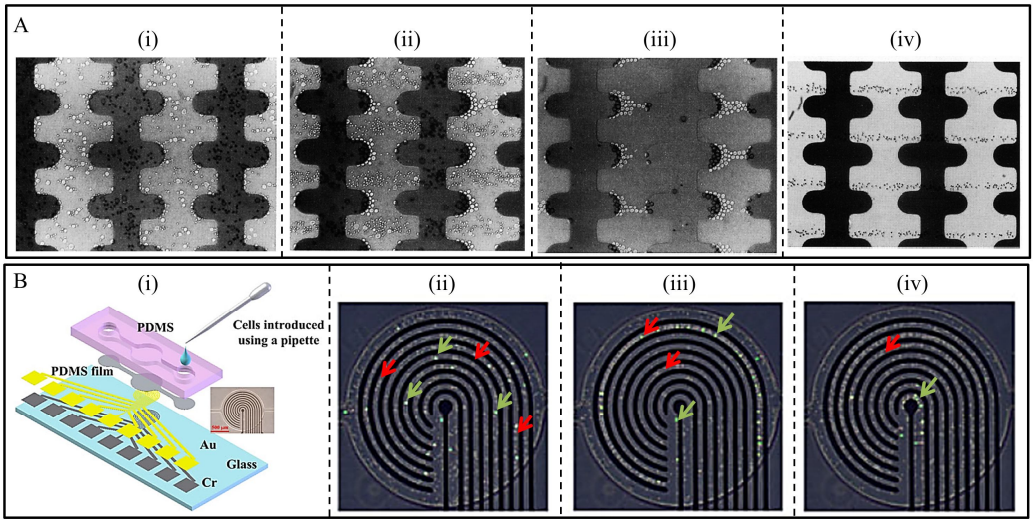


Figure 1.17: Isolation of cancer cells from blood. (A) Separation of metastatic human breast cancer cells from dilute blood utilizing castellated electrode structures. (i) Initial condition, (ii) Starting of trapping of cancer cells, (iii) Trapped cancer cells at the tip of electrodes, (iv) The alignment of blood cells between electrodes [75], (B) Isolation of HeLa (green arrow) cells from RBCs (red arrow). (i) Device structure, (ii) Initial condition (loading of cells), (iii) Starting of DEP operation and cell alignment between spiral electrodes, (iv) Collection of HeLa cells at the center before RBCs [80].

1.2.2.4. Stem Cell Therapy

The destiny of stem cells can be determined by means of DEP, eliminating the requirement of formation of cell-surface markers. Flanagan et al. [83]indicated that undifferentiated fetal derived mouse neuronal stem cells (NSPCs) in different developmental ages had different DEP trapping curves, providing the information about the destiny of them (Fig. 1.18(A)). Moreover, DEP can be utilized for stem cell enrichment [84] and separation as a noninvasive tool. Recently, Agarwal et al. [85] presented that aggregation of stem cells can be provided utilizing DEP, even in the presence of some aggregation inhibitory factors (Fig. 1.18(B)).

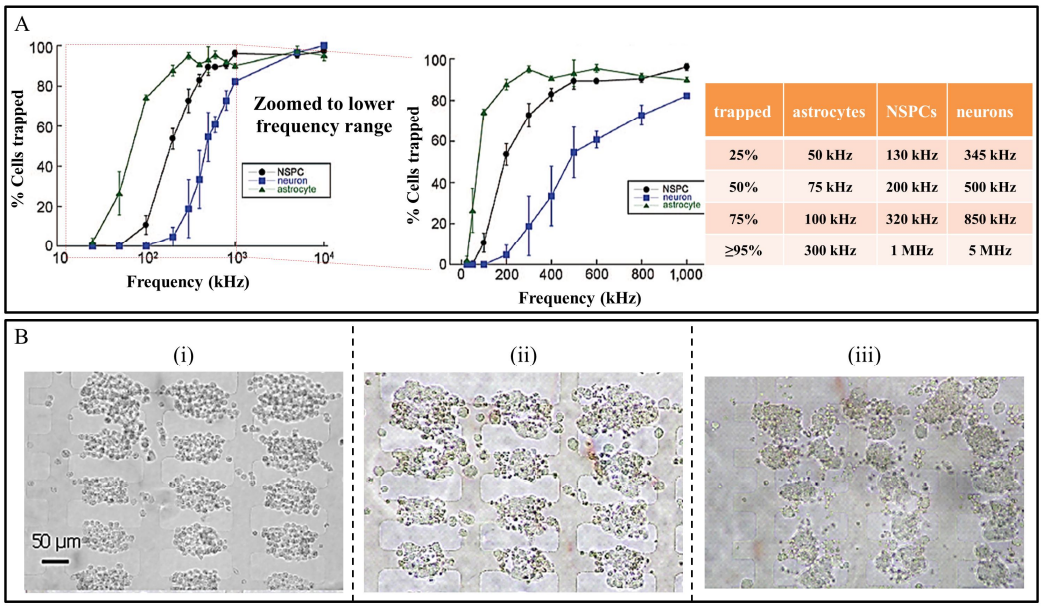


Figure 1.18: DEP research in stem cell therapy. (A) DEP trapping analysis of NSPCs, neurons and astrocytes [83], (B) Aggregation of stem cells at (i) 0 h, (ii) 24 h, (iii) 48h, even in the presence of some inhibitory factors [85].

Table 1.1 summarizes some DEP devices for clinical applications.

Table 1.1: Literature review of DEP for clinical applications [5].

Application	Cells	Applied Voltage Properties	Electrode Type	Reference
Characterization	*HL-60* leukemia cells	AC 1.2 V_{rms} between 10 kHz- 500 kHz	quadrupole	[86]
	oral squamous cell carcinoma (OSCC) (*H357*) and normal epithelial cell	AC between 1 kHz-20 MHz	needle shaped	[74]
Separation	mouse melanocytes (*B16F10*)	AC 5 V_{pp} at 200 kHz, 300 kHz and 400 kHz	castellated	[68]
	Herpes simplex and tobacco mosaic virus	AC at 5 MHz with 5 V_{pp}	polynomial electrodes	[64]
	human breast cancer cells (*MDA 231, MDA 435* & *MDA 468*)	AC 2 V_{rms} at 500 kHz	castellated	[75]
	RBCs and WBCs	AC at 2Mhz with 5 V_{pp}	planar divergent/ convergent type interdigitated electrodes	[53]
	RBCs, T- and B-lymphocytes, monocytes and granulocytes	AC at 100 kHz, 5.8 V_{pp}	planar interdigitated electrodes placed at an angle of 11.3 ° to the direction of flow	[56]
	plasma from blood cells	AC at 1 MHz with 10 V_{pp}	framed rectangle	[57]

Table 1 (continued).

Separation	platelets	AC at 100 kHz with 10 V_{pp}	DEP-FFF / consecutive electrodes on one side of the microchannel	[55]
	platelets	AC at 1 MHz with 100 V_{pp}	2-stage DEP purification/ rachet electrodes	[54]
	B-cell lymphotropic leukemia cells (*BALL-1)*	AC 14 V_{pp} at 37 kHz	creek gap electrodes	[71]
	HL-60 leukemia cells	AC 1.06 V_{rms} between 2kHZ-300 kHz	interdigitated	[70]
	MDA 435 human breast cancer cells and hematopoietic *CD 34+* stem cells	AC between 10 kHz-60 kHz with 4 V_{pp}	interdigitated	[87]
Trapping	*THP-1* human Leukemia monocytes, *MCF 7* breast cancer cells and *MCF 10A* breast cells	AC 250 V_{rms} at 85 kHz	iDEP	[88]
	undifferentiated fetal derived mouse neural stem cells (NSPCs), neurons and astrocytes	AC between 25 kHz-10 MHz at 8 V	interdigitated	[83]
	embryonic stem cells (ESCs) and induced pluripotent stem cells (iPSCs)	AC 10 V_{pp} at 1 MHz	ITO interdigitated	[85]
	MDA-MB-231, MCF 7 and *MCF 10A*	AC 30 V at 164 kHz	iDEP	[72]
Trapping and separation	bacteria-SWNT assemblies	AC at 1 MHz with 10 V_{pp}	parallel, perpendicular and circular electrodes	[62]
	E coli and *S. cerevisiae*	DC between 800 to 200 V/cm	iDEP (external electrodes and cylindrical insulating posts)	[89], [90]
	E. coli from blood	AC at 2 kHz with100 V_{pp}	iDEP (external electrodes and constricted microfluidic channel)	[63]
Trapping and manipulation	Influenza virus	AC at 3 MHz with 20 V_{pp}	planar, interdigitated electrodes	[65]
	nanoparticle	AC between 0-1 MHz with -1.2-1.3 V_{pp}	DEP-integrated CMOS chip	[91]
Trapping/ concentration	proteins	DC at 3 V	microwell electrode system	[92]
Manipulation and concentration	*E. coli* and SEB toxin	NA	immuno-DEP	[93]
Sorting and concentration	*S. aureus*	AC at 500 KHz with 12 V_{pp}	DEP-based cell concentration for SERS analysis	[94]
Detection	positive ABO blood cell types	AC at 1 MHz, 0.025 $V_{pp}/\mu m$	wire electrodes	[59]

Table 1 (continued).

Isolation	colorectal cancer cells (*HCT 116*) and human embryonic kidney cells (*HEK 293*)	scanning of voltage and frequency	ITO thin film bottom electrodes	[45]
	malaria	AC between 1 kHz-5 MHz up to 5 V_{pp}	spiral electrode array	[95]
Differentiation	fibroblasts, macrophages and different stage MOSE cells	AC between 200 kHz-600 kHz with 50-200 V_{rms}	iDEP	[96]
	human myeloid leukemia cells (*K562*) and *K562AR*	scanning of voltage and frequency	needle shaped	[97]
	melanoma (*Colo 38*)	frequency scanning	interdigitated	[69]
Collection & Enrichment	*CD 34+* stem cells	AC 6 V_{pp} at 500 kHz	gold plated interdigitated castellated	[84]
	putative stem cells	AC between 60 kHz-200 kHz at 3 V_{pp}	interdigitated	[98]

1.2.3. Multi Drug Resistance (MDR) Detection in Cancer Cells

Cancer cells can develop resistance to different drugs or chemicals, which have distinct structures and functions, a phenomenon, named as MDR. Patients with MDR do not respond chemotherapy. Two types of MDR exist in cancer patients: 1) Acquired during treatment, 2) Preexisting at the time of diagnosis [99]. The early detection of MDR in cancer cells is critical for the determination of the most suitable treatment method speeding up the recovery period for both 1st and 2nd type of MDR. MDR detection in cancer cells utilizing DEP is one of the main objectives of this thesis. Therefore, this application area will be analyzed in detail in the following subsections.

1.2.3.1. MDR Mechanisms in Cancer Cells

Studies show that MDR is caused by two main mechanisms: 1) Promotion of drug efflux from the cell, 2) Trapping of drug in intracellular vesicles and elimination by exocytosis. In the 1st mechanism, overexpression of cell membrane proteins (P glycoprotein (P-gp) and multidrug resistance associated protein (MRP)), working as drug efflux pumps, is responsible for MDR formation in cancer cells [99]. These proteins, activated by binding ATP, decrease the effective drug concentration inside the cells with evacuating them out (Fig.1.19 (A)). To overcome MDR, modulators, substrate for P-gp and MRP, are used to deactivate these proteins and prevent drug efflux (Fig. 1.19 (B)).

1.2.3.2. The Methods of MDR Detection in Cancer Cells

According to recent studies, MDR detection methods can be separated into three main groups: 1) In vivo imaging, 2) Protein assays, 3) Flow cytometry [99].

To provide the information about dynamic functions of P-gp and MRPs, in vivo imaging techniques, such as single-photon emission tomography and positron emission tomography, are utilized. In these techniques, substrates of P-gp and MRPs, tagged with different isotopes (radiolabelling, or nuclear tagging), are injected to patient's body. Labeling is made with undamaging dosages, but repeated administration of such isotopes is not allowed, due to side effects of radioactive isotopes.

Protein assays give information about the existence of drug efflux pumps, not dynamic functions of them. These are in vitro studies, requiring isolation of cancer cells from the body. Therefore, they are invasive methods.

In flow cytometry, isolated cancer cells are tagged with fluorescently labeled antibodies of membrane proteins to detect MDR. It cannot give information about the activity of the membrane proteins. Moreover, like in vivo imaging techniques, flow cytometry method is expensive one. On the other hand, this method provides quantitative information about the level of MDR proteins' expression.

Commercial MDR detection systems are based on optical techniques. For example, MultiDrugQuant (MDQ) kit, developed by Solvo Biotechnology, utilizes fluorescent staining and intensity measurement technique to determine drug resistivity in tumor cells [100].

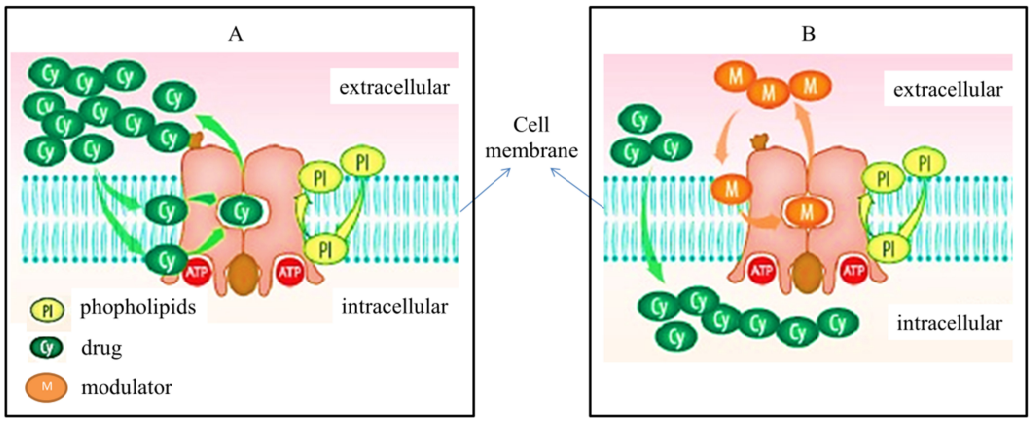


Figure 1.19: Multi drug resistance mechanism in tumor cells. (A) Drug (Cy) efflux through ATP binding cell membrane proteins (P-gp and MRP), (B) Drug intake by means of modulator (M) treatment [100].

1.2.3.3. DEP: A Candidate for MDR Detection Technique

As a more sensitive technique than optical methods, DEP can be utilized for detection of MDR in cancer cells in a label free manner [97], [101], [102]. Labeed et al. showed that P-gp is a membrane bound Cl^- channel, besides being a drug efflux pump. Due to overexpression of P-gp in multidrug resistant cells, ionic concentration of cytoplasm is increased, leading to increased cytoplasmic conductivity, compared to the drug sensitive cells. For example, they reported that the cytoplasmic conductivity of K562AR (doxorubicin resistant leukemia) cells are 2.17 times higher than K562 (sensitive leukemia) cells, by analyzing their DEP collection spectra (Fig. 1.20). In the same study, they also showed that modulator usage does not prevent working of P-gp as a Cl^- channel. Therefore, when a modulator is used, cells become sensitive to chemotherapeutics, while the dielectric properties remain unchanged. Therefore, after modulator therapy is started, DEP cannot be utilized for quantitative analysis of MDR anymore, as this may lead to misinterpretations [97]. As a matter of fact, the usage of DEP after modulator therapy has started is unnecessary since DEP is utilized for the detection of MDR.

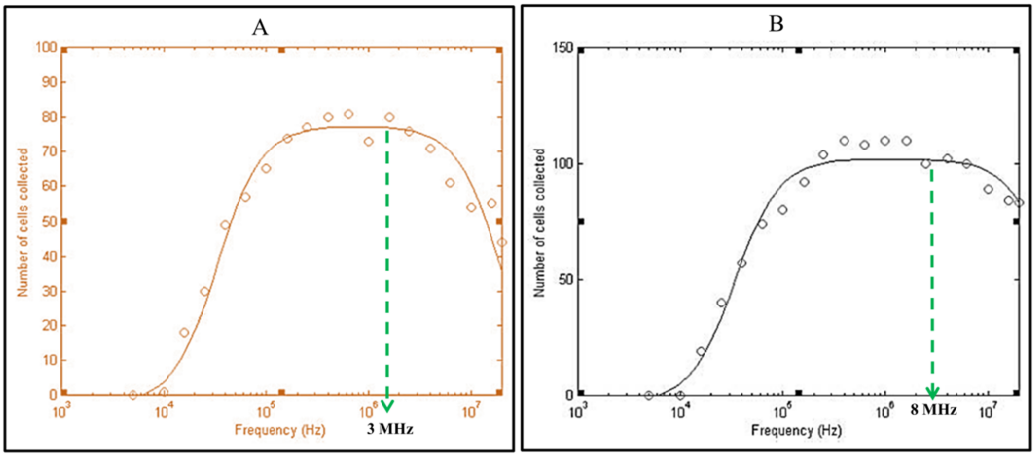


Figure 1.20: DEP collection spectrum of (A) K562 (drug sensitive leukemia) and (B) K562AR (drug resistant leukemia) cells. Collection starts to decrease at 3MHz for sensitive cells while it starts to decrease at 8MHz for resistant ones [97].

1.3. Research Objectives and Thesis Organization

This thesis presents design, fabrication and implementation of a MEMS-based, 3D-electrode contactless dielectrophoresis device for the continuous flow, label-free and real-time detection of MDR in cancer cells.

The main research objective of this thesis is to develop a MEMS-based DEP device for the label-free detection of MDR in cancer. To achieve this objective, following studies need to be carried out in a systematical manner:

1. Realization of DEP-based cell separation based on variations dielectric property only, using viable and non-viable yeast cells, for the proof of concept, through following studies:
   - Accurate dielectric modeling of viable and non-viable yeast cells using MATLAB.
   - Design of the first generation DEP device for separation of viable and non-viable yeast cells under continuous flow conditions, with a novel approach combining the advantages of 3D electrode structures and contactless DEP phenomenon.
   - Hydroelectrodynamic analysis of the design with COMSOL software utilizing finite element model (FEM) simulations.
   - Development of a fabrication flow and fabrication of the first generation DEP device.
   - Development of an experimental procedure and a test setup.
   - Testing of 1st generation DEP devices with viable and non-viable yeast cells, to prove the possibility of DEP-based separation of cells with similar sizes but different dielectrophoretic properties.

2. Accomplishment of DEP-based MDR detection in leukemic K562 cells utilizing dielectric characteristics, through the following studies:

- Dielectric modeling of doxorubicin and imatinib resistant K562 cells and their drug sensitive types using MATLAB, according to their dielectric properties reported in literature.
- Design of a 2nd generation DEP device with 3D contactless electrode structure with improved throughput and detection sensitivity.
- Hydroelectrodynamic analysis of the design with COMSOL software utilizing finite element model (FEM) simulations.
- Development of a fabrication flow and fabrication of the first generation DEP device.
- Development of experimental setup (flow controllers, high speed camera, fluorescent microscopy, etc.) and cells fluorescence staining protocols to observe the movement of cells inside the channel.
- Testing of the devices with sensitive and resistant lines of K562 leukemia cells to detect MDR.
- Performance analyses of the 2nd generation devices by changing experimental parameters, including flow rate, voltage and cell concentration.
- The analysis of the MDR levels using K562 cells with varying degrees of drug (doxorubicin) resistance.
- Evaluation of consistence of experimental results with the available literature and simulations.

Thesis organization is as follows:

Chapter 2 describes the necessary background information and significant analysis parameters about DEP. Moreover, common microelectrode structures for realization of DEP and operating strategies are given in this chapter together with their advantages and disadvantages depending on the applications.

Chapter 3 starts with defining the analogy between biological cells and electrical circuits. Next, it gives the information about cell dielectric modeling, essential for the design of DEP chips. Moreover, the dielectric modeling of viable and nonviable yeast cells, and sensitive and drug (doxorubicin and imatinib) resistant cells, through MATLAB are given.

In chapter 4, design and COMSOL simulations of the DEP devices are presented with detailed structural explanation of them.

Chapter 5 includes the fabrication procedure of DEP devices. Moreover, the images of the fabricated devices at the critical fabrication stages, such as electroplating, are presented in this chapter.

In chapter 6, tests setup and experimental procedure together with the cell preparation and counting protocols are given in detail. The test results are discussed in comparison with the available literature.

Finally, in chapter 7, thesis conclusion elaborating on the accomplishments and possible future works are presented.

CHAPTER 2

THEORY OF DIELECTROPHORESIS

2.1. Dipole Moment

By means of interfacial polarization mechanisms, charge accumulation occurs on the surface between a dielectric particle and suspending medium if particle is exposed to electric field. This polarization leads to formation of dipole moment inside the particle. Equation 1 represents this dipole for a special case: a homogeneous dielectric sphere [103], [104].

$$\vec{p} = 4\pi\varepsilon_m(F_{CM})r^3\vec{E} \tag{1}$$

where ε_m is the suspending medium permittivity, r is the radius of particle, and F_{CM} is Clausius Mossotti factor of the particle, and E presents the electric field.

F_{CM} carries the information about the particle and the medium dielectric properties, and the frequency dependence of dipole moment. For spherical particles, F_{CM} is formulized as:

$$F_{CM} = \frac{\varepsilon_p^* - \varepsilon_m^*}{\varepsilon_p^* + 2\varepsilon_m^*} \tag{2}$$

where ε_p^* and ε_m^* are the complex permittivities of the particle and the suspending medium, respectively (Eqn. 3).

$$\varepsilon_p^* = \varepsilon_p - j\frac{\sigma_p}{w} \tag{3a}$$

$$\varepsilon_m^* = \varepsilon_m - j\frac{\sigma_m}{w} \tag{3b}$$

ε and σ symbolize permittivity and conductivity, respectively, j is $\sqrt{-1}$, and w is the angular frequency.

Due to the formation of dipole moment inside the particle, a dipole force affects the particle in the electric field and is formulized as:

$$\vec{F}_{dipole} = \vec{p}.\nabla\vec{E} \tag{4}$$

In equation 4, ∇ stands for *del* operator. It is utilized to indicate the gradient operation.

These equations have the following outcomes:

- If nonuniform electric field does not exist, net dipole force is zero inside the particle (Eqn. 4).
- Dipole moment cannot be formed if particle and suspending medium have the same complex permittivity since $Re(F_{CM})$ becomes zero in that case (Eqn. 1 & 2).
- For low frequencies, $Re(F_{CM})$ is determined by medium and particle conductivities and for high frequencies, it depends on the particle and medium permittivities. Utilizing these properties, the following boundaries are obtained for $Re(F_{CM})$.

$$\lim_{w\to 0} Re(F_{CM}) = \frac{\sigma_p - \sigma_m}{\sigma_p + 2\sigma_m} \tag{5a}$$

$$\lim_{w\to \infty} Re(F_{CM}) = \frac{\varepsilon_p - \varepsilon_m}{\varepsilon_p + 2\varepsilon_m} \tag{5b}$$

According to equation 5a, if $\sigma_p >> \sigma_m$, maximum value of $Re(F_{CM})$ occurs as 1. If $\sigma_p << \sigma_m$, minimum value of $Re(F_{CM})$ is obtained as -0.5. The same limits are obtained if permittivities are concerned (Eq. 5b).

2.2. Dielectrophoresis

Dielectrophoresis is defined as the relative motion of particles and suspending medium under nonuniform electric field. When equation 1 and 4 are combined, the following equation is obtained and named as dielectrophoretic force [104].

$$\vec{F}_{DEP} = 2\pi\varepsilon_m r^3 \{Re(F_{CM})\nabla|E|^2 + 2Im(F_{CM})\nabla x\vec{E}_i x\vec{E}_r\} \tag{6}$$

In equation 6, E_i and E_r are the imaginary and real parts of alternating electric field, respectively.

The second term of equation 6 is nonzero provided that the rotating nonuniform electric field exists. If electric field does not rotate, common time averaged DEP force is obtained for spherical particles as follows:

$$\vec{F}_{DEP} = 2\pi\varepsilon_m r^3\, Re(F_{CM})\nabla|E|^2 \tag{7}$$

By the combination of equation 2 and 7, if $\varepsilon_p^*>\varepsilon_m^*$, particles are pulled into the stronger electric field region by positive DEP (pDEP) force. If $\varepsilon_p^*<\varepsilon_m^*$, particles are pushed into weaker electric field region by negative DEP (nDEP) (Fig. 2.1).

There exists a frequency at which $Re(F_{CM})$ (Eq. 2) becomes zero. It is named as crossover frequency (f_{cross}) and expressed as [3]:

$$f_{cross} = \frac{1}{2\pi}\sqrt{\frac{(\sigma_m - \sigma_p)(\sigma_m + 2\sigma_p)}{(\varepsilon_p - \varepsilon_m)(\varepsilon_p + 2\varepsilon_m)}} \tag{8}$$

If f_{cross} values of particles are different, they can be separated by DEP based on dielectric property differences between them. If f_{cross} values of them are too close, size-based separation can be achieved since F_{DEP} is directly proportional with the r^3 [5]. Figure 2.2 is an illustration of the separation of three particles depending on their f_{cross} values. It shows

that at the f_{cross} of particle 3, particle 1 ($f_{cross1} > f_{cross3}$) is pulled by pDEP and particle 2 ($f_{cross2} < f_{cross3}$) is pushed by nDEP [105].

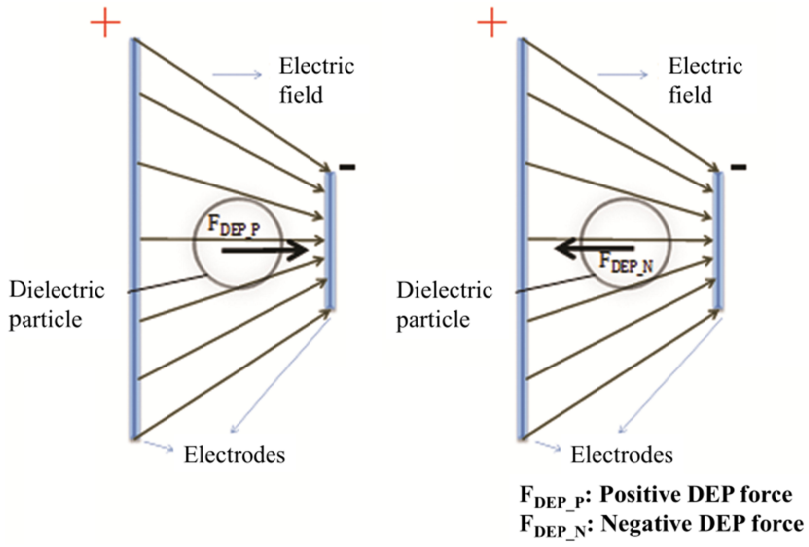


Figure 2.1: Positive and negative DEP force. If $\varepsilon_p^* > \varepsilon_m^*$, particles are pulled into the stronger electric field region by positive DEP (pDEP) force. If $\varepsilon_p^* < \varepsilon_m^*$, particles are pushed into weaker electric field region by negative DEP (nDEP) force [3].

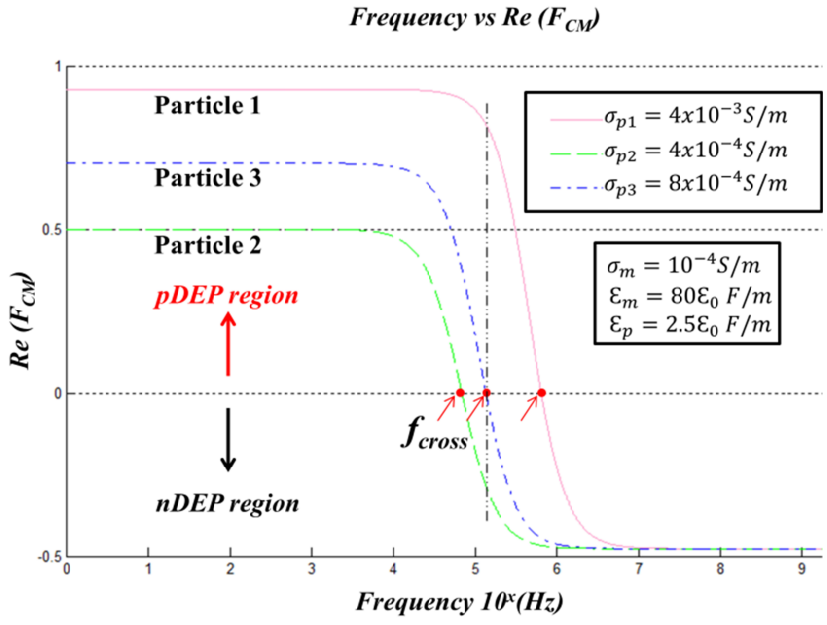


Figure 2.2: *Re(F_{CM})* vs frequency graph of three particles with different conductivities: σ_{P1}=4x10^{-3} S/m, σ_{P2}=4x10^{-4} S/m, σ_{P3}=8x10^{-4} S/m. Conductivity of the medium is taken as 10^{-4} S/m for this illustration [105].

The separation of biological particles, such as tumor cells and blood cells, can be achieved by means of DEP, utilizing differences in their f_{cross} values. f_{cross} coefficients of different tumor cells and blood cells are indicated in Figure 2.3 [3].

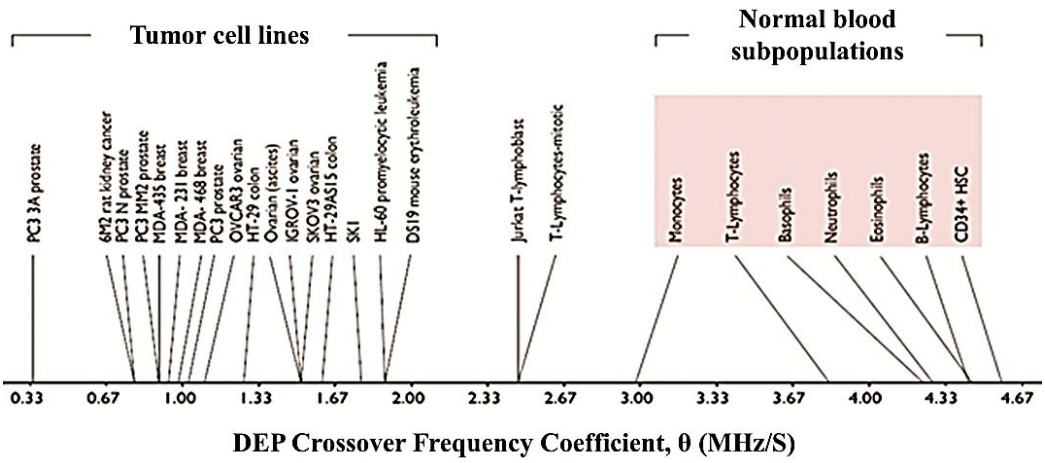


Figure 2.3: Crossover frequency coefficient distribution of different tumor cell lines and normal blood cells. Courtesy of Gascoyne et al. [67], [3].

2.3. Combination of Microfluidics with DEP

Reynolds number determines the type of flow regime. If it is smaller than 2100, flow is laminar. If it is greater than 4000, flow becomes turbulent. For microfluidic systems, Reynolds number can become <<1. Therefore, laminar flow occurs in this type of systems [106]. It is proper flow type for particle manipulation since particles can be directed into needed direction without turbulence effect. Therefore, if a particle is manipulated by DEP to a specific place, flow cannot disrupt its position.

Pressure driven flow is possible in microchannels and named as Poiseuille flow. The velocity distribution is parabolic in this flow type [107]. Parabolic flow profile enables that particles may have different velocities according to the positions of them along channel depth. In addition, by means of DEP, particles can be levitated to different height in channel according to their dielectric properties. Therefore, the combination of parabolic flow profile and this ability of DEP, time varied separation of particles can be achieved [5]. This is one of the operating strategies in DEP and named as DEP- Field Flow Fractionation (DEP-FFF), explained in part 2.5 in detail.

To utilize microfluidics' properties in the design of DEP particle manipulation chip, independent Navier-Stokes equation (Eqn. 9) should be solved with DEP equations, simultaneously, by taking drag, gravity and lifting forces into account.

$$\rho \frac{\partial \vec{u}}{\partial t} + \rho \vec{u}.\nabla \vec{u} = -\nabla \rho + \mu \nabla^2 \vec{u} \qquad (9)$$

where ρ, u and μ are the density, velocity and viscosity of the solution, respectively. To obtain the basic format of this velocity expression, some assumptions can be utilized [107] but in the frame of this thesis, these equations are solved numerically with using COMSOL®, finite-element model (FEM) simulation software.

The forces acting on a suspended particle under the effect of electrohydrodynamic effects are drag, DEP and electroosmotic flow forces in x and y directions. However, if AC field is utilized for DEP operation, electroosmotic flow is negligible. In z direction, lifting and gravity forces are also effective (Fig. 2.4). On the other hand, while studying with DEP for biological cells, lifting and gravity forces are assumed equal because if water based medium is used, medium and particle densities are nearly the same for biological cells (The largest part of the biological cells consists of water.). Since lifting and gravity forces have reverse directions and they are equal, they form zero net force on the particle. Therefore, they cannot affect the particle motion in z direction under these assumptions.

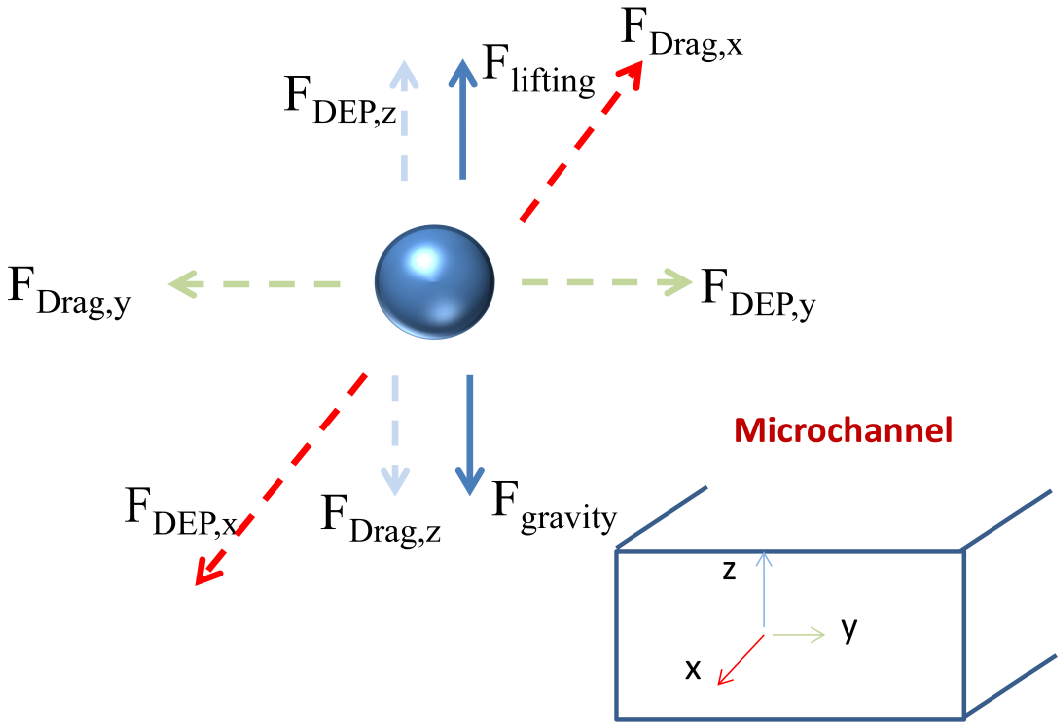


Figure 2.4: Forces acting on a particle inside microchannel.

According to Newton's second law, all forces having same direction should be equal to mass times acceleration in that direction. However, for that analysis, acceleration term is neglected since the time period of the motion is much smaller than the time period of deviation in field variables [108]. Assuming zero electroosmotic flow, only drag and DEP forces remain. Due to neglected acceleration term, the sum of these two forces becomes equal to zero. By this way, the following particle velocity equation is obtained for a particle under the effect of DEP force [105].

$$u_p = u_m + \frac{\varepsilon_m}{\mu}\frac{r^2}{3} Re(F_{CM}) \nabla|E^2| \quad (10)$$

where u_p and u_m are the particle and medium velocities, respectively.
All these equations are for dilute suspensions. For nondilute suspensions, solute-solute interactions become effective in the solution properties. Therefore, interparticle electric and hydrodynamic interactions should be considered. In this case, electrical permittivity of suspension is dependent on particle volume fraction. Therefore, concentration dependent Maxwell-Wagner expressions in quasi-steady state electrodynamics conditions should be studied to acquire the DEP force (Eq. 11) [109].

$$F_{DEP} = \frac{\varepsilon_0 v_p}{2}\left(\frac{\partial \varepsilon_s}{\partial c}\right)_{wt_c} \nabla|E^2| \quad (11)$$

where, ε_0 is the vacuum permittivity, v_p is the particle volume, ε_s is the real part of complex permittivity of suspension, c is the particle volume fraction, and t_c is the relaxation time for dielectric phenomena [110].

Furthermore, interparticle interactions are dominant in nondilute suspensions, when high gradient electric fields are used. Therefore, these particles undergo phase transition by creating highly concentrated regions on DEP gates. Because of this, the efficiency of the DEP system is decreased by affecting the electrodynamics conditions in DEP region. Hence, concentrated suspensions restrain the electric field strength for DEP applications.

2.4. Microelectrode Configurations in DEP Devices

Nonuniform electric field is an essential condition for DEP. To produce nonuniform electric field in DEP devices, different microelectrode configurations are exploited. Based on DEP application, the most proper configuration can be chosen. The principles, advantages and disadvantages of these configurations are examined as the following [111].

In *castellated electrode configuration*, electrodes are placed as reciprocal (Fig. 2.5 (A)) and energized with two signals having 180° phase difference. While weaker electric field formation occurs at the gap between electrodes, stronger electric field is formed at the sharp edges of the electrodes. Although high flow rate and large DEP trapping area are enabled in this configuration, single cell analysis cannot be achieved by this electrode configuration.

Electrodes are placed at an angle to the channel side-walls and energized with two signals having 180° phase difference, in case of *oblique electrode structure*. The stronger electric field is formed at the tip of electrodes while the weaker field occurs at the exterior edges of the electrodes (Fig. 2.5 (B)). Although continuous flow analysis is applicable in this configuration, high flow rate cannot be applied and single cell analysis cannot be achieved.

Quadrupole electrode configuration is composed of four electrodes, placed with an offset by 90°, and they are stimulated with two signals having 180° phase difference between sequential ones (Fig. 2.5 (C)). At the center, weaker electric field region is formed and the stronger field occurs along the arm of the electrodes. Although particles are not exposed to higher electric field, continuous flow analysis is not possible with this configuration.

In *extruded electrode configuration*, electrodes are extruded along the z direction. This provides uniform DEP force along channel height. Although fabrication procedure seems complicated, high flow rate and continuous flow can be achieved.

Electrodes are deposited top and bottom of the channel to provide uniform DEP force along channel height, in case of the *top-bottom patterned electrode structure*. Although fabrication of the electrodes in this configuration is relatively simpler than extruded electrodes, DEP force uniformity is limited with the channel height. This structure is proper only for the microchannels with low height.

In *side-wall patterned electrode configuration*, electrodes are placed on the side-wall of channel along the channel height. It provides uniform DEP force along the channel height and continuous flow DEP operation is independent of the channel height.

Besides electrode based DEP, *insulating DEP (iDEP)* is utilized to generate nonuniform electric field. Insulating arrays or some constrictions inside the channel are used to provide electric field nonuniformity (Fig. 2.5 (D)). iDEP prevents electrode fouling and Joule heating effect [5].

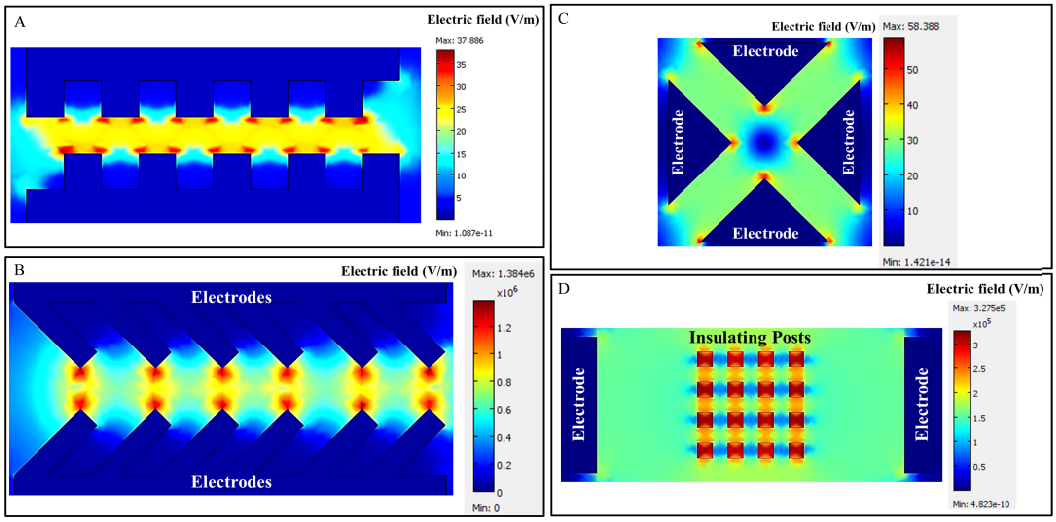


Figure 2.5: The electric field simulations of different electrode configurations utilized in DEP, castellated (A), ratchet (B), and quadrupole (C), and insulating DEP (iDEP).

2.5. Operating Strategies in DEP

To achieve DEP manipulation of particles inside microchannels, electrical and hydrodynamic forces are utilized in interaction with each other and for this purpose, lots of strategies were adapted. Field flow fractionation (FFF), multi-step, travelling wave, multiple frequency, medium conductivity gradient, and immuno-assisted strategies can be listed as the most favorable ones [111].

In *FFF technique*, planar bottom and/or top electrodes are utilized to obtain nonuniform electric field along channel height. Particles are levitated into different heights in the channel by pushing through nDEP due to their different dielectric properties. They also have different velocities at different heights since parabolic flow profile exists in microchannels. As a result of this combination, particles leave the channel at different times. Continuous flow separation can be achieved in this strategy (Fig. 2.6). The main

difference between FFF and the other strategies is not needing different signed $Re(F_{CM})$ values to achieve the DEP separation of particles.

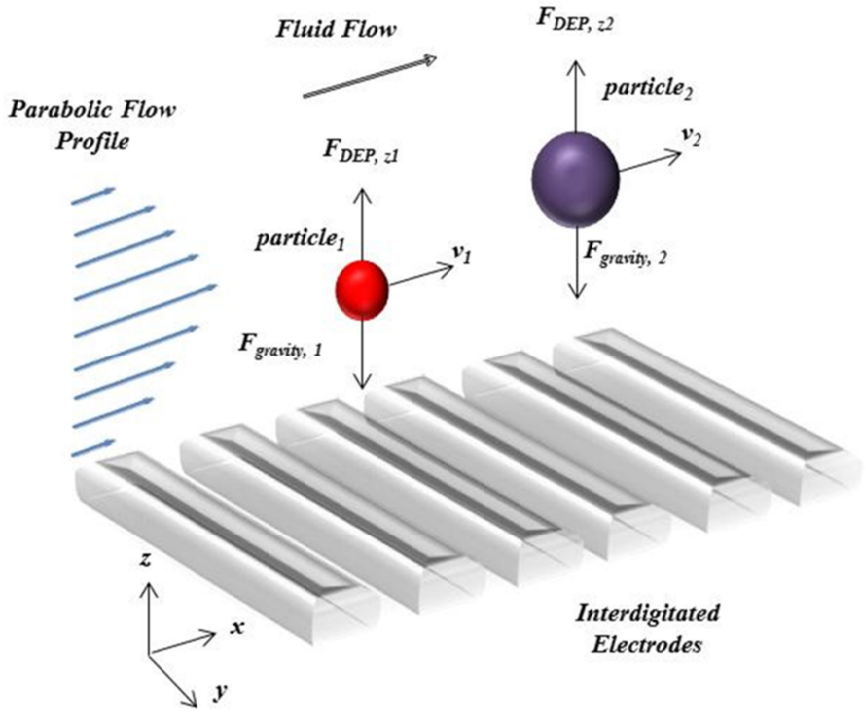


Figure 2.6: The principles of DEP-FFF (Adapted from [67]).

Particle trapping and releasing are utilized in an order in the *multi-step technique* (Fig. 2.7 (A)). The technique is applied to separate particles with oppositely signed $Re(F_{CM})$. While the particle of interest is trapped through pDEP, the others were drifted out of the channel by fluid flow, or vice versa. Removal of DEP force releases the trapped particles, which are collected at the outlet.

In *travelling-wave technique* (Fig. 2.7 (B)), an electric field with 90° phase difference (0°, 90°, 180°, and 270°) is applied to parallel planar bottom electrodes placed along the channel to generate rotating electric field. Due to rotating electric field, imaginary part of the DEP force is used. Like FFF, particle levitation through nDEP is utilized. Continuous flow separation of particles with high separation efficiency can be achieved with higher DEP forces.

As its name suggests, *multiple-frequency technique* (Fig. 2.7 (C)) utilizes electric fields with different frequencies. By means of the application of different frequencies simultaneously, particles having close f_{cross} values can be separated. However, this technique is not proper for continuous flow separation.

Particle and medium conductivity relation in F_{CM} expression is used in the *medium conductivity gradient technique* (Fig. 2.7 (D)) with the assistance of microfluidic flow. Particles are trapped in proper conductivity medium with pDEP and another medium with

different conductivity passes through the channel to release the particles without changing the electric field frequency. This technique is proper for continuous flow separation of multiple particles.

Immunological capture of particles is achieved using antibody-activated surfaces but particles should be close enough to these antibodies to be trapped through them. To bring particles closer to the antibodies, pDEP is utilized in *immuno-assisted method* (Fig. 2.7 (E)). Moreover, when DEP force is not enough to trap the particles in continuous flow, antibodies are coated on microelectrodes and immunological interaction forces can be used to become stronger DEP traps. By this way, immunological and dielectrophoretic particle manipulation techniques can be utilized in a positive feedback relation.

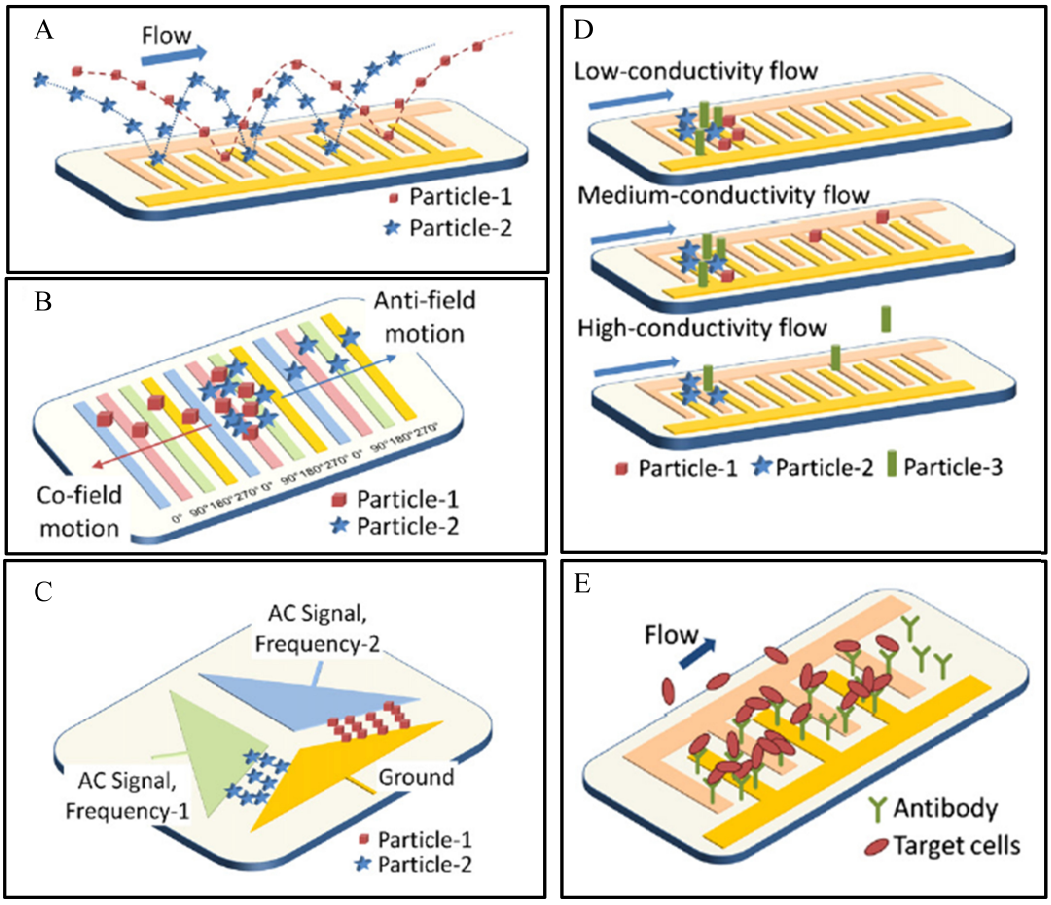


Figure 2.7: The structure and working principle of different operating strategies utilized in DEP: Multi-step (A), Travelling-wave (B), Multiple-frequency (C), Medium conductivity gradient (D), and Immuno-asisted (E) [111].

CHAPTER 3

DIELECTRIC MODELING OF CELLS

Re(F_{CM}) depends on the particle and medium dielectric properties. Medium dielectric properties can be adjusted but particle dielectric properties should be measured. After determination of the dielectric properties, particles are modeled to simulate DEP microfluidic system with FEM. Proper structures for DEP operation are determined based on these models. Therefore, dielectric modeling of particles is one of the key points in the design of DEP system.

3.1. The Analogy between Biological Cells and Electrical Circuit Elements

Biological cells are the smallest living things and they have the complex structures. To understand their mechanisms, chemistry, biology, and genetics should be deeply comprehended. Moreover, to explain most of the events inside the cell, signaling pathways and ion exchange mechanisms should be understood. In these mechanisms, some charged or polarizable molecules (Fig. 3.1) are utilized and due to presence of these molecules, biological cell membranes and cytoplasm have some various electrical properties, such as capacitance and resistance [112].

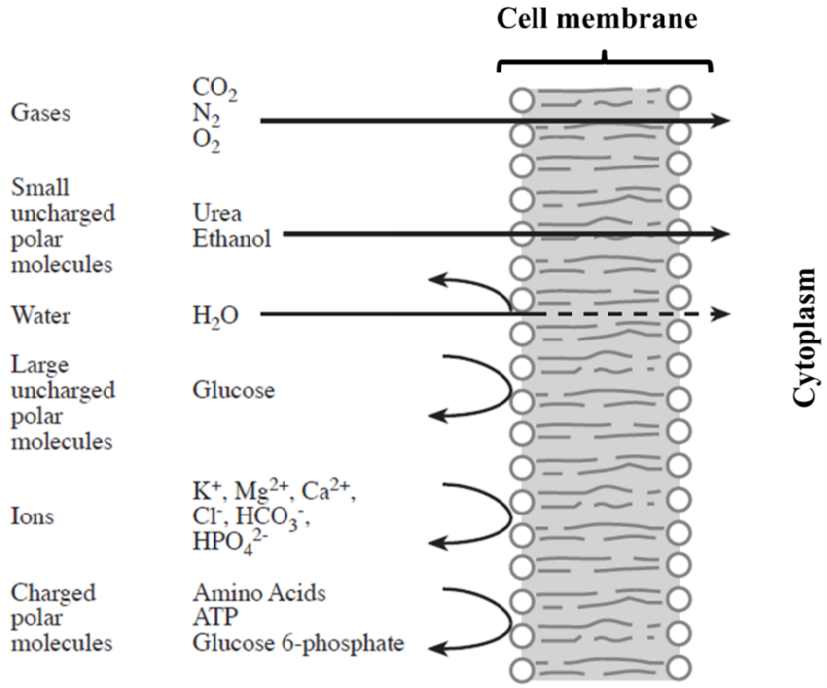


Figure 3.1: Charged or polarizable molecules exchange from cell membrane [112].

Gases and small uncharged molecules can be transported inside the cell without using energy. However, large uncharged or charged molecules and ions transportation needs energy. In addition, their transportation needs some protein gates (Fig 3.2).

Biological cell membrane works like a shield for cells to protect them from the environmental damages and it enables semi-permeability to the cell, by letting some molecules inside while leaving the others out. It is composed of two unbroken hydrophilic phospholipid shields with their hydrophobic fatty acid tails and membrane proteins inside this structure. The thickness of cell membrane is between 5 to 10 nm [113](Fig.3.2).

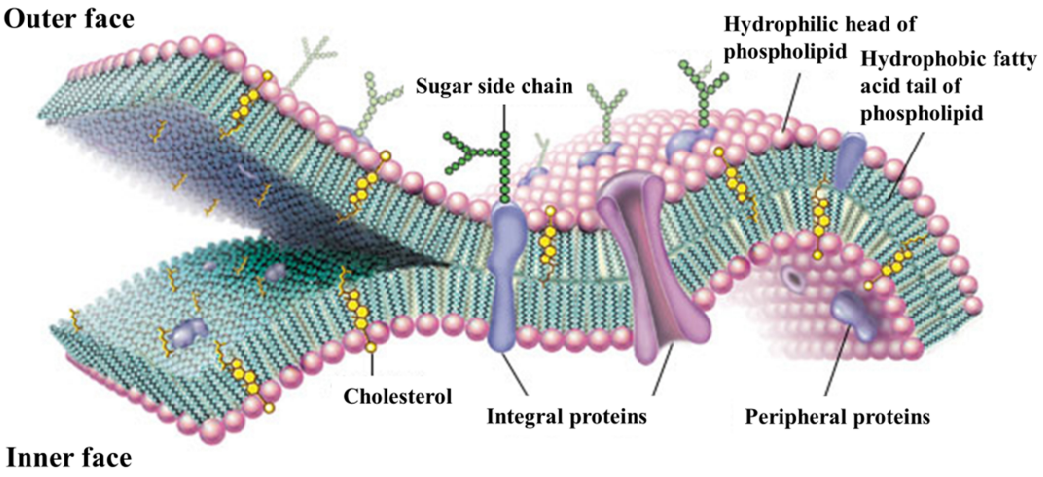


Figure 3.2: Biological cell membrane structure (Encyclopedia Britannica, Inc., 2007).

This membrane acts like a capacitor parallel with a resistor since two phospholipid layers are conductive and a dielectric structure is placed between them. Impedance of the cell membrane is calculated utilizing the following formulas for its resistance and capacitance, respectively.

$$R = \frac{L}{\sigma A} \tag{12}$$

$$C = \varepsilon \frac{A}{d} \tag{13}$$

In equation 12 and 13, R and C describe the resistance and capacitance, respectively. σ and ε is used for conductivity and permittivity, and L and A stand for perimeter and crossectional area, respectively. d is the thickness of cell membrane for this case. L is calculated as 2*π*r and A is calculated as $\pi*r^2$. After the necessary cancellation, L/A becomes 2/r (r is the radius of the cell).

The cytoplasm of biological cells is composed of cytosol and organelles (only for eukaryotic cells). Cytosol consists of mostly water besides protein, ions, fatty acids, etc. Because of ions, cytoplasm is much more conductive than the cell membrane. Moreover, it can be modeled with its impedance like the cell membrane.

Figure 3.3 shows the modeled biological cell inside a medium, utilizing general analogy between them and electrical circuit.

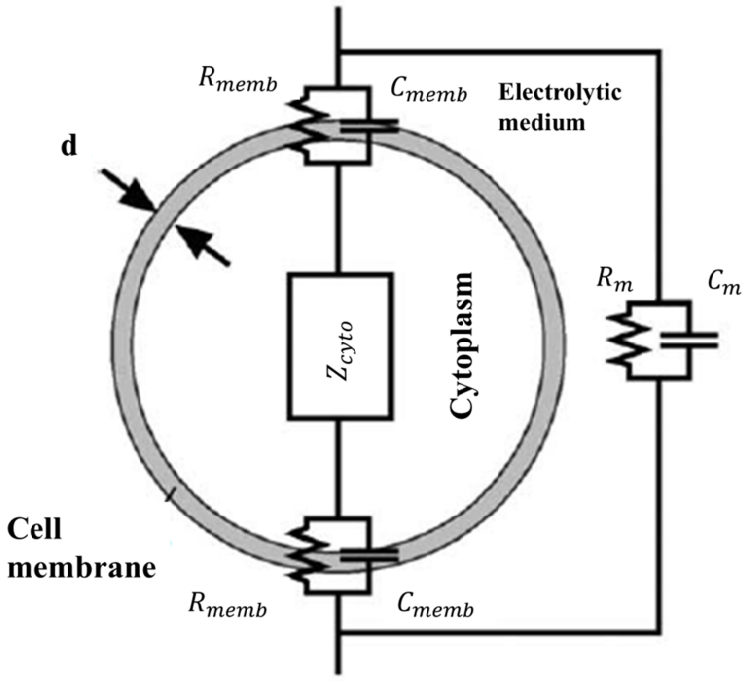


Figure 3.3: The analogy between biological cell and suspending medium, and electrical circuit [12].

The electrical parameters, such as R_{memb}, C_{memb}, Z_{cyto} (R_{cyto}, C_{cyto}), can be determined with electrorotation method, where peak rotational rate of a cell is measured under uniformly rotating electric field at varying medium conductivities and electric field frequences to obtain a linear formulation as a function of frequency, cell radius and medium conductivity, which is utilized to estimate cell dielectric properties [12].

As cells vary in their molecular content, these electrical properties provide a kind of cell-specific characteristics that can be utilized as a selective feature in cell identification, manipulation, or separation by DEP. For example, Flanagan et al. reported that even the dielectric properties of different progenies of stem cells are different and their destiny can be known with dielectrophoretic trapping before they differentiate [83].

3.2. Cell Dielectric Modeling Techniques

Cells can be modeled as electrical circuit elements as it is seen in figure 3.3. However, to use those parameters in DEP system design, they should be converted into a single complex permittivity for membrane and cytoplasm.

To achieve this conversion, some models have been developed. Biological cells are generally modeled with spherical or ellipsoidal models. However, they can have other geometries. The exact modeling of the cell geometry is not achievable due to some

mathematical challenges. Although more realistic techniques have been actualized, the assumptions made in the spherical or ellipsoidal modeling do not cause significant errors for most of the cells. Besides, biological particles are not homogenous because of their cell membrane, cytoplasm, and nucleus structures. Therefore, cell modeling techniques are generally based on the shell number around the cell, such as single or double shell modeling. In these modeling techniques, effective complex permittivity (Eq. 14 for spherical cell with single shell) is utilized instead of ε_p^* in F_{CM} expression (Eq. 2) [114].

$$\varepsilon_{eff,p}^* = \varepsilon_{memb}^* \left\{ \frac{[(r+d)/r]^3 + 2\left[(\varepsilon_{cyto}^* - \varepsilon_{memb}^*)/\varepsilon_{cyto}^* + 2\varepsilon_{memb}^*\right]}{[(r+d)/r]^3 - \left[(\varepsilon_{cyto}^* - \varepsilon_{memb}^*)/\varepsilon_{cyto}^* + 2\varepsilon_{memb}^*\right]} \right\} \quad (14)$$

In this equation, ε_{memb}^* and ε_{cyto}^* stand for membrane and cytoplasm complex permittivities, respectively. According to equation 3, they have conductivity, permittivity and frequency information inside them.

3.3. Dielectric Modeling of Yeast Cells

Yeast cells have both cell membrane and cell wall unlike mammalian cells. Therefore, they should be modeled with triple shell cell modeling. In this modeling, equation 14 is utilized twice. In first usage of the equation 14, ε_{memb}^* and ε_{cyto}^* are used for membrane and cytoplasm complex permittivities and an effective complex permittivity is obtained. In second usage, obtained effective complex permittivity is used instead of ε_{cyto}^* and ε_{wall}^* is used instead of ε_{memb}^*. Next, finally obtained effective complex permittivity is used as the particle complex permittivity in the expression of F_{CM} (Eq. 2).

Viable and nonviable cells dielectric properties are different (Table 2.1) and their radius are similar, 4 μm for viable yeasts and 3.5 μm for nonviable ones. Figure 3.4 shows the $Re(F_{CM})$ characteristics of these cells in a medium with 3 mS/m conductivity and 78 permittivity coefficient. MATLAB is used for this analysis and code is available in Appendix A.

Table 3.1: The dielectric properties of viable and nonviable yeast cells [114].

	viable	**nonviable**
σ_{wall}**(S/m)**	0.014	0.0015
σ_{memb}**(S/m)**	2.5×10^{-7}	1.6×10^{-4}
σ_{cyto}**(S/m)**	0.2	0.007
ε_{wall}	60	60
ε_{memb}	6	6
ε_{cyto}	50	50
t_{memb}	8 nm	8 nm
t_{wall}	0.22 μm	0.25 μm

According to this simulation, crossover frequency of nonviable yeast cells is 1.45 MHz and at that frequency, viable yeast cells can be pulled/ manipulated through pDEP force while nonviable ones observe zero DEP force.

Viable and nonviable yeast cells were used in the 1st generation devices for the proof of DEP concept. Tests were made at the f_{cross} (1.45 MHz) of nonviable cells.

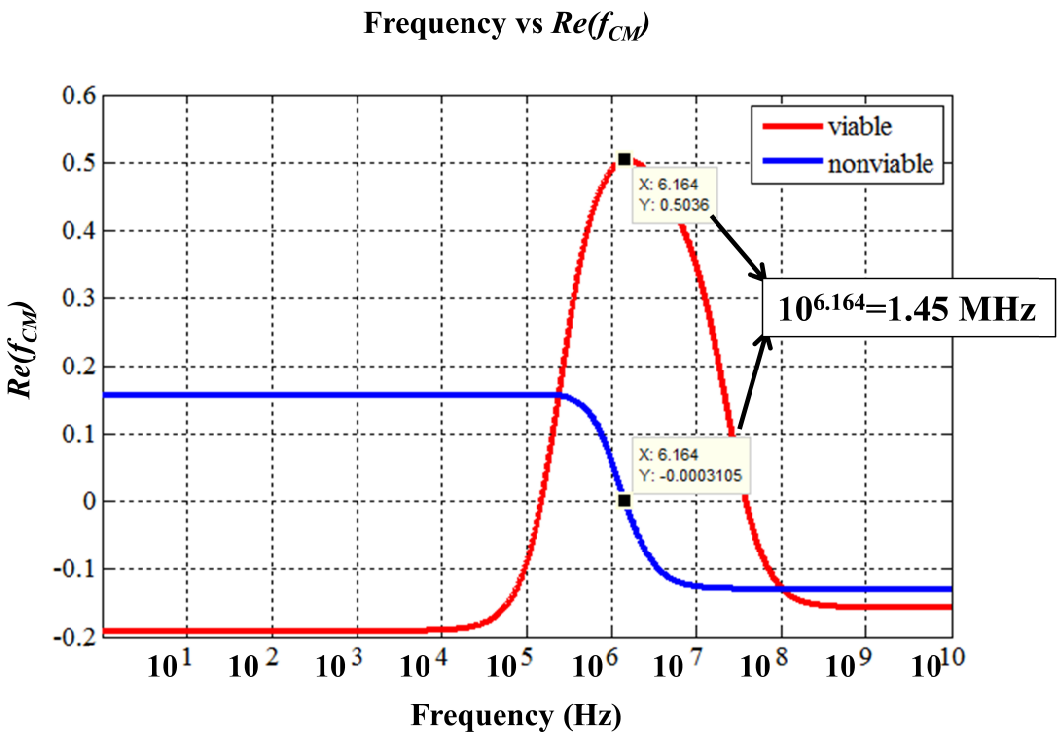


Figure 3.4: $Re(F_{CM})$ vs. frequency graphs of viable and nonviable yeast cells in a medium with 2.5 mS/m conductivity and 78 permittivity coefficient [115].

3.4. Dielectric Modeling of K562 (Human Chronic Myeloid Leukemia (CML)) cancer cells

Because of biological cells' dynamics, the expression level of the proteins embedded in the cell membrane can vary. These proteins can be utilized for the transportation of molecules (Fig. 3.1 & 3.2). When they are overexpressed, the number of molecules transported may increase, or vice versa. Therefore, cells can differentiate from their progenies.

As it is explained in detail in Chapter 1, cytoplasmic conductivity of P-gp related MDR cells is different than the sensitive ones since P-gp is a Cl^- channel and overexpression of it affects the cytoplasmic ion level [105].

Labeed et al. [97] reported the dielectric properties of 100 nM doxorubicin resistant (K562/dox100) and sensitive K562 cells as in the table 2.2. According to this table, cytoplasmic conductivity of doxorubicin resistant K562 cells is 2.17 times greater than that of sensitive ones.

Table 3.2: Dielectric properties of K562 and K562/100dox [97]. * is used to mark average values.

	σ_{cyto}(S/m)	ε_{cyto}	σ_{memb}(S/m)	ε_{memb}
K562	0.23 (0.22-0.24)*	40	1.8×10^{-6}	8
K562/dox100	0.5 (0.48-0.52)*	40	2×10^{-6}	9

In this study, the values in table 2.2 are used for the modeling of K562 sensitive and K562/dox100 cells. These dielectric properties are also utilized in the modeling of 200 nM imatinib resistant K562 cells (K562/ima200) since there is no information about their dielectric properties. While utilizing these data for imatinib resistant K562 cells, it was assumed that the error is not in considerable amount because imatinib resistance is caused by P-gp overexpression. This means that the reason behind the resistance is the same in both doxorubicin and imatinib resistant cells.

Moreover, to model the cells with double shell cell modeling, membrane thickness and cell radius are needed. Throughout this study, cell membrane thickness is assumed as 10nm [116] and the radius of the cells were measured as 7-8 μm. While measuring the cell radius, 10 μm polystyrene beads were used as reference, and the cell radius were estimated using a pixel counting software.

Utilizing the equations 2 and 14, frequency dependent $Re(F_{CM})$ characteristics of K562 and K562/dox100 cells was obtained through MATLAB (code is available in Appendix A). Figure 3.5 shows the $Re(F_{CM})$ characteristics of these cells in a medium with 2.5 mS/m conductivity and 78 permittivity coefficient. This medium was used for all cancer cells tests in this study since the dielectric properties of doxorubicin resistant and sensitive K562 cells were measured and reported in this medium according to literature. The analyses of $Re(F_{CM})$ characteristics of doxorubicin resistant K562 cells were performed with in different conductivity (0.25, 2.5 and 25 mS/m) media (Appendix B). Figure B.1 in appendix B shows that at high frequencies (>10 MHz), $Re(F_{CM})$ characteristics does not change considerably as expected. Moreover, the analyses of $Re(F_{CM})$ characteristics for both doxorubicin resistant and sensitive K562 cells in media with different conductivities (25 mS/m and 0.25 mS/m, appendix B, figure B.2 and B.3, respectively) were performed. According to these analyses, while crossover frequency of sensitive K562 cells changes, $Re(F_{CM})$ values of doxorubicin resistant ones does not change considerably at that crossover frequencies.

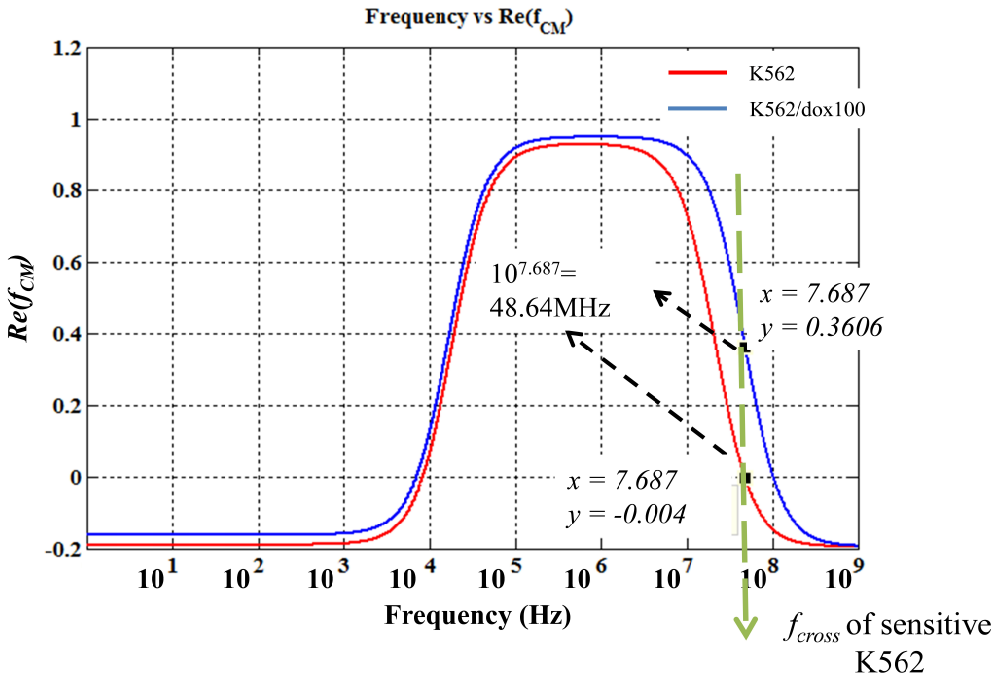


Figure 3.5: *Re(F_{CM})* vs. frequency graphs of K562 & K562/dox 100 cells in a medium with 2.5 mS/m conductivity and 78 permittivity coefficient [105].

According to this simulation, crossover frequency of K562 sensitive cells is 48.64 MHz and at that frequency, K562/dox100 cells can be pulled/ manipulated through pDEP force while K562 sensitive cell observe zero DEP force.

The aim of this study is the detection of doxorubicin and imatinib resistance in K562 leukemia cells, using a custom-designed, MEMS-based dielectrophoretic cell-trapping device. In the analysis of dielectrophoretic response, the same frequency was utilized for both doxorubicin and imatinib resistant K562 cells. Moreover, the effect of degree of drug (doxorubicin) resistance on dielectrophoretic response of K562 cells is also investigated. For this, the dielectrophoretic response of 300 nM and 500 nM K562/dox cells were analyzed at the same frequency. Due to variation in P-gp expression levels, and hence, the cytoplasmic conductivity, dielectrophoretic response of these cells is expected to be different, under the same experimental conditions.

CHAPTER 4

DESIGN AND SIMULATION

In this chapter, the designs of the dielectrophoresis devices, achieved in this study, are presented. First, the design of the 1st generation devices, used for the proof of concept, is given. Next, 2nd generation devices design is explained. The modifications in the design of 1st generation devices to form the 2nd generation devices with reasons are also discussed in detail. Finally, the finite element simulations of these designs are demonstrated with the detailed explanation of simulation method in COMSOL software.

4.1. Design of the DEP Devices

In order to design a DEP device, three main points should be considered: 1) The aim of the DEP device (e.g., separation, trapping, concentration, focusing, etc.), 2) Electrode structure (e.g., interdigitated, quadruple, 3D, etc.) and operating strategy (e.g., continuous flow, batch, etc.), 3) Design parameters (flow rate, channel dimensions, voltage and frequency of applied electric field, electrode size, etc.). As it is explained in chapter 2, various electrode structures and operating strategies are utilized in DEP, based on the application. For example, for continuous flow analysis, quadruple electrodes cannot be used, or, for label free detections, immuno-assisted DEP operating strategy cannot be preferable. Therefore, the aim of the DEP device should be well-defined before starting the selection of electrode type and operating strategy. Next, electrode type and operating strategy with specific design parameters should be determined. For example, in FFF DEP strategy, the depth of the channel is the most important parameter since cells are levitated in the channel and the length of channel depth should be high enough for separation of cells with DEP.

4.1.1. The Design of 1st Generation DEP Devices

The aim of the 1st generation DEP devices is to make proof of DEP concept utilizing viability test for yeast cells. Viable and nonviable yeast cells have nearly the same radius. Therefore, this design should be suitable to achieve separation based only on the differences in dielectric properties. In addition, separation should be realized under continuous flow conditions. Therefore, side-wall electrodes were used with the combination of extruded electrode type to provide uniform DEP force along channel depth, which increases the separation efficiency. Contactless DEP strategy, which prevents Joule heating and cell damaging, was also utilized by coating the electrodes with a thin layer of insulating polymer, parylene. As the operating strategy, multi-step was chosen, in which particle trapping and releasing are utilized in an order. The f_{cross} of nonviable cells was chosen as the electric field frequency since at that frequency, viable cells are pulled by pDEP while nonviable ones are drifted out of the channel by continuous fluid flow. Moreover, two inlets in side channel type to provide pressure driven focusing of the cells into DEP area and two outlets in T-shaped to obtain better control on flow were chosen. Figure 4.1 illustrates the physical structure of proposed device. In this design, pressure driven flow of buffer medium from the side-channel provides the focusing of all cells into

the DEP area, formed in the side of long electrode. At the f_{cross} of nonviable yeasts, viable yeasts are pulled towards the short electrodes. Sectional 3D short electrodes were utilized to increase the effect of DEP force throughout DEP area.

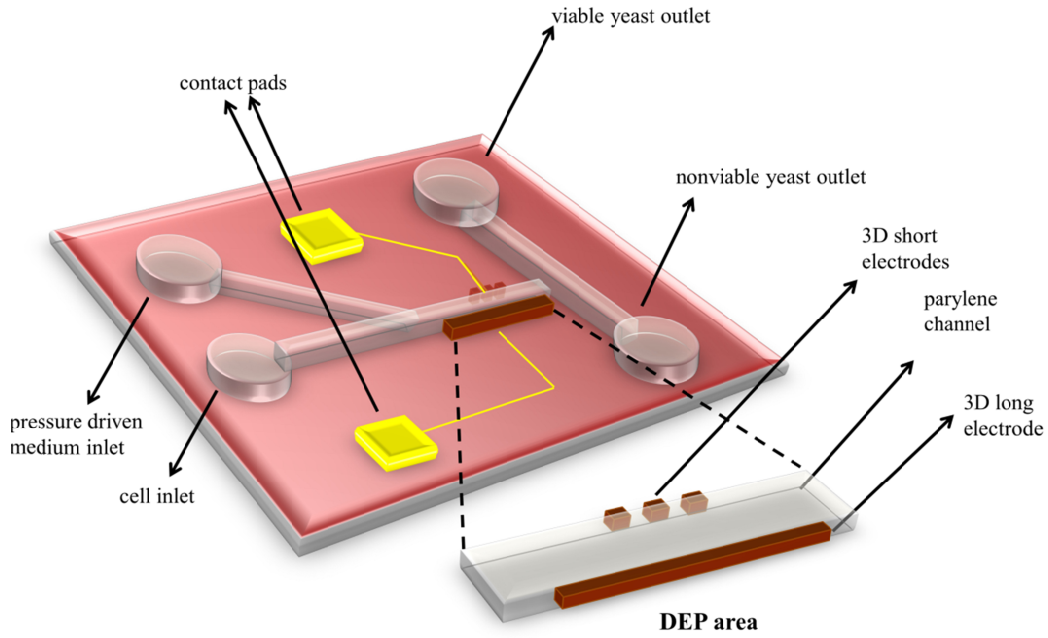


Figure 4.1: The illustration of the 1st generation DEP devices, with an enlarged view of DEP area.

According to these decisions, the design parameters, namely, the electrodes shape, width and height; channel depth, width and length; insulating parylene layer thickness; and magnitude and frequency of the voltage were determined.

Electrode shapes were chosen as rectangular for the ease of fabrication. One long electrode and three short electrodes were utilized to provide nonuniform electric field in both channel length and width. Analytical calculation of nonuniform electric field in these structures is problematic and has considerably low accuracy. Therefore, to decide those parameters, iterations should be utilized with simulations. Long electrode length was kept constant at 1000 µm to provide large but microscale DEP area. Short electrode's length was determined as 40 µm after lots of iteration with the consistency of simulations. The gap between short electrodes was chosen as 20 µm taking care of the limits of Cu electroplating, used to fabricate 3D electrode structure. Channel depth was chosen as 20 µm considering the size of the cells and Cu-electroplating limits. Channel depth and electrode height have almost the same size, since, DEP force should be uniform along channel depth. The optimum channel width was chosen as 75 µm, at which highest possible flow rate could be achieved without compromising the necessary DEP force. Since, flow rate is directly proportional with the cross-sectional area (width x height) of the channel and DEP force is inversely proportional with the gap between electrodes through channel width.

A particle should follow nearly 250 μm inside the microchannel before entering into DEP area to reach steady state velocity. This value is specific to this design and calculated with the MATLAB. Therefore, the length of channel inlet should be at least 300 μm to be on the safe side. However, because of fluidic connections and inlet reservoirs, inlet and outlet dimensions were determined with the physical connectors, such as nanoports which have almost 5 mm radius. The total size of the device is 1.5 x 1.8 cm.

Insulation parylene thickness was determined as the minimum parylene thickness, ~0.3 μm that can be coated in METU-MEMS Center facilities, in order not to affect the electric field strength, significantly.

The magnitude of the voltage was determined iteratively within 10 - 16V_{pp} interval, through simulations. The frequency of the voltage was chosen as the f_{cross} of nonviable yeasts, which is 1.45 MHz according to cell dielectric modeling.

Table 4.1 shows all related parameters, utilized in the design of 1st generation devices.

Table 4.1: Design parameters utilized for the 1st generation devices.

Parameters	Values
Short electrode width (μm)	40
Short electrode height (μm)	15-20
Long electrode width (μm)	1000
Long electrode height (μm)	15-20
Channel width (μm)	75
Channel depth (μm)	20-22
Insulating parylene thickness (μm)	0.3
Voltage magnitude (V_{pp})	10-16
Voltage frequency (MHz)	1.45

4.1.2. The Design of 2nd Generation DEP Devices

The aim of 2nd generation DEP devices is to provide the detection of doxorubicin and imatinib resistance in K562 leukemia cells. Like viable and nonviable yeast cells, resistant and sensitive K562 cells have almost the same radius. Therefore, dielectric property based separation under continuous flow conditions should be achieved. For this purposes, side-wall patterned, sectional 3D-electrode arrays were chosen.

After testing of the 1st generation devices, it was concluded that the use of two different external pressure actuation devices (a pressure controller and a syringe pump) complicates the operation, due to different steady state times and difficulty in simultaneous control of the both. In the 2nd generation device, this difficulty was overcome by using V-shaped parylene obstacles inside the channel for hydrodynamic focusing of the cells to DEP area. This design eliminated the need for the second inlet, used for pressure driven flow for cell focusing. Moreover, a single outlet was used, as the main purpose is the trapping of resistant K562 cells at the f_{cross} of sensitive K562 cells. Figure 4.2 illustrates the structure of the 2nd generation device.

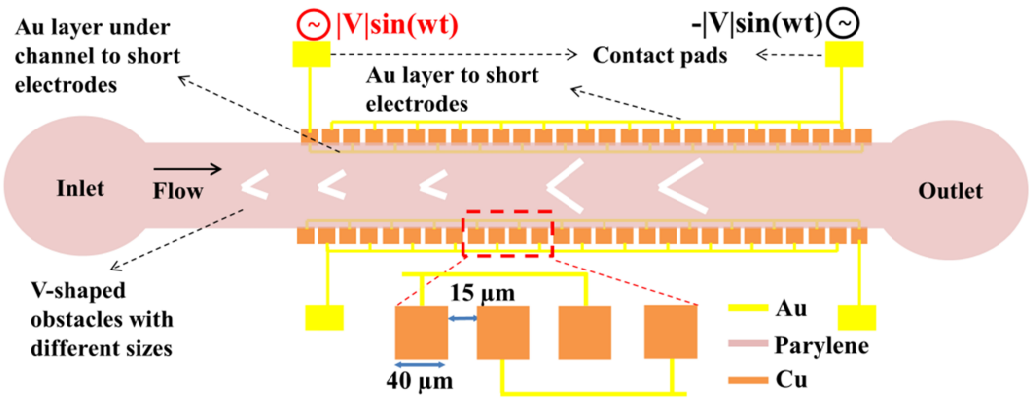


Figure 4.2: Illustration of the 2nd generation device structure.

According to these decisions, the design parameters, namely, the electrode number, width and height; the gap between electrodes; channel depth, width and length; insulating parylene thickness; the number and dimensions of V-shaped obstacles; magnitude and frequency of the voltage; and the parylene thickness used to prevent parasitic capacitances, were determined.

Electrode shapes were chosen as rectangular like in the 1st generation. Electrode width was chosen the same with the previous design as 40 µm since it worked in the proof of concept tests. In the previous design, the gap between short electrodes was 20 µm due to fabrication limits. In this design, with an addition of a new mask to fabrication, electrode gaps could be decreased to 15 µm, which increases the DEP force, as it is inversely proportional to the distance between electrodes. The total length of the DEP area is fixed to 1500 µm, containing 27 sectional electrodes. Electrode height is chosen as 25-30 µm since the average cancer cell's diameter is15 µm.

In this design, a larger channel width (300 µm) was utilized to obtain a higher flow rate, which is significant in analyzing higher sample volumes in a shorter period of time. It is four times greater than the 1st generation devices. Therefore, DEP force along channel width decreases sharply. However, in this design, two symmetrical electrode arrays were used reciprocally and DEP force between them was not utilized. Channel depth was determined as 30 µm according to electrode height to provide uniform DEP force along channel depth.

The total length of the channel was 1.6 cm, with only an inlet nanoport. No nanoport was used in the outlet, for the ease of testing.

The thickness of insulating parylene layer was chosen as 0.3 µm as in the 1st generation devices. Another parylene layer was also utilized in this design to prevent the parasitic capacitances between Au layer under the channel (used for contacts) and 3D-electrodes. Its thickness was determined as 5 µm with COMSOL simulations.

Five V-shaped obstacles were used to direct all cells to DEP area. These V-shaped obstacles were rotated 90° right and their center passed from the device center to obtain better control on flow. The degree between its arms was determined as 90° for the same reason.

The half-length of the channel width is 150 µm and cell diameter is 15 µm, on the average. The length between the tip of the arms of the 1st and 2nd obstacles and the channel wall was chosen as 60 µm, providing the passage of four cells without clogging. This is because the trapping starts at the first two obstacles where the cell concentration is high. After the first two obstacles, cell concentration decreases due to trapping. Therefore, the length between arm tips and channel wall was decreased to 50 µm to increase hydrodynamic leading force on cells. As a result, the arm lengths of V-shaped obstacles became different (1st-120 µm, 2nd-120 µm, 3rd-140 µm, 4th -140 µm, 5th -140 µm). The length between obstacles was chosen according to the simulations and iterations since for particle velocity and hydrodynamic focusing, numerical solutions, coupling the equations of microfluidic and DEP forces, should be utilized. Figure 4.3 shows lengths mentioned above.

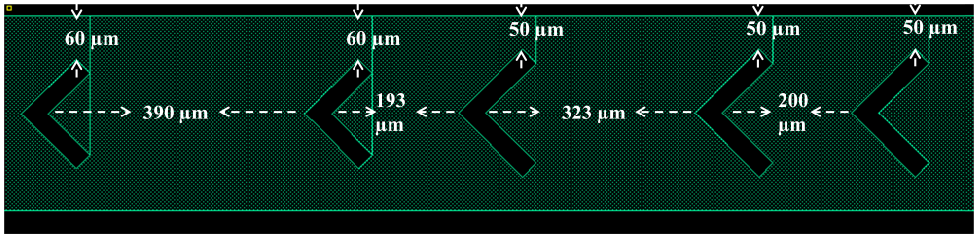


Figure 4.3: The dimensions of V-shaped obstacles.

The trapping efficiency changes with the magnitude of the applied voltage. According to the simulations, the device is expected to work at voltages as low as 1 V_{pp}. Frequency of the voltage is chosen as 48.64 MHz, the f_{cross} of sensitive K562 cells found through dielectric cell modeling.

Table 4.2 shows all related parameters, utilized in the design of 2nd generation devices.

Table 4.2: Design parameters utilized for the 2nd generation device.

Parameters	**Values**
Electrode width (µm)	40
Electrode height (µm)	20-25
Electrode number in one array	27
The gap between electrodes (µm)	15
Channel width (µm)	300
Channel depth (µm)	30
Insulating parylene thickness (µm)	0.3
(Parasitic capacitance) parylene thickness (µm)	5
Voltage magnitude (V_{pp})	>1
Voltage frequency (MHz)	48.64
The number of V-shaped obstacles	5

4.2. Simulation Method

Before starting to simulations, device structure is exported from CADENCE, the software used for mask plotting for micro fabrication, as *.gds* file. Then, this file is imported to COMSOL. Therefore, simulated structures are exactly the same with the fabricated ones.

In both designs, 3D-electrodes were used to provide a uniform DEP force along the channel depth. Therefore, first, the uniformity of DEP force through channel depth should be proved with the simulations even it was proven in [117]. In DEP equation, all parameters are constant except for the gradient of electric field square term (∇E^2), which changes with the position information. Hence, the uniformity of this term through channel depth was shown to prove the DEP force uniformity in the same direction. To achieve this simulation, Equation 15 was utilized, where V is the voltage.

$$\nabla E^2 = \left| \begin{array}{l} \left(\frac{\partial^3}{\partial x^3} + \frac{\partial^3}{\partial y^2 \partial x} + \frac{\partial^3}{\partial z^2 \partial x}\right)\hat{x} \\ \left(\frac{\partial^3}{\partial y^3} + \frac{\partial^3}{\partial x^2 \partial y} + \frac{\partial^3}{\partial z^2 \partial y}\right)\hat{y} \\ \left(\frac{\partial^3}{\partial z^3} + \frac{\partial^3}{\partial x^2 \partial z} + \frac{\partial^3}{\partial y^2 \partial z}\right)\hat{z} \end{array} \right| * V^2 \qquad (15)$$

While converting this equation to COMSOL language, Vx stands for the derivative of voltage in terms of x and Vxx is used for the 2nd derivative of V in terms of x. Moreover, Vxy means the 1st derivative of voltage in terms of x and 2nd derivative in terms of y. Following this notation, "***sqrt(((2*(Vx*Vxx+Vy*Vyx+Vz*Vzx))^2) +((2*(Vx*Vxy+Vy*Vyy+Vz*Vzy))^2)+((2*(Vx*Vxz+Vy*Vyz+Vz*Vzz))^2))***" expression was obtained. 3D-electrode simulation was utilized for only 1st generation design since it is same for the 2nd generation. Figure 4.4 shows the 3D simulation of ∇E^2 term.

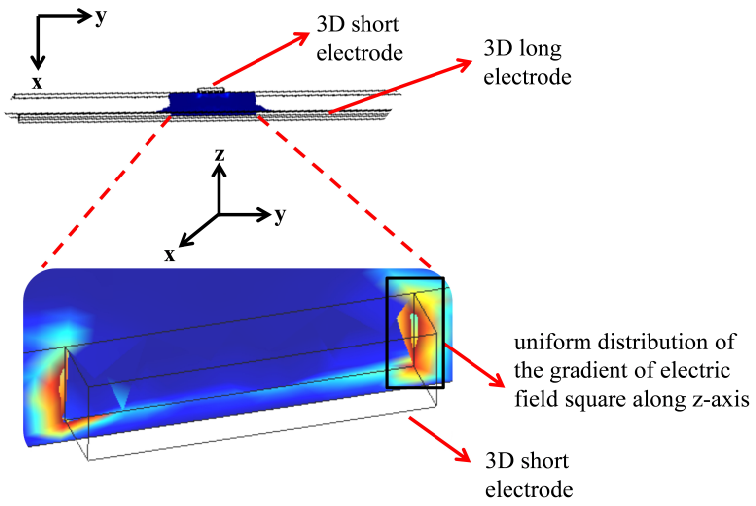


Figure 4.4: 3D simulation of the gradient of electric field square.

After obtaining these simulation results for uniformity of DEP force, all simulations were made in 2D.

First, it should be shown that the gradient of electric field square is greater than 10^{12} (kg^2m/s^6A^2), necessary for the manipulation of biological cells [118]. Therefore, the electric field was simulated in 2D utilizing the following expression: ***sqrt(((2*(Vx*Vxx+Vy*Vyx))^2)+((2*(Vx*Vxy+Vy*Vyy))^2)).*** As it is seen in this expression, only the voltage change in x and y directions were taken into account.
Voltage is sinusoidal since frequency creates differences in the DEP responses of biological cells. Therefore, electric field simulations should be solved time dependently. Time dependent simulation has three different parameters (Fig. 4.5). Relative tolerance and absolute tolerance were not changed in this study but *times* is the key parameter for those simulations. This parameter shows the starting and ending time of simulation with time step. Starting and ending times are determined by frequency of the simulation. Time step changes according to the required resolution. Therefore, for different designs and biological cells, these parameters should be changed.

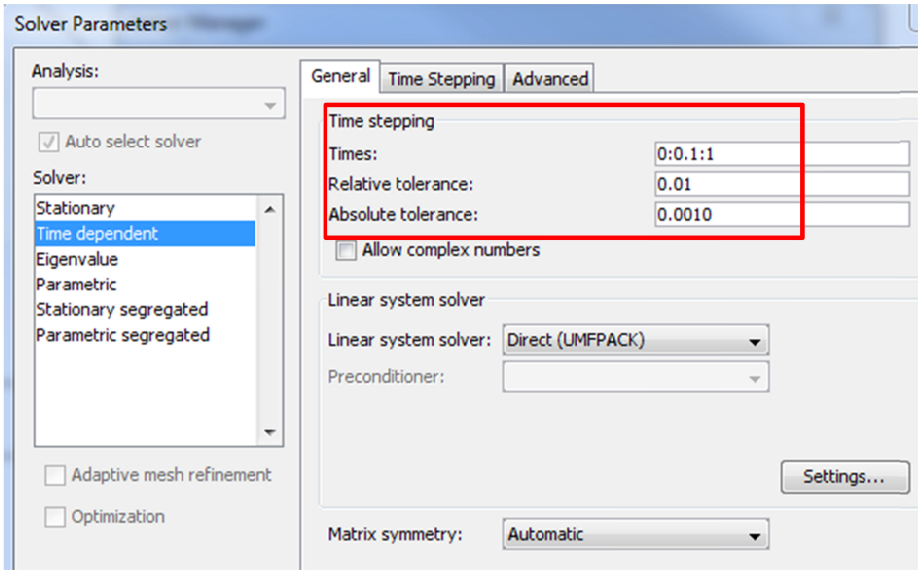


Figure 4.5: Key paramters in time dependent simulations of COMSOL

After time dependent solution is completed, solutions should be stored to provide the stationary analysis of particle trace at determined time. For this purpose, store solution is chosen in solver manager.

Sinusoidal voltage becomes zero for each half of its period and it reaches maximum value twice through its period. Therefore, DEP force changes in the period of sinusoidal voltage and it becomes zero for each half of its period. However, in this study, very high frequencies were used like 1.45 MHz and 48.64 MHz. Therefore, the time between each maximum (344 ns and 10.3 ns) is much lower than the average duration (49 ms) of cell remaining in DEP area. As a result, particle tracing simulations were achieved with stationary solutions at time where maximum voltage occurs.

Particle tracing simulations were achieved with the solution of *Independent Navier-Stokes* equations numerically in COMSOL. The stationary solution of these equations is enough for the simulations of both designs. While solving these equations, particle velocity equation (Eq. 10) was utilized for x and y direction, in COMSOL language as follows: (x direction) ***u+((constant)*(2*(Vx*Vxx+Vy*Vyx)))*** and (y direction) ***v+((constant)*(2*(Vx*Vxy+Vy*Vyy))),*** where u and v are the medium velocity in x and y directions, respectively, and ***constant*** stands for the following in these expressions:

$$constant = \frac{\varepsilon_m}{\mu}\frac{r^2}{3}\,Re(F_{CM}) \qquad (16)$$

As it is seen in above equation, constant is dependent to the medium and particle dielectric properties, and medium viscosity (8.92 x 10^{-4} kg/m.s was utilized for all simulations in this study).

u and ***v*** are calculated by COMSOL with numerical solutions. However, the starting velocities are chosen by designer using boundary settings. While selecting these velocities, one should take into account the losses due to tubing used in testing. For this purpose, laminar inflow is chosen as boundary condition in boundary settings (Fig. 4.6). By means of laminar inflow choice, entrance length (L_{entr}), used by tubing, can be chosen as a simulation parameter. It was 15 cm in this study for all designs. Average velocity is the needed velocity for syringe pump adjustments in tests.

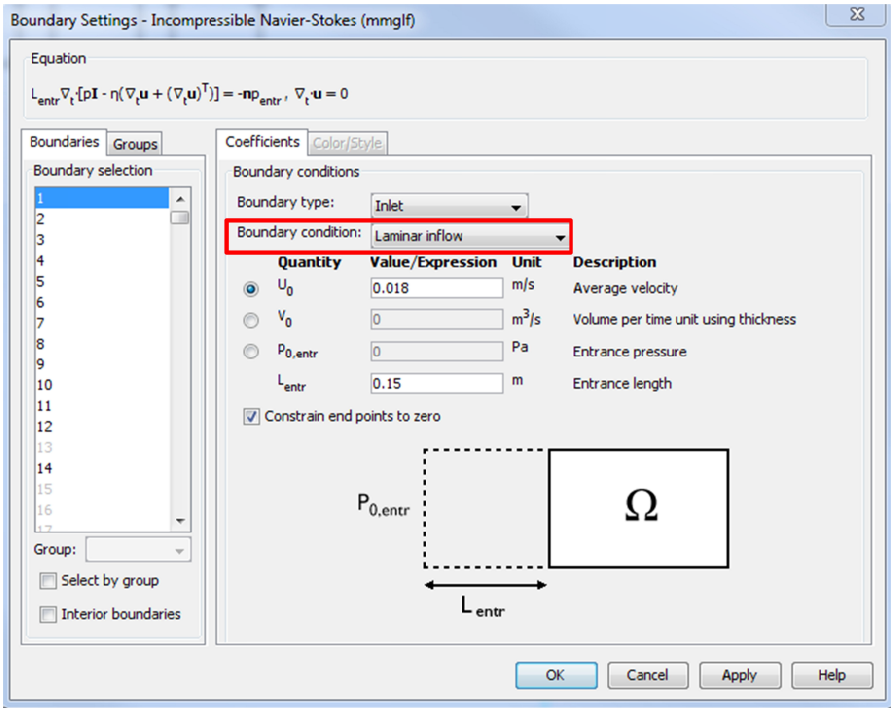


Figure 4.6: Key parameters for particle tracing simulatins in COMSOL

General simulation method, explained above in detail, is as follows:

1. The gradient of electric field square is simulated in 2D time dependently and should be $>10^{12}$ kg^2m/s^6A^2.
2. Results of the simulations in step 1 are stored.
3. Constant is determined according to cell and medium properties.
4. Stationary simulations of particle velocity are made at a time where maximum voltage occurs with taking care of pressure losses in tubing, used in tests.

4.2.1. Simulations of 1st Generation DEP Devices

Following the steps of general simulation method, first, 2D electric field simulation of the 1st generation devices was made. Figure 4.7 shows that the gradient of electric field square along channel width and length in DEP area is greater than 10^{12} kg^2m/s^6A^2 at 16 V_{pp}.

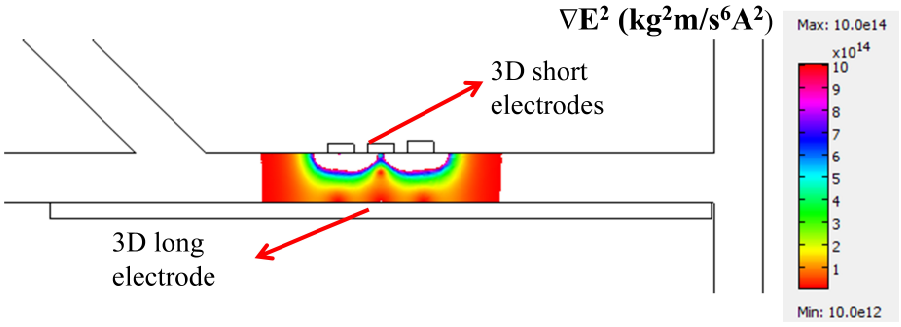


Figure 4.7: The gradient of electric field square for 1st generation design.

For this design, the frequency was 1.45 MHz. Therefore, ending time was chosen as 0.69 µs and time step was one fourth of it (0.17 µs). Solutions were stored and for stationary simulation 0.17 µs solution was chosen as 2nd step. Then, constants (Eq. 15) were determined as 5.29 x 10^{-20} (Fm^2s/kg) x $Re(f_{CM})$ and 4.05 x 10^{-20} (Fm^2s/kg) x $Re(f_{CM})$ for viable and nonviable yeasts, respectively. However, according to dielectric modeling of nonviable yeasts, their $Re(f_{CM})$ value is almost zero at 1.45 MHz. Therefore, they cannot be pulled into short electrodes and they flow with medium velocity (***u*** and ***v***). Finally, particle tracing simulations were achieved as step 4. By using streamline tool in postprocessing of COMSOL, particle path in the channel was visualized (Fig. 4.8).

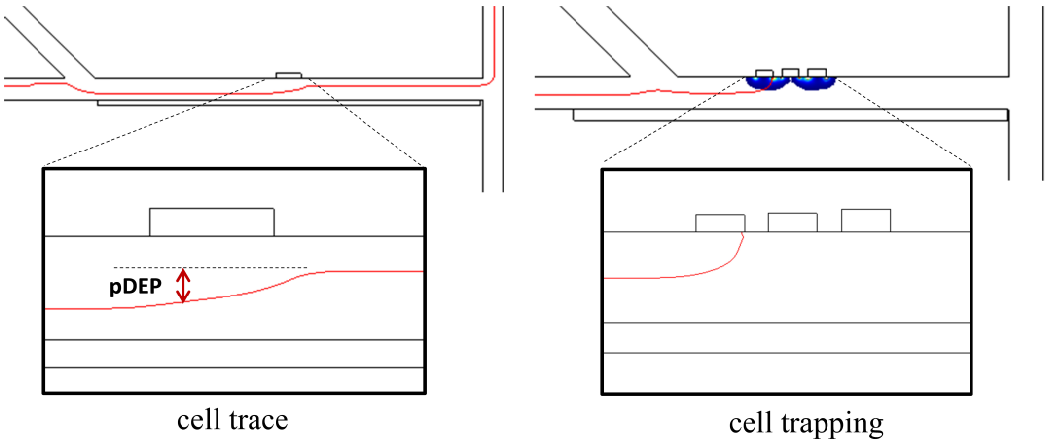


Figure 4.8: Yeast cells path in 1st generation devices. In the left figure, voltage is not enough to trap the cell on electrode but it still affects the cell by pulling it to short electrode. In the right figure, voltage is high enough to trap the cell.

According to this simulation, viable yeast cells can be pulled by pDEP in DEP area. However, if the distance between cell and short electrode is increased, DEP force becomes smaller. Therefore, cell trapping cannot be achieved when they move away from short electrodes. On the other hand, when separation of cells is needed, trapping should be avoided. While designing the 1st generation device, the main aim was the proof of DEP concept with separation of biological cells. However, because of experimental problems, the aim of this design was converted into proof of DEP concept with trapping of biological cells.

The side channel was going to be used as the inlet of pressure driven fluid (as explained in design part of this chapter). The selection of the pressure magnitude was one of the key parameters of this design, together with the selection of cell velocity. These parameters were determined, but devices were tested under capillary flow conditions only, due to problems in experimental setup. Trapping of viable yeast cells could be achieved under capillary flow at the f_{cross} of nonviable yeasts. Therefore, parameters, related with pressure and velocity, are not given in this thesis to prevent confusion of concepts.

Moreover, when cells are trapped in DEP area, they should be lined up on electric field lines, if short and long electrodes are used reciprocally. Therefore, electric field line simulation was also achieved as it is seen in Figure 4.9. According to this simulation, yeasts should form a line when they are trapped between short and long electrodes. Moreover, if yeasts are trapped at tip of short electrodes they should form an angle with channel walls.

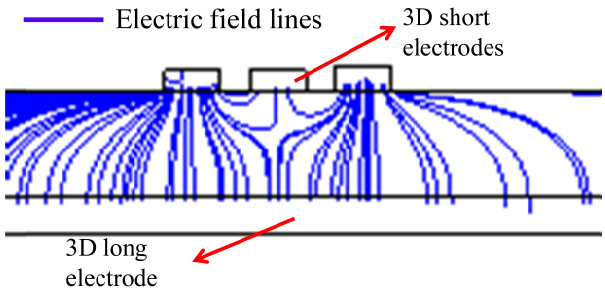


Figure 4.9: Electric field line simulations in DEP area of 1st generation dev ices.

4.2.2. Simulations of 2nd Generation DEP Devices

As in the case of 1st generation devices' simulations, general simulation steps were followed. Firstly, the gradient of electric field square simulation was made (Fig. 4.10). It provides the necessary magnitude. To increase the electric field magnitude, a voltage was applied to consecutive electrodes with 180° phase difference in testing and simulation of this design. The frequency of this design is the f_{cross} of sensitive K562 cells (48.64 MHz). Therefore, ending time of time dependent solution was chosen as 20.5 ns and time step was 5.14 ns.

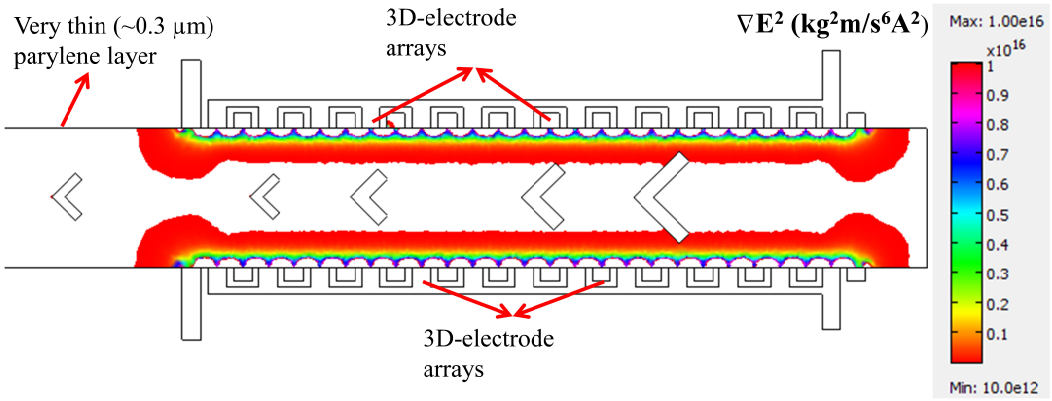


Figure 4.10: The gradient of electric field square for 2nd generation design.

Solutions were stored and for stationary simulation the solution at 5.14 ns was chosen as 2nd step. Then, constants (Eq. 15) were determined as 17.62 x 10^{-20} (Fm^2s/kg) x $Re(f_{CM})$ and 16.2 x 10^{-20} (Fm^2s/kg) x $Re(f_{CM})$ for resistant and sensitive K562 leukemia cells, respectively. According to dielectric modeling of sensitive K562 cells, their $Re(f_{CM})$ value is almost zero at 48.64 MHz. Therefore, they cannot be pulled towards the electrodes and flow with medium velocity (***u*** and ***v***) (Fig. 4.11 (A)). Finally, particle tracing simulations of resistant K562 cells were achieved as step 4. By using streamline tool in postprocessing of COMSOL, the path of them in the channel was visualized (Fig. 4.11 (B)). As it is seen

in these simulations, sensitive cells are lead to DEP area and touch to electrodes due to hydrodynamic forces, but they are not trapped and flow with the fluid. However, resistant cells are trapped in DEP area. On the other hand, some resistant cells can escape form DEP traps, since the device was not designed to have 100% efficiency. The aim is to show the possibility of the DEP-based separation of sensitive and resistant cancer cells. Yet, the design can be improved to have 100% separation efficiency.

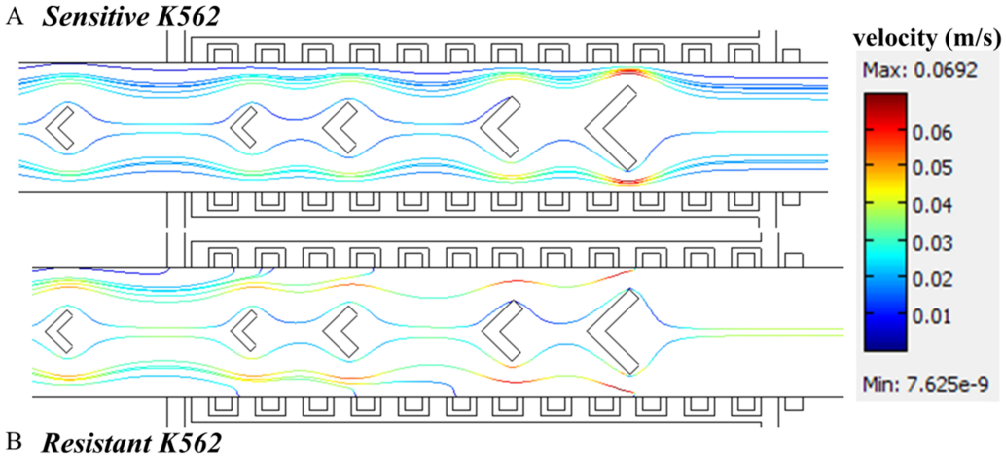


Figure 4.11: The path of K562 sensitive (A) and resistant (B) cells under DEP effect in 2nd generation devices (*flow rate=10 µl/min, voltage=20 V_{pp}*).

CHAPTER 5

FABRICATION

To be able to fabricate the 1st and 2nd generation DEP devices, surface micromachining techniques were mainly utilized. Parylene microchannel fabrication processes on 4" glass wafer, which was developed in our group, were adapted and optimized for these two designs. Process flow of the 1st and 2nd generation designs are almost the same for basic operations but there are some differences and in this section, all process flows are explained in detail with the photos showing important stages of fabrication.

5.1. Fabrication of the 1st Generation Devices

This fabrication is a three mask process and it consists of metal sputtering, wet and dry etching, photolithography, electroplating and polymer (parylene) coating steps. All related parameters are given in Appendix C as Table C.1. Figure 5.1 presents the whole fabrication process.

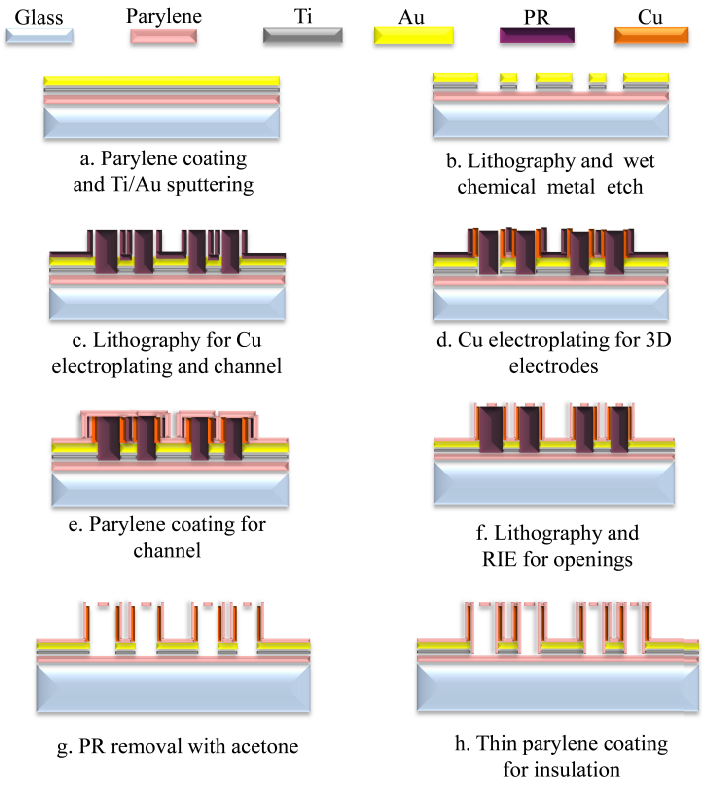


Figure 5.1: The fabrication flow of 1st generation devices.

Before starting fabrication, the piranha cleaning of the 4" glass wafers was made. To obtain a rugged surface which makes material coating possible on glass wafer, buffered hydrofluoric (BHF) etch was utilized for one minute. After these steps, thin parylene coating (~2 µm) was made with silane. Parylene coating can be made with silane, providing stiction of parylene to surface, only when there is no photoresist on the wafer surface. However, if photoresist is coated before parylene, silane cannot be used since it damages the structure of photoresist. Therefore, the initial thin parylene layer was coated to provide the stiction of other parylene layers to wafer. According to the parylene coater optimization, all coatings were performed by a ratio of 1:2, layer thickness in micrometers to parylene weight in grams.

After parylene coating step, Ti & Au were sputtered on the wafer to form a seed layer, providing contact for electroplating. Then, these metal layers were patterned by mask 1 (fig. 5.2), with utilizing S1813 photoresist, which is used when thin coatings are needed. After patterning, wet etching of Ti & Au layers were made with commercial Au etchant and freshly prepared Ti etchant, consisting of 10 ml HF, 10 ml H_2O_2 and 80 ml DI water. The seed layer formation was completed at the end of this steps and Figure 5.3 presents that structure.

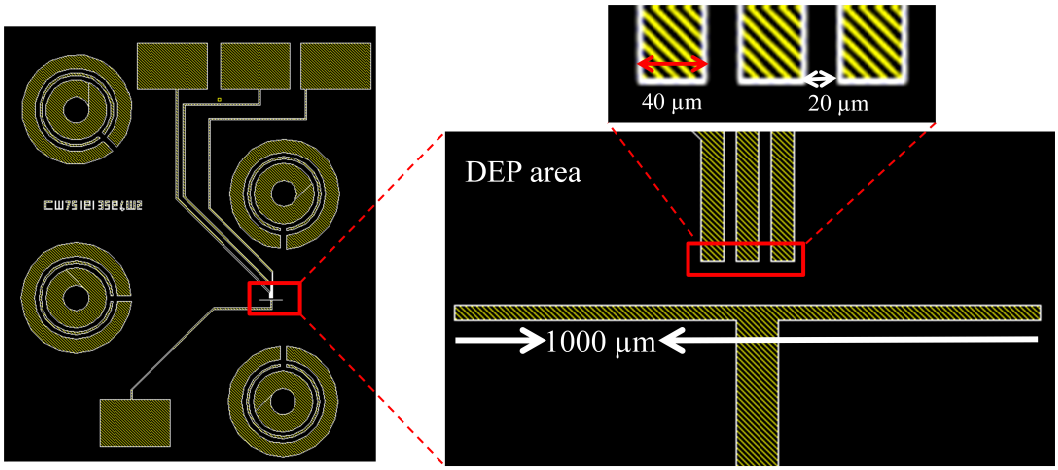


Figure 5.2: Mask 1 of the 1st generation devices. This mask is used for the patterning of seed layer.

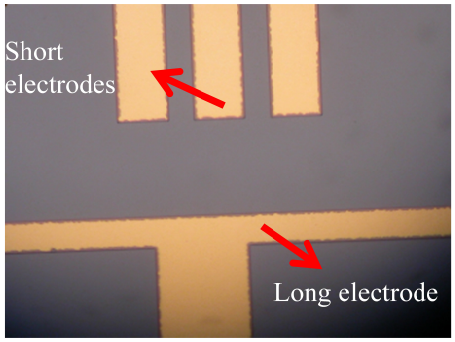


Figure 5.3: The image of seed layer after wet metal etching step.

After seed layer preparation, the photoresist was stripped from the surface by acetone. With utilizing mask 2 (Fig. 5.4), lithography was made to determine the electroplating area. For this lithography, thick resist (~20 µm) was needed. Therefore, AZ9260 photoresist was used by performing single spin. Figure 5.5 shows the channel structure after resist patterning. This image is green because of the filter which prevents the degeneration of photoresist under the light of microscope. In figure 5.5, a photoresist layer was seen on short electrodes. This layer provides to decrease surface tension on thin electrode layers (especially at corners of layers) while electroplating is done. In addition in figure 5.4, electrode places determined by small photoresist layers (8 µm x 10 µm x 20 µm) are seen. These small layers were utilized for the prevention of joining of 3D-electrodes while electroplating. Then, Cu electroplating was achieved with 50 mA current for 90 minutes to form 3D-electrodes. After this process, 3D-electrode height was measured as 15-19 µm. The aim of 3D-electrodes is to provide uniform DEP force along channel depth. Therefore, the difference between channel top layer and the top of electrodes should be smaller than the radius of cells, to be on the safe side by being sure that the higher portion of the cells' volumes would be within the DEP region. Figure 5.6 shows the electroplated 3D-electrodes. This figure also shows that thin photoresist layers between short electrodes did not work properly and electrodes were joined during growing of the metal. Without photoresist strip, thick parylene coating (~20 µm) was done to form the channel top layer and walls. By this way, mask 2 could be utilized for channel formation and electroplating as well.

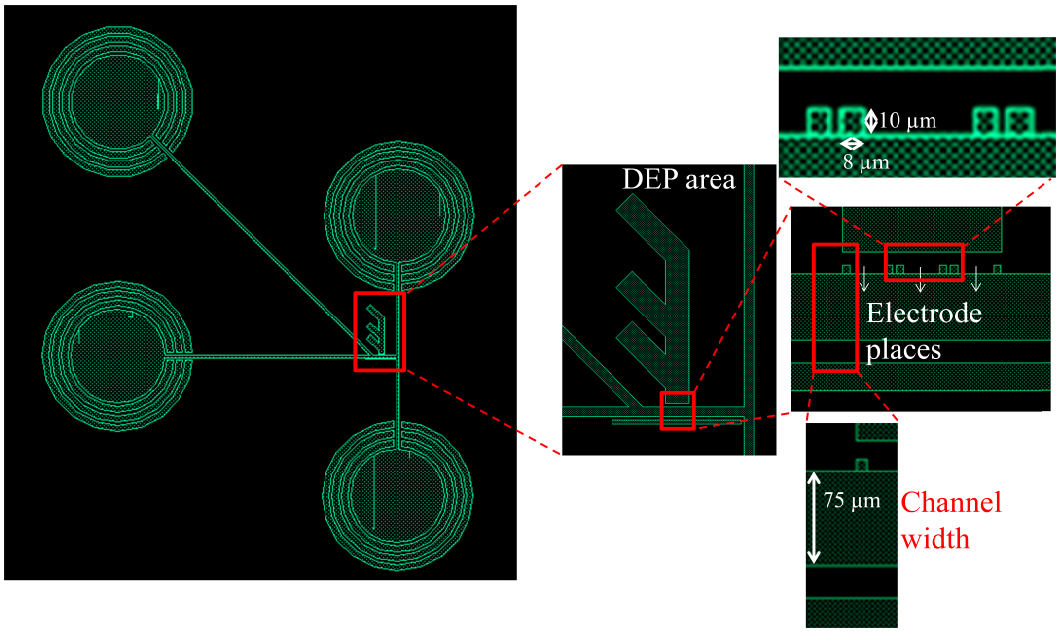


Figure 5.4: Mask 2 of the 1st generation devices. This mask is utilized for the determination of electroplating area.

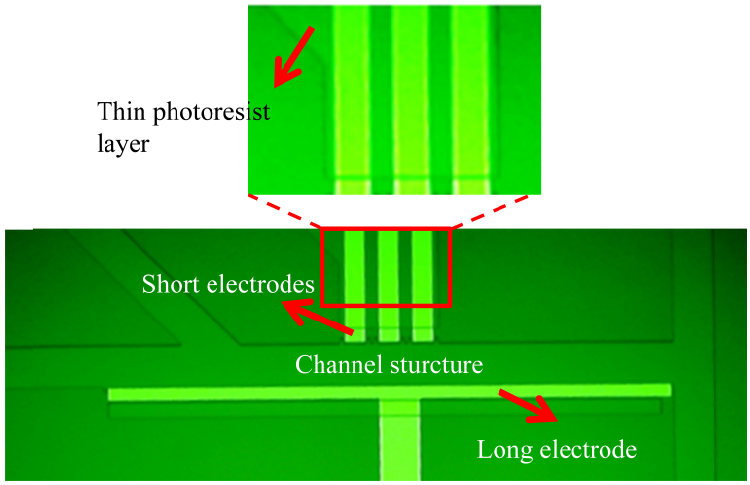


Figure 5.5: Channel structure after the AZ9260 photoresist photolithography step.

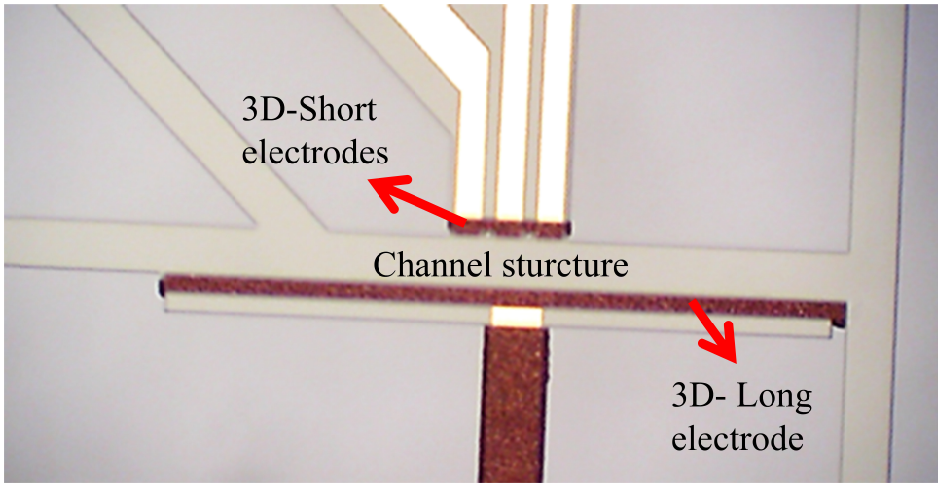


Figure 5.6: Device structure with 3D-electrodes after electroplating step.

The place of electrode contact pads, inlets and outlets were patterned with mask 3, by utilizing AZ9260 (double spin) (Fig. 5.7), and contact pads, inlet and outlet reservoirs were formed with reactive ion etching (RIE). Finally, each wafer was diced and 12 devices were obtained per one wafer.

After dicing, each device was inserted in acetone for 2 days to strip the photoresist, used as sacrificial layer. Then, each die was placed inside parylene coater and a very this parylene layer was coated for insulation of electrodes preventing contact of the electrodes with inside of the channel. Figure 5.8 presents the fabricated device just before testing.

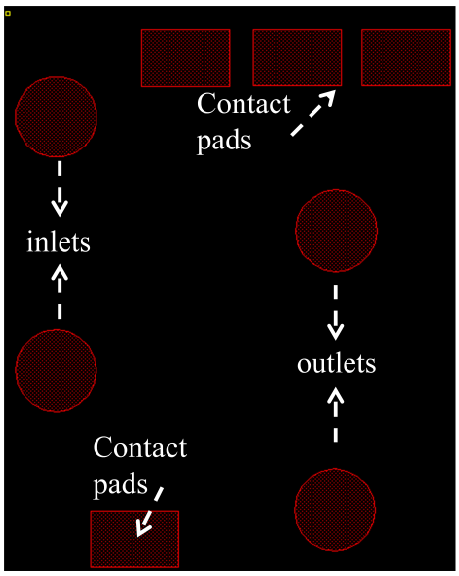


Figure 5.7: Mask 3 of the 1st generation devices. This mask is used for the determination of inlet and outlet reservoirs places.

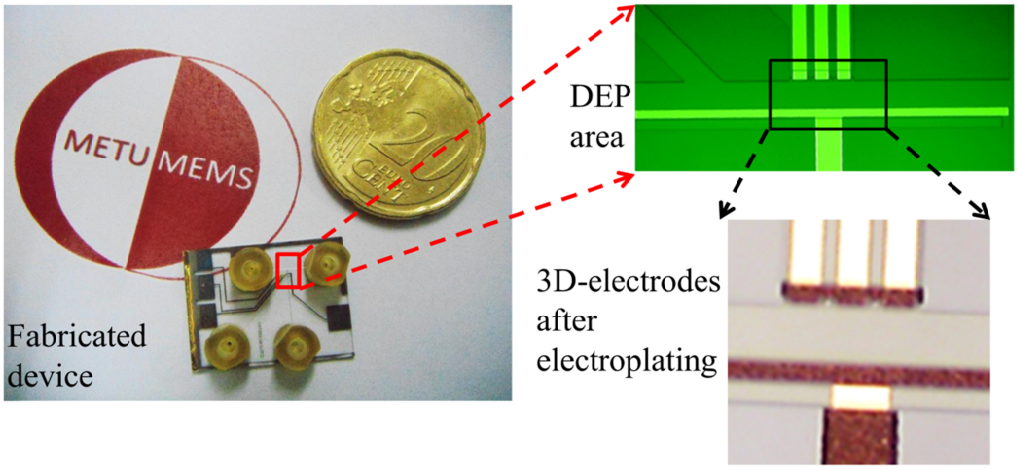


Figure 5.8: Fabricated device for the 1st generation.

5.2. Fabrication of the 2nd Generation Devices

In the fabrication of the 2nd generation devices, one more mask was added and four mask surface micromachining process was utilized to prevent merging of 3D-electrodes. All related parameters are given in Appendix C as Table C.2. Figure 5.9 presents whole fabrication process. Besides, mask 2 was used twice. In this fabrication, wafer cleaning, BHF etch and the 1st two steps were the same until the end of the metal seed layer formation. Figure 5.10 shows the 1st mask, which was used in the patterning of seed layer, and figure 5.11 presents the patterned seed layer. After this step, photoresist was stripped with acetone and a thin parylene layer (5 µm) coating was utilized to prevent the parasitic

capacitances between the Au layer, which was used to short electrodes, and the 3D-electrodes.

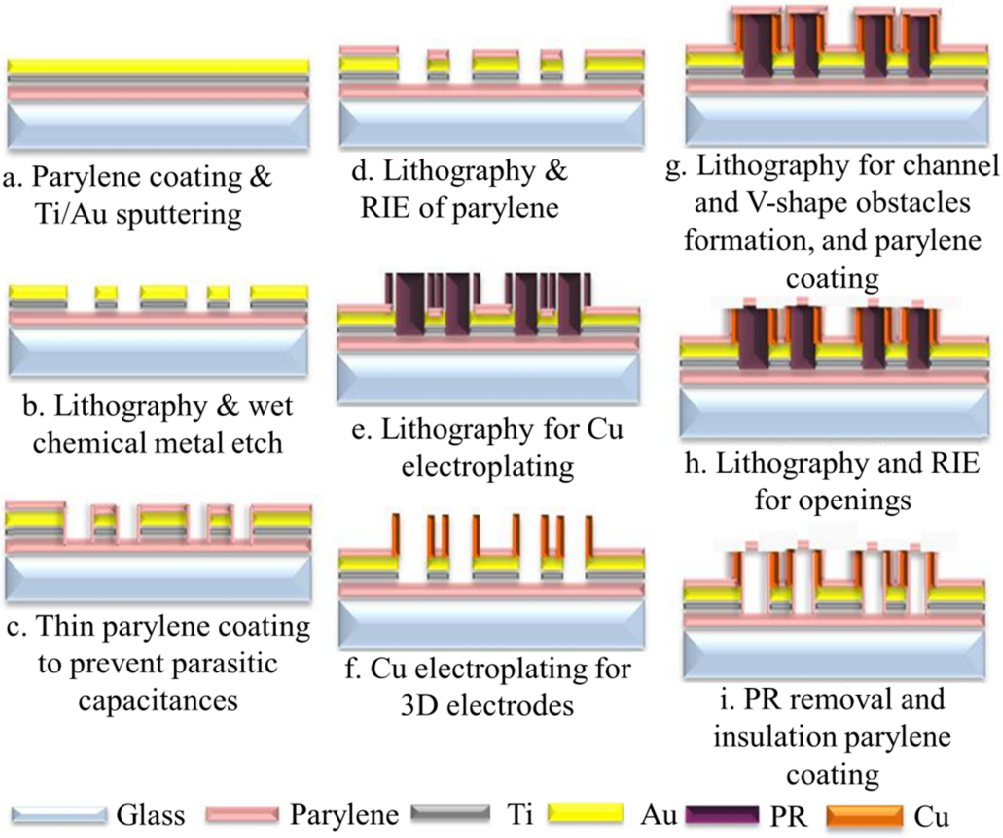


Figure 5.9: Fabrication flow of the 2nd generation devices.

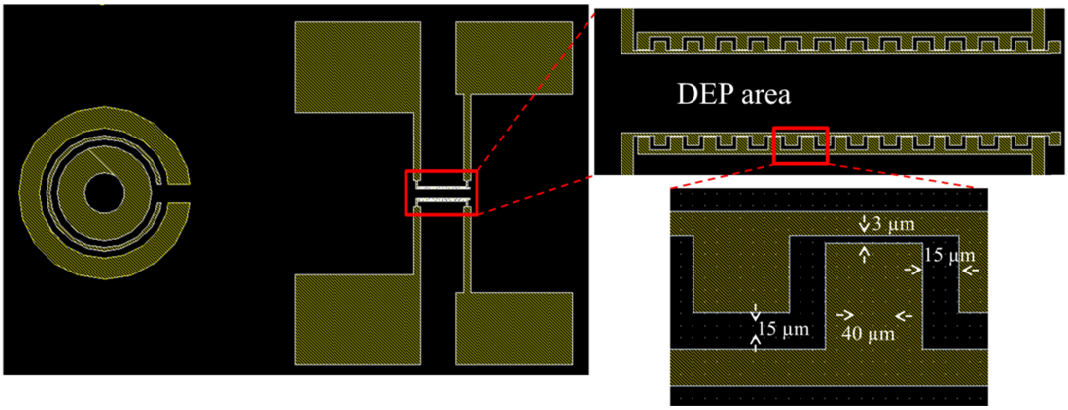


Figure 5.10: Mask 1 for seed layer paterning in the 2nd generation devices.

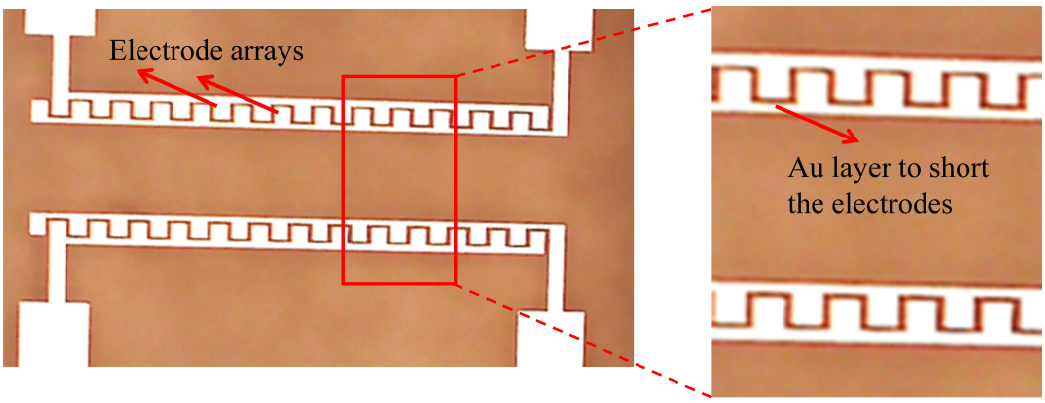


Figure 5.11: Seed layer in the 2nd generation devices.

Parylene has a very uniform coating property, so it coated the whole wafer. Therefore, the electrode places were needed to be opened. For this purpose, parylene RIE was used and a patterning was done. To etch 1 µm parylene, 2 µm photoresist is needed. Therefore, to etch 5 µm parylene, thick (10 µm) photoresist coating was performed with AZ9260, by performing single spin. Mask 2 (Fig. 5.12) was used as dark field for the patterning of AZ9260. After that, with the application of RIE for 20 minutes, electrode places were determined and photoresist was stripped.

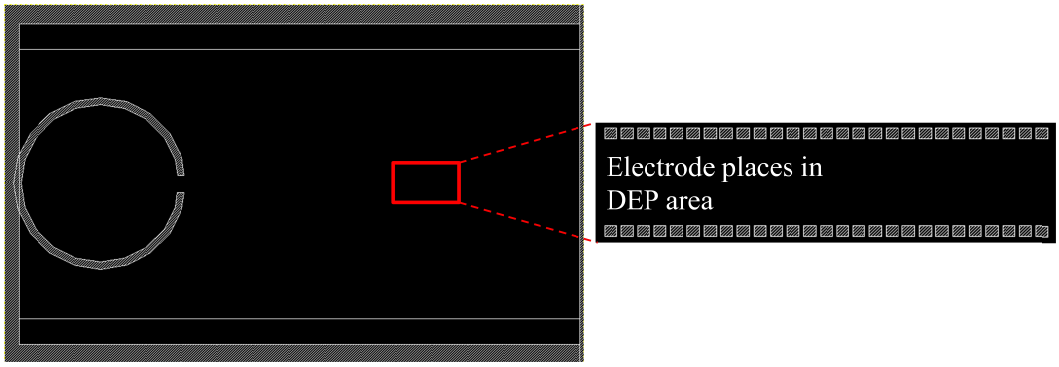


Figure 5.12: Mask 2 as dark field for the determination of electrode places in the 2nd generation devices.

Before fabrication of 3D-electrodes, electrode wells were required to be formed with photoresist patterning. For this purpose, first, AZ9260 patterning by performing double spin was utilized since 30 µm thick wells were needed. Mask 2 was utilized again at this step, as clear field. Then, Cu electroplating was performed with 100 mA current, for 90 minutes. Figure 5.13 shows the electroplated 3D-electrodes. This figure also reveals that the merging problem of 3D-electrodes was solved by the addition of one more mask.

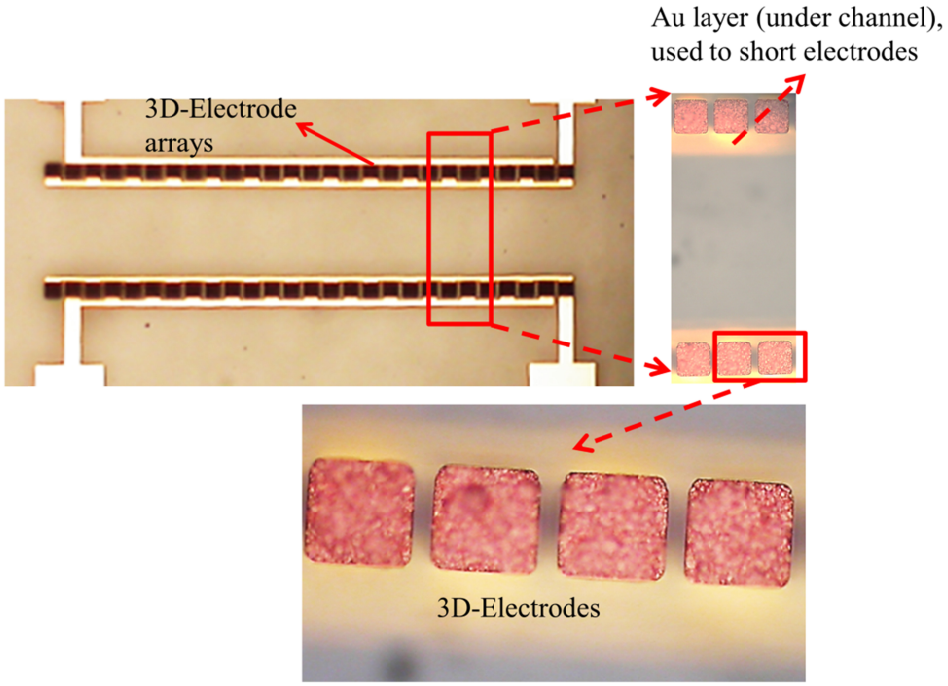


Figure 5.13: 3D-electrode structure in 2nd generation devices.

After electrode formation, channel structure and V-shaped obstacles were patterned with AZ9260, by performing double spin, with utilizing the mask 3 (Fig. 5.14). Thick (20 µm) parylene coating was performed for channel formation. The following steps are the same with the 1st generation devices. Mask 4 for the determination of contact pads, inlet and outlet reservoirs can be seen in Figure 5.15.

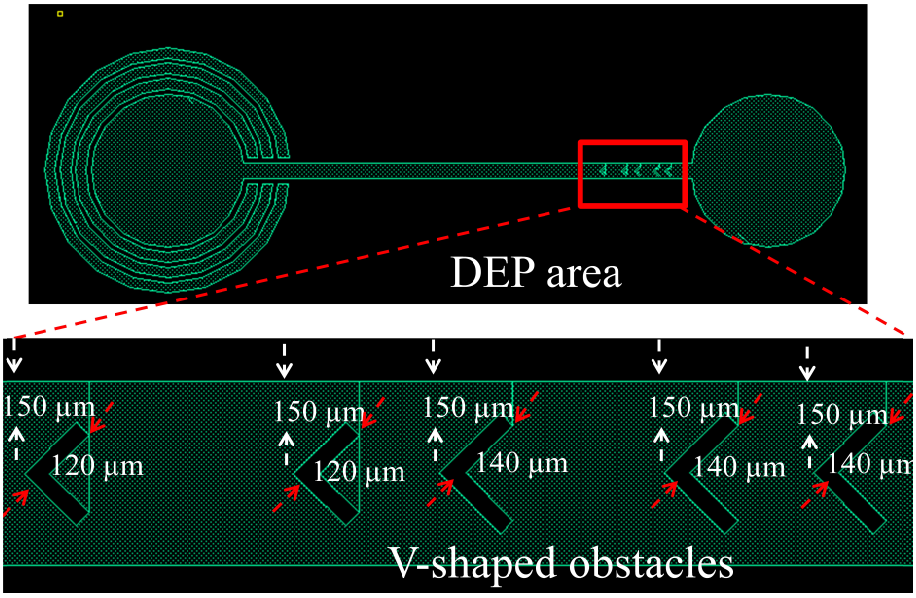


Figure 5.14: Mask 3 for the formation of channels in 2nd generation devices.

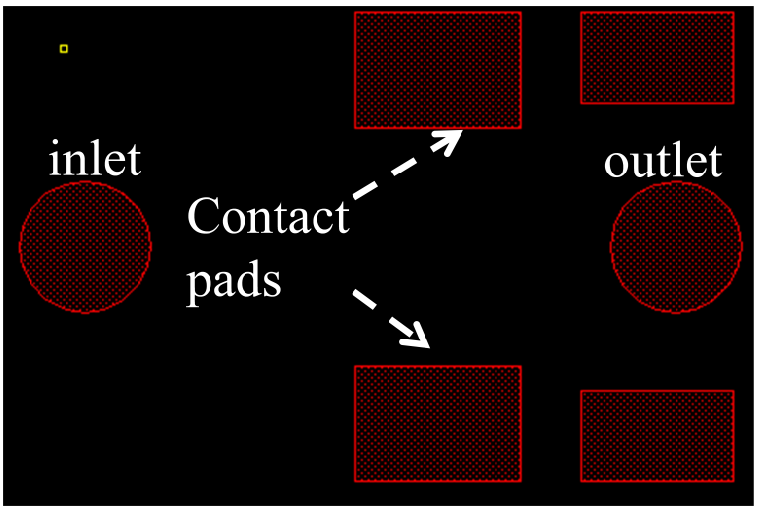


Figure 5.15: Mask 4 for the determination of inlet and outlet reservoirs in the 2nd generation devices.

Finally, figure 5.16 presents the fabricated devices, which are ready for testing.

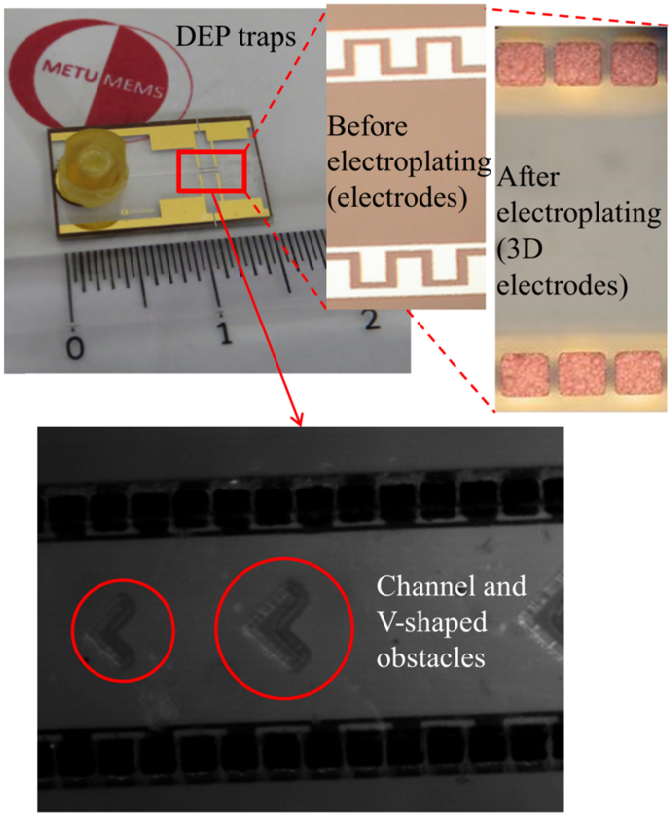


Figure 5.16: Fabricated device.

As it is seen in both designs, DEP area is the smallest part of the devices. However, due to the nanoport dimensions, with a radius of approximately 0.5 cm (Fig. 5.17), inlet and outlet reservoirs occupy most of the device. In addition, three layer Cu was used to carry the nanoports, preventing the collapse of parylene channels (Fig. 5.2 and Fig. 5.10).

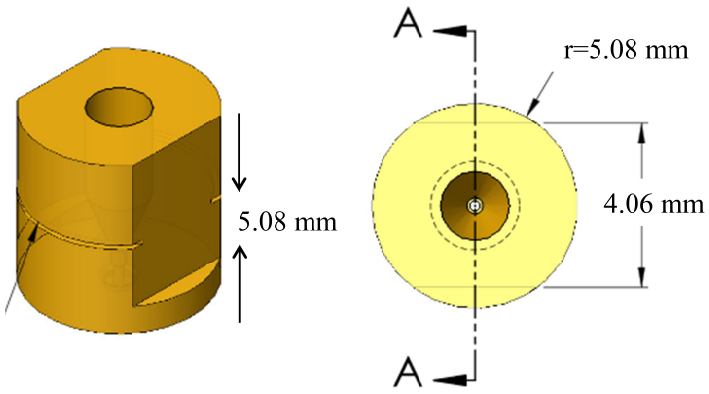


Figure 5.17: The dimensions of nanoports used for the fluidic connections [119].

CHAPTER 6

RESULTS AND DISCUSSION

This chapter presents the experimental results on the 3D-electrode contactless DEP devices and discusses them in comparison with the literature data. First, the test results of the proof of DEP concept with the 1st generation devices utilizing yeast cells are presented. Discussions about these results are given by explaining the necessary revisions in the 1st generation devices. Next, the preparation procedure of sensitive and drug resistant K562 cells is given. Then, experimental setup and methodology are presented. After, the performance analyses of the 2nd generation devices, utilizing different parameters, including different cell concentration, flow rate and the magnitude of voltage, are demonstrated. Finally, the analyses of drug molarity effect on DEP response of doxorubicin resistance K562 cells are given.

6.1. Proof of DEP Concept with 1st Generation Devices

Yeast cells, *Saccharomyces cerevisiae*, are more stable cells than cancer cells since they have rigid cell wall and the molecular change in cytoplasmic content is not fast as much as in cancer cells. Therefore, to be able to make proof of concept analyses, yeast cells are commonly used. In this study, viability analysis of yeasts was made to test DEP devices since the dielectric properties of viable and nonviable yeasts are different [114]. According to their cell modeling (Fig. 3.4), while viable cells are trapped/ manipulated, nonviable cells are not affected by DEP at 1.45 MHz. It is expected that nonviable yeast cells flow with the fluid.

Yeast cells preparation, and test procedure and test results with discussions are given in the following subsections.

6.1.1. Preparation of Yeast Cells

Baker's yeasts were bought from the market. One gram of yeast was added to 2 ml of water and grown with glucose (50 mg/mL in deionized H_2O) at 37°C for 2 hours for activation and growth. Then, the half of the cell suspension was incubated at 95°C for 20 minutes to obtain nonviable yeast cells. Finally, viable and nonviable populations were mixed and washed twice in a medium with a conductivity of 2.5 mS/m. Cells were stained with trypan blue (1:5 (v/v) trypan blue: cell suspension), a viable cell stain, to discriminate between viable and nonviable yeast cells. Figure 6.1 summarizes the whole procedure.

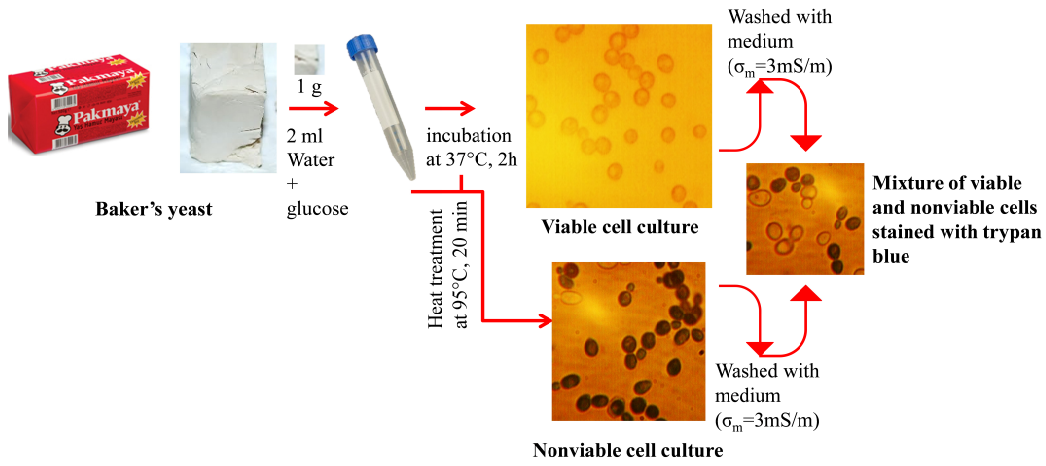


Figure 6.1: Yeast cell preparation for testing of the 1st generation devices.

6.1.2. Test Procedure, Test Results and Discussions

While designing the 1st generation devices, the main aim was the proof of DEP concept through the continuous flow separation of viable and nonviable cells. However, because of experimental problems associated with simultaneous control of two different pressure actuation devices, the analyses were carried out with the capillary flow, instead of pressure driven flow. After cell suspension injection to the channel, sinusoidal voltage was applied at 16 V_{pp} and 1.45 MHz. The yeast cells' motion was observed under microscope connected to a probe station. According to these tests, device has a trapping capability with 96.8 % purity. It means that if 100 cells are trapped, 97 of them are viable and 3 of them are nonviable. The formation of pearl chain structure of viable cells under DEP effect was observed (Figure 6.2). As it is explained in Chapter 4 with Figure 4.9, these viable yeast cells should be lined up on the electric field lines. Yellow lines in Figure 6.2 symbolize the electric field lines (originated from figure 4.9). Viable cells were pulled to short electrodes while nonviable ones were not affected by DEP [115].

Moreover, the manipulation of viable yeasts was achieved with the 1st generation devices. The video of manipulation of viable yeast cells is delivered in supplementary CD (Video 1). The stop motion images of the manipulation are presented in Figure 6.3. In this manipulation, capillary flow was used. By means of DEP force, 4 viable cells stayed without flowing at middle of electrodes. At t=2s, power was turned OFF and DEP effect was removed. Therefore, 2 of 4 trapped cells were split and flowed with the fluid. At t=7s, power was turned ON again and DEP force pulled these 2 cells and they trapped in a different place at t=8s.

These results proved the DEP concept for the 3D-electrode contactless DEP devices, designed in this study. Studies with the 1st generation devices has also been useful in identifying the problems associated with fabrication and testing, and designated the necessary improvements for the 2nd generation devices. As explained in Chapter 5, separated electrodes were merged while growing. This prevented the uniformity of DEP force along channel depth. However, as the electrodes were still separated at the bottom of the channel, the effect of increasing the DEP force along channel length could be seen.

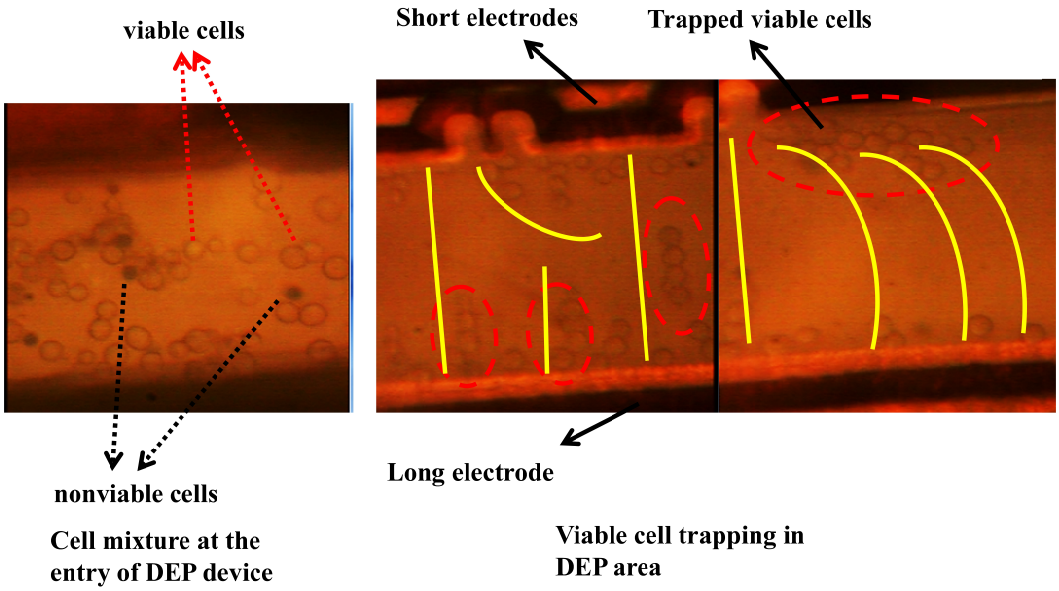


Figure 6.2:.Viable yeast cells' trapping, forming pearl chain structure on electric field lines, in DEP area [115].

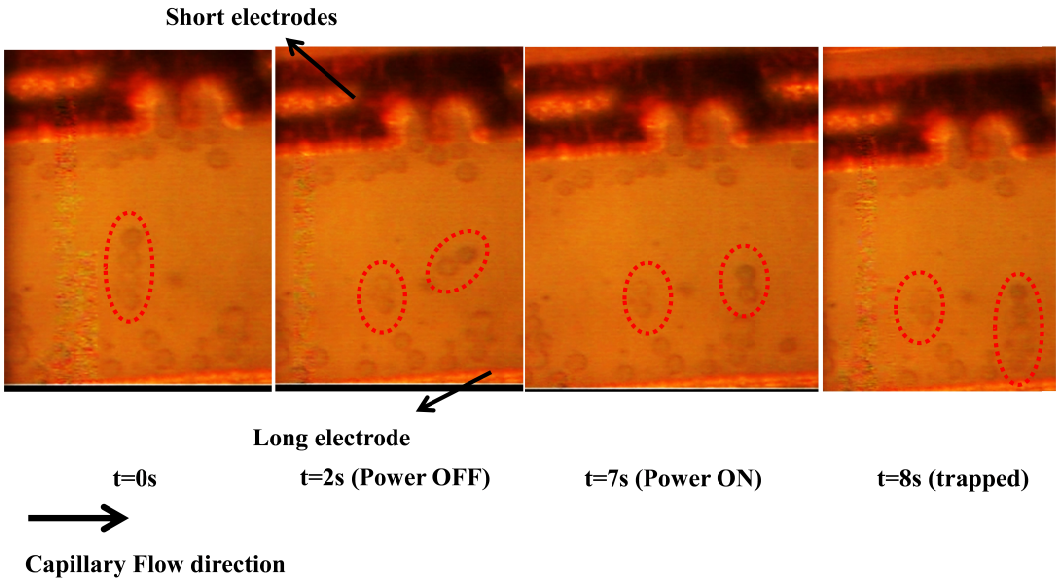


Figure 6.3: Viable yeast cells manipulation with the 1st generation devices. At t=0s, by means of DEP force, 4 viable yeast cells formed a pearl chain structure. Next, at t=2s, power was turned off and 2 of them flowed with the capillary flow. At t=7s, power was turned on again. At t=8s, 2 viable yeast cells were trapped at a different place on long electrode [115].

6.2. Imatinib and Doxorubicin Resistance Detection in K562 Cells

After the proof of DEP concept with the 1st generation devices, the 2nd generation devices were designed and fabricated as explained in detail in the previous sections. In this section, preparation of K562 cells, experimental setup for the 2nd generation DEP devices, test procedure and test results with discussions are presented.

6.2.1. Cell Preparation

K562 sensitive and drug (imatinib and doxorubicin) resistant cells were cultured in RPMI 1640 medium containing 10% (w/v) fetal bovine serum (FBS) and 0.2% (w/v) gentamicin, at 37°C with 5% CO_2 in humidified incubator (in the Department of Biology, METU). Before each tests, these cells were washed twice with a medium with a conductivity of 2.5 mS/m (adjusted using 1X phosphate buffered saline (PBS)). The medium contained 8.5 % (w/v) sucrose and 0.3 % (w/v) dextrose to adjust osmotic pressure inside the cell. By means of this, the burst of cells is prevented [70]. According to the tests, cell concentration was adjusted with counting of cells through hemacytometer.

To monitor cells inside DEP devices fluorescein diacetate (FDA), a fluorescent stain used for viable cell staining, was utilized. FDA was dissolved in DMSO (10 µg/ml) and 1µl of it was used to stain 10^6 cells. If cells are viable, they are stained with FDA after 15 minutes incubation and monitored with GFP filter as green. The cell preparation procedure was summarized in Figure 6.4.

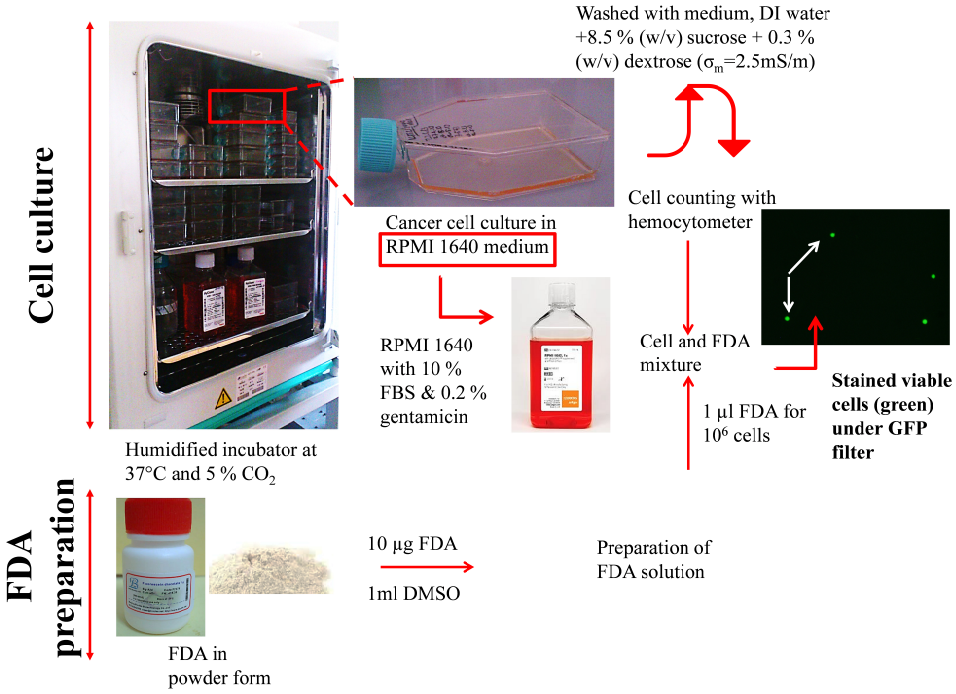


Figure 6.4: Cancer cell preparation for testing of the 2nd generation devices.

6.2.2. Experimental Setup

For the detection of imatinib and doxorubicin resistance in K562 cells, continuous flow DEP analyses were carried. The test setup is demonstrated in figure 6.5. To adjust the flow rate, a programmable syringe pump (*Lab Smith*) and its software (*µProcess Scanner*) were used with different sized syringes, such as 8 µl and 20 µl. Probe station provided to take contact from micro DEP devices. Moreover, to fulfill the camera need for high speed monitoring of living cells in low intensity light, *Evolve 128* high speed camera and its free software (*µManager*) were used. This camera is monochrome so images are in gray scale.

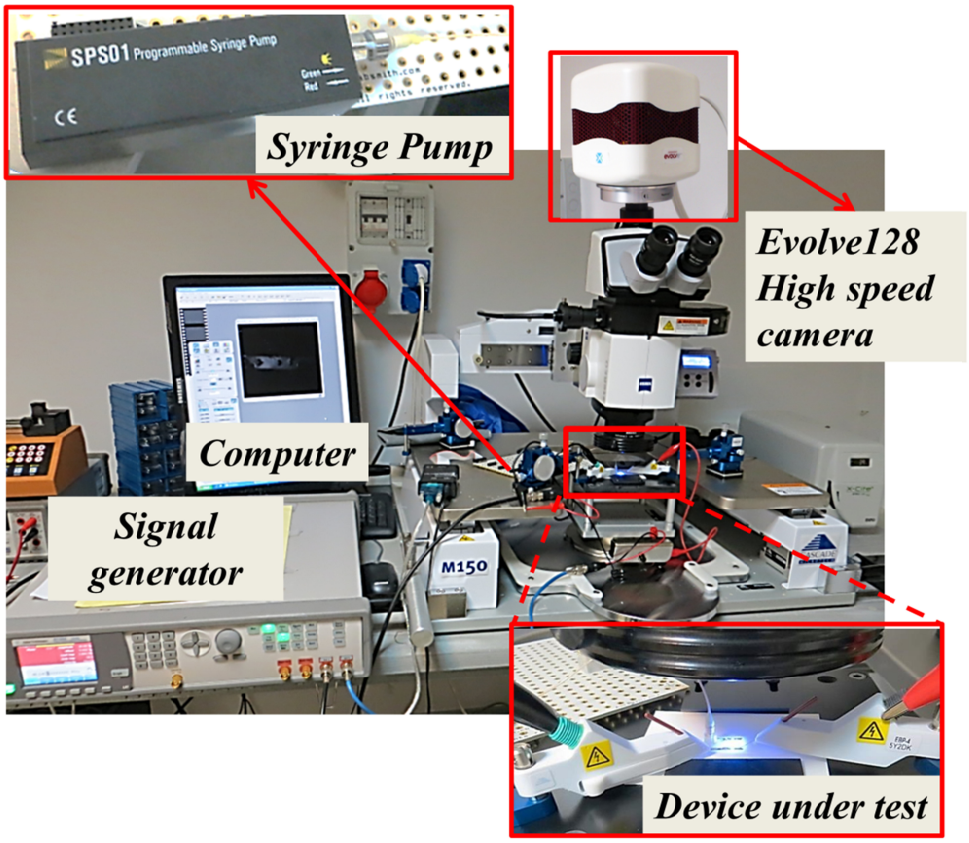


Figure 6.5: Experimental test setup for the 2nd generation devices.

6.2.3. Test Results and Discussions

To show the detection of imatinib and doxorubicin resistance in K562 cells by using the 2nd generation DEP devices, first, the trapping of resistant K562 cells were achieved at 48.64 MHz, at which sensitive K562 cells were not affected by DEP force. This frequency is the crossover frequency of K562 sensitive cells in a medium with 2.5 mS/m conductivity (as determined in Chapter 3, Fig. 3.5). Figure 6.6 shows the trapping of imatinib (A) and doxorubicin (B) resistant K562 cells in the 2nd generation devices with 10 µl/min flow rate and 9 V_{pp} voltage at 48.64MHz. Figure 6.7 presents the pathway of sensitive K562 cell while they pass through the microchannel through fluid flow without trapping, under the

same experimental conditions of resistant cell lines [105]. Moreover, in the supplementary CD, trapping of imatinib (video 2) and doxorubicin (video 3) resistant K562 cells, and the pathway of sensitive K562 cells (video 4) are available. In video 4, a high intensity area is seen at left side of the screen. It is caused that there is no outlet port in the 2nd generation devices. Therefore, waste is taken from outlet reservoir with syringe by hand. While taking the waste fluid out, the intensity of the whole image changes. Moreover, air bubble formation is also seen in this video but it did not affect the DEP effect in the top electrode array.

The main problem of this design is the formation of air bubbles inside the channel (Figure 6.7). The sharp arms of V-shaped obstacles cause this problem. Air is trapped between the arms of V-shaped obstacles and while fluid flows rapidly, trapped air forms air bubbles. With the fluid motion, these bubbles move to any place in channel. They close the electrodes randomly and prevent the DEP operation at this side. Therefore, for the next generation devices, the shape of the obstacles will be modified to prevent the bubble formation.

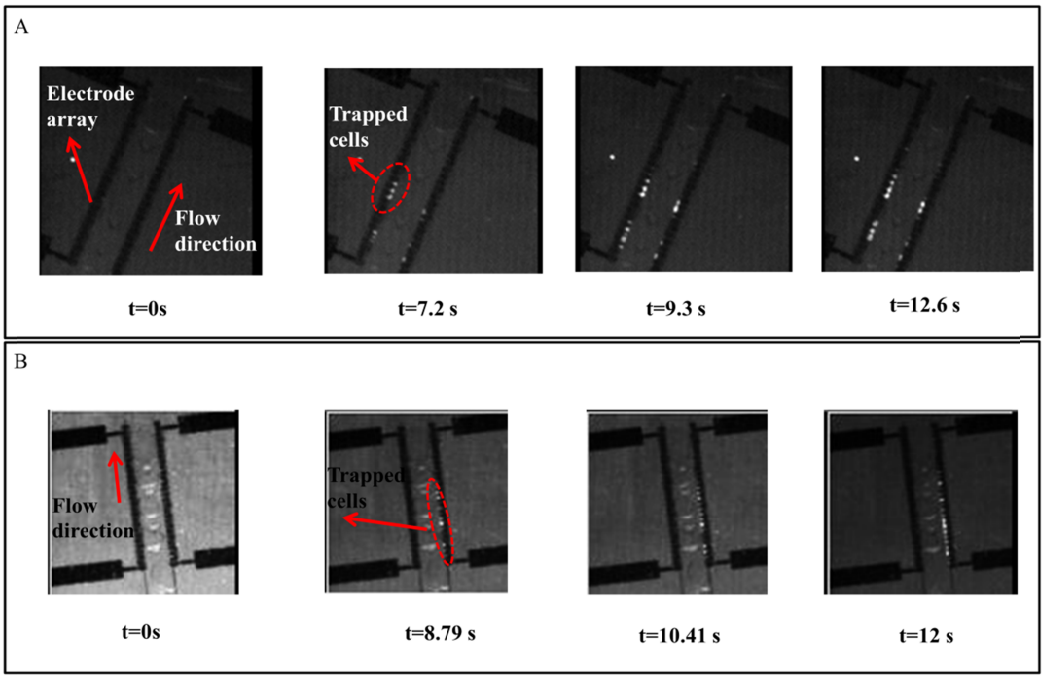


Figure 6.6: The trapping of imatinib (A) and doxorubicin (B) resistant K562 cells with the 2nd generation devices (flow rate = 10 µl/min, voltage = 9 V_{pp}, frequency = 48.64MHz) [105].

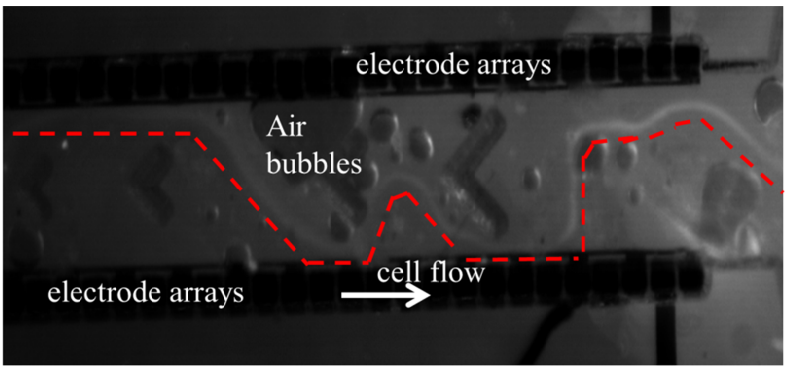


Figure 6.7: The pathway of sensitive K562 cells while they flow through the microchannel in the 2nd generation devices (flow rate = 10 µl/min, voltage = 9 V_{pp}, frequency = 48.64 MHz) [105].

With these results, the assumption made while cell modeling is certified. Doxorubicin and imatinib resistance are caused by P-gp overexpression. Therefore, DEP responses of them are similar at the same frequency. Moreover, these results showed that drug resistant K562 cells and their sensitive ones could be separated at 48.64 MHz frequency.

After determination of the frequency as 48.64 MHz for DEP trapping of imatinib resistant K562 cells, performance tests of the devices were carried out. For this purpose, a systematical study for the determination of optimum voltage, cell concentration and flow rate was performed. First, all test parameters remained the same except for the magnitude of the voltage. Cell concentration and flow rate was kept constant at 625000 cells/ml and 10 µl/min, respectively, while voltage was varied between 1 and 20 V_{pp}. At 20, 15, 12, 10, 9 and 5 V_{pp}, imatinib resistant K562 cells were trapped. The voltage values below 5 V_{pp} were not enough for trapping. Although cells were trapped at 20 V_{pp}, this voltage was not proper for detection as the cells were damaged and burst at 20 V_{pp} since very thin parylene (~0.3 µm) insulation is not enough for that much voltage. Table 6.1 shows the results of performance tests of devices in terms of voltage magnitude. Besides, these results also show that trapping can be achieved at considerably lower voltages (5 V_{pp}) than reported in the literature for contactless DEP devices [72], [120].

Table 6.1: Perfomance test results of the 2nd generation devices for different voltages at 10 µl/min flow rate and 625000 cells/ml cell concentration.

voltage (V_{pp})	20	15	12	10	9	5	1
trapping	+	+	+	+	+	+	-

Figure 6.8 shows the sample images for trapped imatinib resistant K562 cells at different voltages. The results prove that when voltage is decreased, trapping efficiency declines since DEP force is directly proportional to the square of applied voltage.

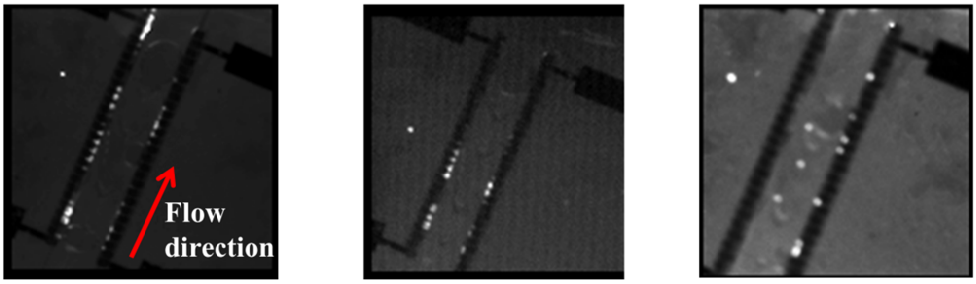


Figure 6.8: Sample images of trapped imatinib resistant K562 cells under different voltages.

In addition, video 5 in supplementary CD demonstrates the trapping test results for imatinib resistant K562 cells at varying voltages. In this video, the voltage was $1V_{pp}$ at the beginning, where cells flow with the fluid at a flow rate of 10 µl/min. When the voltage was increased to 10 V_{pp}, trapping started suddenly.

After completing the voltage performance analyses, flow rate analyses were performed at two different concentrations of imatinib resistant K562 cells, 625000 cells/ml and 300000 cells/ml (Table 6.2). The voltage was kept constant at 15 V_{pp}. According to these analyses, at 1, 3, 6.67, 10 and 20 µl/min flow rates, trapping can be achieved when cell concentration is 625000 cells/ml. However, when the cell concentration is decreased, trapping cannot be achieved at 10 and 20 µl/min flow rates. This means that the efficiency of the devices is reduced with decreasing cell concentrations or increasing flow rate for low cell concentrations.

Table 6.2: Perfomance test results of the 2nd generation devices for different flow rates and cell concentrations (voltage=$15V_{pp}$).

flow rate (µl/min) / **concentration**	1	3	6.67	10	20
625000 cells/ml	+	+	+	+	+
300000 cells/ml	+	+	+	-	-

6.3. The analyses of the Effect of Drug Resistance Level on DEP Response

One of the mechanisms in developing MDR in cancer cells is mediated by increased P-gp expression level, which functions in drug efflux, whereby cells decrease the effective drug concentration inside the cytoplasm. P-gp also functions as Cl^- channel; hence, cells with different P-gp expression levels have different cytoplasmic conductivities. It can be hypothesized that the variation in cytoplasmic conductivity in resistant cells can be used to assess the degree of drug resistance, as the P-gp expression level, hence the cytoplasmic conductivity, may vary depending on the level of resistance. Although increased P-gp expression in resistant cells is well known, no correlation with the drug resistance level with the cytoplasmic conductivity, and hence the DEP response has been reported, so far. In this study, K562 cells with varying doxorubicin resistance levels (100 nM, 300 nM and 500 nM) were examined with the 2nd generation DEP devices to evaluate the variation in their DEP response, through trapping tests. Cells were examined under the same

experimental conditions, and the numbers of trapped cells were counted. Based on the preliminary test results, a relationship between the drug resistance level and DEP response has been proposed.

In the following subparts, experimental approach, procedures, and results are given in detail together with the discussions and challenges.

6.3.1. Cell Preparation

100, 300 and 500 nM doxorubicin resistant K562 cells were developed in METU Biology Department (thanks to Murat Erdem from Cancer Research Lab of Prof. Dr. Ufuk Gündüz). Basically, the cells were grown in culture media with a certain drug concentration. They are repeatedly sub-cultured until they adapt to live in that drug concentration. Then, the cells were transferred to an increased drug concentration and cultured there until they get adapted. The procedure is repeated until the desired resistance level is achieved. For the quantitative verification of drug resistance IC_{50}, the half maximal inhibitory drug concentration, of resistant cells were determined through XTT analysis. In other words, XTT test determines the drug concentration at which 50% reduction in the cell viability is observed, relative to the untreated ones [97]. Figure 6.9, 6.10 and 6.11 present the results of XTT tests for 100, 300 and 500 nM doxorubicin resistant K562 cells, respectively. According to this analysis, IC_{50} values of 100 nM, 300 nM and 500 nM doxorubicin resistant K562 cells were determined as 0.996 μM, 2.492 μM, and 4.337 μM, respectively.

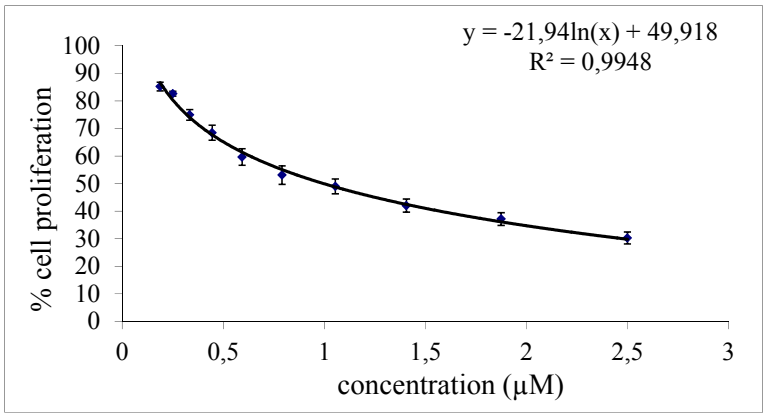


Figure 6.9: XTT results for the determination of IC_{50} values of 100 nM doxorubicin resistant K562 cells.

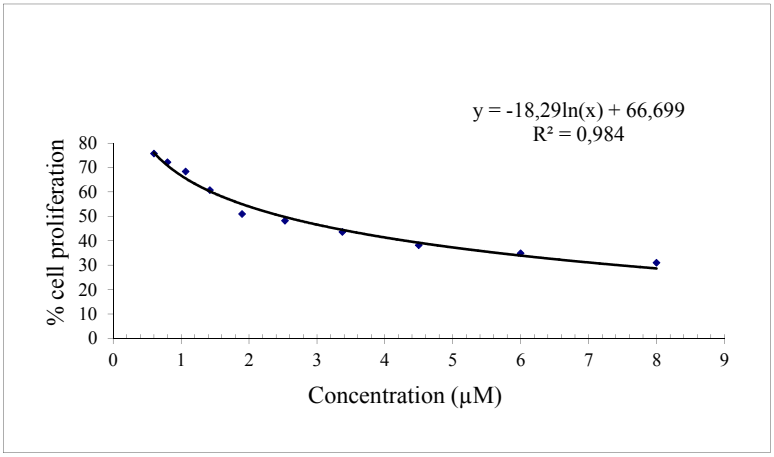


Figure 6.10: XTT results for the determination of IC_{50} values of 300 nM doxorubicin resistant K562 cells.

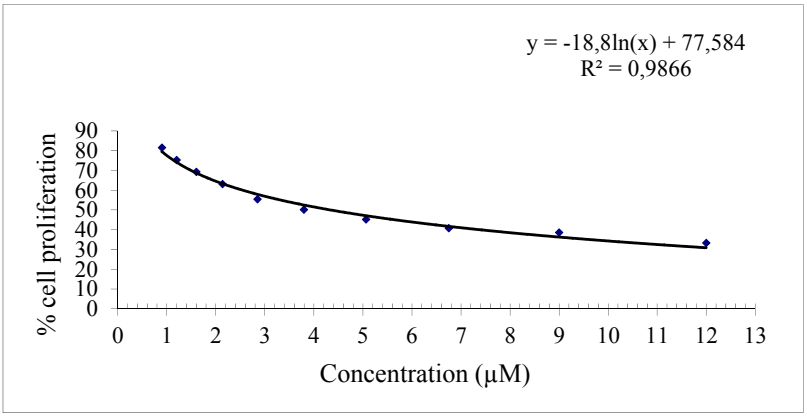


Figure 6.11: XTT results for the determination of IC_{50} values of 500 nM doxorubicin resistant K562 cells.

For the DEP analysis, cells were prepared as described in Figure 6.4. For the determination of the effect of drug resistance level on DEP response, DEP trapping and cell counting analysis were performed, which requires lower cell concentrations. Moreover, since the DEP area is 1500 µm, it should not be saturated or clogged with the trapped cells during the analyses. To optimize the cell concentration, 20 µl of 2500 cells/ml, 25000 cells/ml, and 250000 cells/ml cell suspensions were injected to the channel. In the former two cell concentrations, no cells could be observed in the channel, most probably due to high precipitation level occurring in the macro scale tubing and ports, before they can reach the microchannel. Therefore, if cell concentration is too low, almost all cells remain in the fluidic connections. Finally, 250000 cells/ml cell concentration was decided to be used for these tests.

6.3.2. DEP Trapping Test and Cell Counting

DEP trapping tests with the 2nd generation devices were performed immediately after transferring the cells into suspension solution (8.5 % (w/v) sucrose, 0.3 % (w/v) dextrose, 2.5 mS/m conductivity). Each set should be completed in almost 2-3 hours, since, the cells' physiology changes when they are removed from the CO_2 incubator, in which they are cultured. Tests were repeated at least 4 times using separate cultures of cells, for each cell type, and in each test, 100 µl of cell suspension were examined in 5 parts (20 µl, each). In addition, in each set, the same DEP device was used for each type of cells.

Test parameters were fixed as: voltage = $9V_{pp}$, frequency = 48.64 MHz, flow rate = 5 µl/min, cell concentration = 250000 cells/ ml. The test setup shown in Figure 6.5 was utilized for these analyses.

Cell counting was performed by measuring the variation in light intensity, using an image analysis software (*Image J*). The high speed camera (*Evolve 128*) has the ability to take screen shot images at every 10 ms. Therefore, cell trapping can be monitored in microchannel easily. Cells were stained fluorescently. Therefore, when a cell is trapped, light intensity changes. Utilizing differential analysis between images, cell counting was achieved. Figure 6.12 shows two sample images, examined for cell counting. In the top image, only one cell was trapped and in light intensity analysis, 1 peak is seen. In the bottom image, although 4 more cells were trapped, there are only 3 peaks, but the gray value of the 3rd peak, which belongs to previously trapped cell, is increased. In addition, the gray value of the second peak is as high as the third one, so, there should be 2 cells, too. This means that a new cell was trapped on the same place of the previously trapped one. Due to transparency of cell cytoplasm, cells trapped on top of each others can be discriminated with this method.

While trapped cell number increases, discrimination of the difference between the peaks in light intensity analysis become difficult and the error ratio increases. Therefore, first, all gray values in light intensity analysis are extracted to *Excel* with the help of *Image J*. Next, difference analyses were performed for different images. If the difference amount is between 200000 and 400000, there exist two cells. If the difference amount is between 400000 and 600000 and the difference value for the consecutive pixels is smaller than 400000, there exist three cells. If difference value of the consecutive pixels is greater than 400000, one cell exists at that pixel and another one is on the consecutive pixel. If the difference amount is between 600000 and 800000 and the difference value for the consecutive pixels is smaller than 600000, there exist four cells. Table 6.3 summarizes cell-counting rules.

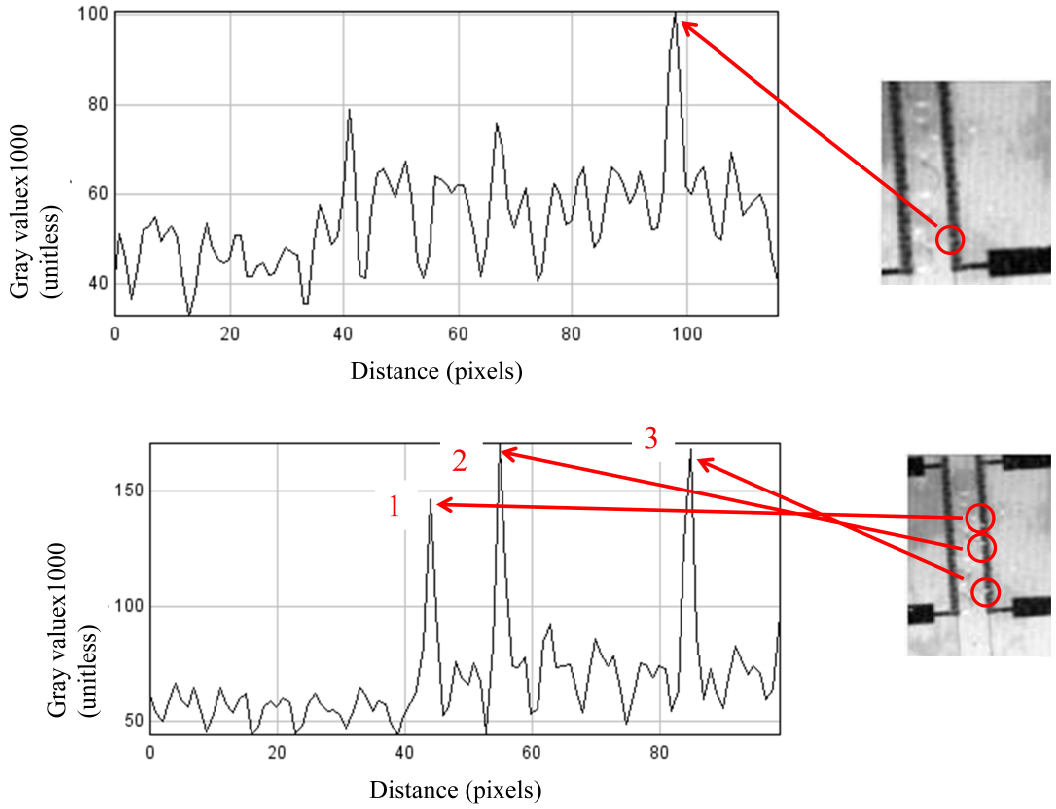


Figure 6.12: Example images used in cell counting with ligth intensity analysis in *Image J*. In top image only one cell is trapped. In bottom image, 4 more cells are trapped.

Table 6.3: The principles of cell counting utilizing light intensities. "X" means not considerable.

evaluated pixel gray value	**consecutive pixel gray value (Left & Rigth)**	**cell number**
<200000	X	0
>200000	<200000 & <200000	1
>200000	>200000 & <200000	1
>200000	>200000 & >200000	0
>200000 & <400000	<200000 & <200000	2
>200000 & <400000	>200000 & <200000	2
>200000 & <400000	>200000 & >200000	1
>400000 & <600000	<400000 & <400000	3
>400000 & <600000	>400000 & <400000	3
>400000 & <600000	>400000 & >400000	1
>600000 & <800000	<600000 & <600000	4
>600000 & <800000	>600000 & <600000	4
>600000 & <800000	>600000 & >600000	2

Examined images were chosen by examining all photos by eyes. Therefore, some images at which cells are trapped may escape observation. This is the error part of this analysis. However, these images cannot be examined with a software, one by one, since there exist some problems caused by the design of the device. The first problem is air bubble formation due to sharp arms of the V-shaped obstacles. These bubbles move in the channel with the flow. Therefore, they can damage the trapped cells (Fig. 6.13). If a software is utilized for each image, one by one, this issue cannot be discriminated and cells trapped and damaged by the air bubble cannot be counted as trapped. On the other hand, this air bubble problem does not affect the general test flow since, as it is seen in figure 6.13., it damage the system only for ~1 second while whole test duration is 4 minutes. Although the number of this type of situation is not considerably high, it affects the cell counting. Therefore, as a future work, V-shape obstacles and device efficiency should be improved in the 3rd generation DEP device design.

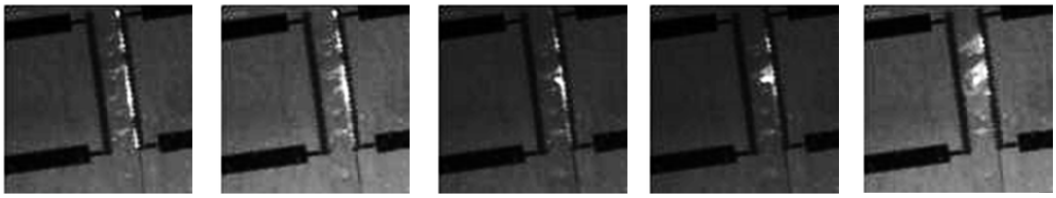


Figure 6.13: Due to sharp arms of V-shaped obstacles, air bubble forms and damages the trapped cells in microchannels.

The second problem is that there is no outlet port in the 2nd generation devices. Therefore, waste is taken from outlet reservoir with syringe by hand. While taking the waste fluid out, the intensity of the whole image changes (Fig. 6.14). It causes the sharp increase in the intensity of cells even there is the same number of cells. Therefore, while choosing images for light intensity analysis with eye, this difference can be seen and one more light intensity analysis was performed with the area at which cells are not trapped. The minimum change in light intensity is determined with this method and it is extracted from the real images at which cells are trapped.

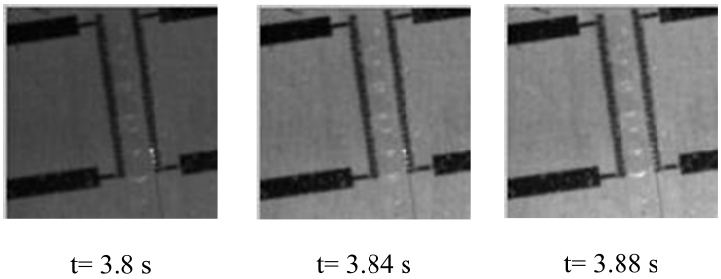


Figure 6.14: Intensity change in whole image because of waste fluid in outlet resorvoir although there is not trapped cell.

As only one device was used in all the tests for the homogeneity of the results, the device got damaged (especially the V-shaped obstacles, because of the pressure) during the fourth run. So, although 4 sets of tests with each cell type were performed, the results of the first 3 were counted.

6.3.3. Test Results

Cells were counted according to the above procedures and the average number of the trapped cells was calculated, for each cell type. Figure 6.15 presents the results.

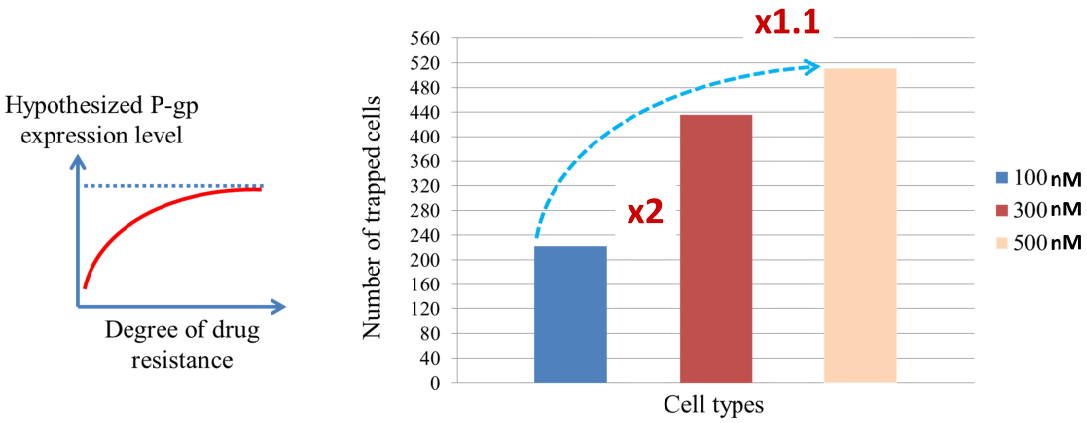


Figure 6.15: Trapped cell number belongs to the different degree of doxorubicin resistant K562 cells (100, 300 & 500 nM). Comparing the hypothetical P-gp expression, the increase in the trapping cell number is in saturation trend.

According to this result, there is a non-linear relationship between the drug resistance level and DEP response of cells. The number of trapped cells is almost 2 times higher for 300 nM resistant cells, compared to the 100 nM ones. Yet, when 300 nM and 500 nM cells are compared, the trapped cell number increases only by 1.1 times. This may imply that P-gp expression level may reach to saturation after a point, and cells develop another mechanism for survival. Or, although P-gp expression in resistant cells increases with the drug resistance level, cell conductivity does not increase after a point, as this may be harmful for the cell metabolism. These results form a very important basis for the proof of hypothesis. However, more data should be collected with cells having different drug resistance levels, and these data should be supported with the biological/molecular analyses, to prove the hypotheses.

CHAPTER 7

CONCLUSION AND FUTURE WORK

The main objective of this study is to achieve the continuous flow, label-free and real-time detection of MDR in K562 leukemia cells, through the design, fabrication and implementation of a MEMS-based, 3D-electrode contactless dielectrophoresis device. To reach this goal, first the DEP-based cell detection based only on the variation in dielectric properties was realized utilizing viable and nonviable yeast cells. This was achieved through cell dielectric modeling followed by design, extensive simulations, fabrication and testing of the 1st generation DEP devices. Consistency of the results with the simulations and literature data has proven the possibility of DEP-based cell detection, separation and manipulation. Next, dielectric modeling of the sensitive and resistant lines of leukemic K562 cells was carried out. Based on the experiences gained in the 1st generation devices and the developed models, design, simulation and fabrication of the 2nd generation DEP devices were performed. Results obtained with K562 cells revealed that MDR detection is possible in leukemia cases. Besides, with further tests, the designed DEP devices have shown to be capable of determining the level of MDR.

The achievements throughout this study, in relation with the proposed objectives, can be listed as follows:

1. The proof of DEP concept for DEP-based cell separation, based only on differences in dielectric properties, was achieved using viable and nonviable yeast cells, through following studies:
   - Accurate dielectric modeling of viable and nonviable yeast cells were obtained by applying triple shell cell modeling with the dielectric properties of these cells, available in literature, and utilizing MATLAB.
   - For the proof of DEP concept, studies on the separation of cells with similar sizes but different dielectric properties, the 1st generation DEP device design was achieved with a novel approach combining the advantages of 3D-electrode structures and contactless DEP phenomenon.
   - Hydroelectrodynamic analysis of the 1st generation DEP device design was achieved through COMSOL software utilizing FEM simulations.
   - A fabrication flow was developed for the 1st generation DEP devices.
   - Fabrication of the 1st generation DEP device was achieved. The problems of fabrication were discussed and ameliorated in the 2nd generation DEP device's fabrication.
   - An experimental procedure and test setup were developed for testing of the 1st generation DEP devices.
   - Testing of the 1st generation DEP devices was performed. However, separation tests became challenging due to experimental problems. Therefore, trapping of viable yeast cells in DEP area were achieved at the crossover frequency (1. 45 MHz) of nonviable yeast cells with a purity of 96.8 %, at capillary flow

conditions. At the same frequency, it was proven that nonviable yeast cells are carried away with the capillary flow.

2. A DEP-based MDR detection in K562 leukemia cells utilizing dielectric characteristics was accomplished, through the following studies:
   - According to the dielectric properties of doxorubicin resistant and sensitive K562 cells reported in literature, accurate dielectric modeling of imatinib and doxorubicin resistant, and sensitive K562 cells were obtained by applying double shell cell modeling and utilizing MATLAB.
   - The design of the 2nd generation DEP device with 3D contactless electrode structure with enhanced throughput and detection sensitivity was accomplished.
   - Hydroelectrodynamic analysis of the 2nd generation DEP device design was achieved through COMSOL software utilizing FEM simulations.
   - Fabrication flow of the 2nd generation DEP devices was developed through some modifications of the fabrication flow of the 1st generation device
   - Fabrication of the 2nd generation DEP devices was achieved.
   - Development of the experimental setup (flow controllers, high speed camera, fluorescent microscopy, etc.) and cells fluorescence staining protocols to observe the movement of cells inside the channel were accomplished.
   - Testing of the 2nd generation DEP devices was performed. Trapping of imatinib and doxorubicin resistant K562 cells were achieved at the crossover frequency (48.64 MHz) of sensitive K562 cells at a flow rate of 10 µl/min and voltage magnitude of $9V_{pp}$ while sensitive cells were not trapped at the same experimental conditions.
   - Performance analyses of the 2nd generation devices were performed by changing the experimental parameters, including flow rate, voltage and cell concentration. Devices have the trapping capability up to 20 µl/min flow rate for 625000 cells/ ml. Although contactless DEP phenomenon was utilized, device has trapping capability at considerably lower voltages (5 V_{pp}) than reported in the literature for contactless DEP devices.
   - The analysis of the MDR levels using doxorubicin resistant K562 cells with varying degrees of drug resistance was achieved. 100, 300 and 500 nM doxorubicin resistant K562 cells were subjected to cell trapping analysis and the number of trapped cells was compared. Results revealed that as the degree of drug resistance increases, trapped cell number also increases. However, it was shown that this increase is not in linear trend. This can be caused by the saturation in cytoplasmic ion level or P-gp expression level. To find the real reasons, tests should be repeated and verified with biological analysis.
   - Evaluation of the consistence of experimental results with the available literature and simulations were performed. There is not any discrepancy between them.

As a future work, modification of the 2nd generation DEP device for the continuous flow separation, not trapping, of the MDR and sensitive K562 cells, with a higher sensitivity and throughput, are planned. This can be achieved by adding two outlets for the collection of sensitive and resistant cell lines, separately. The applied voltage and frequency can be adjusted through simulations, to lead the cells to different outlets without trapping. The channel width and length and electrode dimensions can be modified to obtain higher sensitivity and throughput. The inner walls of the channels can be modified with heparin to prevent blood clogging during studies with real blood. Moreover, the shape of the obstacles will be changed and air bubble formation will be prevented. Therefore, the

automatized analyses for the determination of the drug resistance degree in K562 cells can become possible. These are the short term, future studies.

In long term several other challenges need to be solved to obtain a stand-alone and portable DEP device for cancer cell detection and separation from whole blood, in a label free manner. The next generation devices should be designed to comply with the following requirements:

- Should be able to operate at higher flow rates to decrease the time-to-result in high sample volume applications,
- Should operate at low voltages to allow development of a hand-held, portable device in future,
- Device should have higher sensitivity for the separation of very low concentration of cells,
- Cells should remain viable after the separation to allow downstream molecular analysis.

Apart from the above parameters, as the final aim of such studies is to develop a portable device working on whole blood, design parameters like medium conductivity, viscosity, cell concentration, etc., should be selected to as close as possible to the blood. For example, the conductivity of buffer used in this study is much lower than that of the blood. Low conductivity was selected, as all the dielectric parameters related with K562 cells were determined at this conductivity. Increasing the conductivity of the solution may result in significant changes in the whole design and operation. Or, the designs may be modified to have buffer inlet and a mixer to adjust the conductivity. Like conductivity, fluid viscosity and cell concentration are important design considerations. For these reasons, developments of a MEMS-based DEP device for rapid and sensitive separation of cancer cells from whole blood requires major improvements and that can be solved in long time.

REFERENCES

[1] World Health Organization, from “http://www.who.int/en/”, retrieved on May 2013.

[2] M. Kermode, “Unsafe injections in low-income country health settings: need for injection safety promotion to prevent the spread of blood-borne viruses.,” *Health Promotion International*, vol. 19, no. 1, pp. 95–103, Mar. 2004.

[3] Y. Demircan, G. Yılmaz, and H. Külah, in: Microfluidic Technologies for Human Health, U. Demirci, A. Khademhosseini, R. Langer, J. Blander (Eds.), *Electrophoresis and Dielectrophoresis for Lab-on-a-Chip (LOC) Analyses*, World Scientific Publishers, 2012, ISBN-10: 9814405515 | ISBN-13: 978-9814405515.

[4] K. C. Cheung and P. Renaud, “BioMEMS in medicine: diagnostic and therapeutic systems,” *Proceedings of 35th European SolidState Device Research Conference 2005 ESSDERC 2005*, vol. 345, pp. 345–350, 2005.

[5] Y. Demircan, E. Özgür, and H. Külah, "Dielectrophoresis: Applications and future outlook in point of care", *Electrophoresis*, vol. 34, no. 7, pp. 1008-1027, Apr. 2013.

[6] R. Sista, Z. Hua, P. Thwar, A. Sudarsan, V. Srinivasan, A. Eckhardt, M. Pollack, and V. Pamula, “Development of a digital microfluidic platform for point of care testing.,” *Lab on a chip*, vol. 8, no. 12, pp. 2091–104, Dec. 2008.

[7] A. J. Tudos, G. J. Besselink, and B. M. Schasfoort, “Trends in miniaturized total analysis systems for point-of-care testing in clinical chemistry.,” *Lab on a chip*, vol. 1, no. 2, pp. 83–95, Dec. 2001.

[8] M. J. Lawrence and G. D. Rees, “Microemulsion-based media as novel drug delivery systems.,” *Advanced Drug Delivery Reviews*, vol. 45, no. 1, pp. 89–121, Dec. 2000.

[9] V. Gupta, I. Jafferji, M. Garza, V. O. Melnikova, D. K. Hasegawa, R. Pethig, and D. W. Davis, “ApoStream^{TM}, a new dielectrophoretic device for antibody independent isolation and recovery of viable cancer cells from blood,” *Biomicrofluidics*, vol. 6, no. 2, p. 024133, 2012.

[10] M. Cormier, B. Johnson, M. Ameri, K. Nyam, L. Libiran, D. D. Zhang, and P. Daddona, “Transdermal delivery of desmopressin using a coated microneedle array patch system.,” *Journal of Controlled Release*, vol. 97, no. 3, pp. 503–511, Jul. 2004.

[11] M. Pearton, V. Saller, S. A. Coulman, C. Gateley, A. V. Anstey, V. Zarnitsyn, and J. C. Birchall, “Microneedle delivery of plasmid DNA to living human skin: Formulation coating, skin insertion and gene expression,” *Journal of Controlled Release*, vol. 160, no. 3, pp. 1–9, Jun. 2012.

[12] M. A. Burns, B. N. Johnson, S. N. Brahmasandra, K. Handique, J. R. Webster, M. Krishnan, T. S. Sammarco, P. M. Man, D. Jones, D. Heldsinger, C. H. Mastrangelo, and D. T. Burke, “An integrated nanoliter DNA analysis device.,” *Science*, vol. 282, no. 5388, pp. 484–487, Oct. 1998.

[13] J. T. Lin, "Cell manipulations with dielectrophoresis", Waterloo, Orlando, Canada, 2007.

[14] Y. D. Jung, "Microfabricated continuous flow separation and manipulation systems for human whole blood", Georgia Institute of Technology, Atlanta, USA, 2010.

[15] H. Maruyama, S. Sakuma, Y. Yamanishi, and F. Arai, “Size-dependent filtration and trapping of microparticle in a microfluidic chip using centrifugal force and a graduated mechanical gap,” *2009 IEEESICE International Symposium on System Integration SII*, vol. 22, no. 3, pp. 7–12, 2009.

[16] D. Di Carlo, D. Irimia, R. G. Tompkins, and M. Toner, “Continuous inertial focusing, ordering, and separation of particles in microchannels.,” *Proceedings of the National Academy of Sciences of the United States of America*, vol. 104, no. 48, pp. 18892–7, 2007.

[17] A. J. Mach and D. Di Carlo, “Continuous scalable blood filtration device using inertial microfluidics.,” *Biotechnology and bioengineering*, vol. 107, no. 2, pp. 302–11, Oct. 2010.

[18] M. Zborowski, G. R. Ostera, L. R. Moore, S. Milliron, J. J. Chalmers, and A. N. Schechter, “Red Blood Cell Magnetophoresis,” *Biophysical Journal*, vol. 84, no. 4, pp. 2638–2645, Apr. 2003.

[19] K.-H. H. K.-H. Han and B. Frazier, “Paramagnetic capture mode magnetophoretic microseparator for blood cells.,” *IEE proceedings Nanobiotechnology*, vol. 153, no. 6, pp. 67–73, 2006.

[20] J. Jung, S.-K. Seo, Y.-D. Joo, and K.-H. Han, “Label-free continuous lateral magneto-dielectrophoretic microseparators for highly efficient enrichment of circulating nucleated cells from peripheral blood,” *Sensors and Actuators B: Chemical*, vol. 157, no. 1, pp. 314–320, Sep. 2011.

[21] N. Pamme and C. Wilhelm, “Continuous sorting of magnetic cells via on-chip free-flow magnetophoresis.,” *Lab on a Chip*, vol. 6, no. 8, pp. 974–980, Aug. 2006.

[22] H. Lee, Y. Liu, S. Member, R. M. Westervelt, and D. Ham, “IC / Microfluidic Hybrid System for Magnetic Manipulation of Biological Cells,” vol. 41, no. 6, pp. 1471–1480, 2006.

[23] D. Robert, N. Pamme, H. Conjeaud, F. Gazeau, A. Iles, and C. Wilhelm, “Cell sorting by endocytotic capacity in a microfluidic magnetophoresis device.,” *Lab on a Chip*, vol. 11, no. 11, pp. 1902–1910, Jun. 2011.

[24] Z. Chen, G. Hong, H. Wang, K. Welsher, S. M. Tabakman, S. P. Sherlock, J. T. Robinson, Y. Liang, and H. Dai, “Graphite-coated magnetic nanoparticle microarray

for few-cells enrichment and detection.," *ACS nano*, vol. 6, no. 2, pp. 1094–101, 2012.

[25] H. A. Rendall, R. F. Marchington, b. B. Praveen, G. Bergmann, Y. Arita, A. Heisterkamp, F. J. Gunnmoore, and K. Dholakia, "High-throughput optical injection of mammalian cells using a Bessel ligth beam. ", *Lab Chip*, vol. 12, pp. 4816-4820, 2012.

[26] L. Paterson, M.P. MacDnald, J. Arlt, W. sibbett, P. E. Bryant and K. Dholakia, "Controlled rotation of optically trapped microscopic particles.", *Science*, vol. 292, pp. 912-914, 2001.

[27] Y. Y. Sun, X.-C. Yuan, L. S. Ong, J. Bu, S. W. Zhu, and R. Liu, "Large-scale optical traps on a chip for optical sorting," *Applied Physics Letters*, vol. 90, no. 3, p. 031107, 2007.

[28] M. Ozkan, M. Wang, C. Ozkan, R. Flynn, A. Birkbeck, and S. Esener, "Optical Manipulation of Objects and Biological Cells in Micro ¯ uidic Devices," *Electrical Engineering*, vol. 5, no. 1, pp. 61–67, 2003.

[29] S. Sato, M. Ishıgure and H. Inaba, "Optical trapping and rotational manipulation of microscopic particles and biological cells using higher-order mode Nd.:Yag laser beams.", *Electronics Letters*, vol. 27, pp. 1831–1832, 1991.

[30] R. W. Applegate, J. Squier, T. Vestad, J. Oakey, D. W. M. Marr, P. Bado, M. Dugan, and A. Said, "Microfluidic sorting system based on optical waveguide integration and diode laser bar trapping.," *Lab on a Chip*, vol. 6, no. 3, pp. 422–426, Mar. 2006.

[31] M. M. Wang, E. Tu, D. E. Raymond, J. M. Yang, H. Zhang, N. Hagen, B. Dees, E. M. Mercer, A. H. Forster, I. Kariv, P. J. Marchand, and W. F. Butler, "Microfluidic sorting of mammalian cells by optical force switching.," *Nature Biotechnology*, vol. 23, no. 1, pp. 83–87, Jan. 2005.

[32] Y.-H. Lin and G.-B. Lee, "Optically induced flow cytometry for continuous microparticle counting and sorting.," *Biosensors & bioelectronics*, vol. 24, no. 4, pp. 572–8, Dec. 2008.

[33] J. J. Hawkes and W. T. Coakley, "Force field particle filter, combining ultrasound standing waves and laminar flow.", *Sensors and Actuators B*, vol. 75, pp. 213–222, 2001.

[34] F. Petersson, L. Aberg, A.-M. Swärd-Nilsson, and T. Laurell, "Free flow acoustophoresis: Microfluidic-based mode of particle and cell separation.", *Analytical Chemistry*, vol. 79, no. 14, pp. 5117–5123, 2007.

[35] F. Petersson, A. Nilsson, C. Holm, H. Jonsson, and T. Laurell, "Continuous separation of lipid particles from erythrocytes by means of laminar flow and acoustic standing wave forces.", *Lab on a Chip*, vol. 5, no. 1, pp. 20–22, Jan. 2005.

[36] P. Y. Kwok, "Single nucleotide polymorphism: Methods and protocols.", Humana Press, 2003.

[37] S. I. Dirks-Go and H. C. Zanen, “Latex agglutination, counterimmunoelectrophoresis, and protein A co-agglutination in diagnosis of bacterial meningitis.,” *Journal of Clinical Pathology*, vol. 31, no. 12, pp. 1167–1171, 1978.

[38] S. Sukas, "Design and fabrication of a DNA electrophoresis chip based on MEMS technology", METU, 2007.

[39] H. Pohl, “The Motion and Precipitation of Suspensoids in Divergent Electric Fields,” *Journal of Applied Physics*, vol. 22, no. 7, p. 869, 1951.

[40] R. Pethig, “Review article-dielectrophoresis: status of the theory, technology, and applications.,” *Biomicrofluidics*, vol. 4, no. 2, Jan. 2010.

[41] H. Shafiee, M. B. Sano, E. Henslee, J. L. Caldwell, and R. V Davalos, “Selective isolation of live/dead cells using contactless dielectrophoresis (cDEP).,” *Lab on a chip*, vol. 10, no. 4, pp. 438–45, Feb. 2010.

[42] T. Heida, W. L. Rutten, and E. Marani, “Dielectrophoretic trapping of dissociated fetal cortical rat neurons.,” *IEEE transactions on bio-medical engineering*, vol. 48, no. 8, pp. 921–30, Aug. 2001.

[43] P. Zellner, A. Sahari, Y. Hosseini, B. Behkam, and M. Agah, “Selective E. coli trapping with 3D insulator-based dielectrophoresis using DC-biased, AC electric fields.,” *Conference proceedings : Annual International Conference of the IEEE Engineering in Medicine and Biology Society. IEEE Engineering in Medicine and Biology Society. Conference*, vol. 2012, pp. 6285–6288, Jan. 2012.

[44] L. Yang, “Dielectrophoresis assisted immuno-capture and detection of foodborne pathogenic bacteria in biochips.,” *Talanta*, vol. 80, no. 2, pp. 551–8, Dec. 2009.

[45] F. Yang, X. Yang, H. Jiang, P. Bulkhaults, P. Wood, W. Hrushesky, and G. Wang, “Dielectrophoretic separation of colorectal cancer cells.”, *Biomicrofluidics*, vol. 4, pp. 013204–1-013204-13, 2010.

[46] A. Y. Wu and D. M. Morrow, “Clinical use of Dieletrophoresis separation for live Adipose derived stem cells.,” *Journal of translational medicine*, vol. 10, no. 1, p. 99, Jan. 2012.

[47] M. Eguchi, H. Imasato, and T. Yamakawa, “Separation of Blood Cells by Employing Dielectrophoresis and Traveling-wave Electric Fields,” pp. 1–6, 2012.

[48] S. H. Ling, Y. C. Lam, and K. S. Chian, “Continuous cell separation using dielectrophoresis through asymmetric and periodic microelectrode array.,” *Analytical chemistry*, vol. 84, no. 15, pp. 6463–70, Aug. 2012.

[49] W. Braff, A. Pignier, and C. R. Buie, “High sensitivity three-dimensional insulator-based dielectrophoresis.,” *Lab on a chip*, vol. 12, no. 7, pp. 1327–31, Apr. 2012.

[50] C. Yu, J. Vykoukal, D. M. Vykoukal, J. A. Schwartz, L. Shi, P. R. C. Gascoyne, and I. T. Cytometry, “A Three-Dimensional Dielectrophoretic Particle Focusing Channel for Microcytometry Applications,” vol. 14, no. 3, pp. 480–487, 2005.

[51] K. Asami, “Dielectric dispersion in biological cells of complex geometry simulated by the three-dimensional finite difference method,” *Journal of Physics D: Applied Physics*, vol. 39, no. 3, pp. 492–499, Feb. 2006.

[52] V. Raicu, T. Sibara, H. Enzan, and A. Irimajiri, "Dielectric properties of rat liver in vivo: Analysis by modeling hepatocytes in the tissue architecture. ", *Bioelectrochemistry and Bioenergetics*, vol. 47, pp. 333-342, Sep 1998.

[53] K.-H. Han and B. Frazier, “Lateral-driven continuous dielectrophoretic microseparators for blood cells suspended in a highly conductive medium.,” *Lab on a chip*, vol. 8, no. 7, pp. 1079–86, Jul. 2008.

[54] M. S. Pommer, Y. Zhang, N. Keerthi, D. Chen, J. Thomson, C. D. Meinhart, and H. T. Soh, “Dielectrophoretic separation of platelets from diluted whole blood in microfluidic channels.,” *Electrophoresis*, vol. 29, no. 6, pp. 1213–1218, Mar. 2008.

[55] N. Piacentini, G. Mernier, R. Tornay, and P. Renaud, “Separation of platelets from other blood cells in continuous-flow by dielectrophoresis field-flow-fractionation.,” *Biomicrofluidics*, vol. 5, no. 3, pp. 34122–341228, Sep. 2011.

[56] S.-I. Han, S.-M. Lee, Y.-D. Joo, and K.-H. Han, “Lateral dielectrophoretic microseparators to measure the size distribution of blood cells.,” *Lab on a chip*, vol. 11, no. 22, pp. 3864–72, Nov. 2011.

[57] Y. Nakashima, S. Hata, and T. Yasuda, “Blood plasma separation and extraction from a minute amount of blood using dielectrophoretic and capillary forces,” *Sensors and Actuators B: Chemical*, vol. 145, no. 1, pp. 561–569, Mar. 2010.

[58] M.-W. Wang, K.-S. Jeng, M.-C. Yu, and J.-C. Su, “Using a Microfluidic–Microelectric Device to Directly Separate Serum/Blood Cells from a Continuous Whole Bloodstream Flow,” *Japanese Journal of Applied Physics*, vol. 51, p. 037002, Feb. 2012.

[59] S. K. Srivastava, P. R. Daggolu, S. C. Burgess, and A. R. Minerick, “Dielectrophoretic characterization of erythrocytes: positive ABO blood types.,” *Electrophoresis*, vol. 29, no. 24, pp. 5033–46, Dec. 2008.

[60] M. Borgatti, N. Bianchi, I. Mancini, G. Feriotto, and R. Gambari, “New trends in non-invasive prenatal diagnosis : Applications of dielectrophoresis-based Lab-on-a-chip platforms to the identification and manipulation of rare cells (Review),” pp. 3–12, 2008.

[61] G. H. Markx, Y. Huang, X. Zhou, and R. Pethig, "Dielectrophoretic characterization and separation of micro-orgaisnms.", *Microbiology*, vol. 140, pp. 585-591, 1994.

[62] R. Zhou, P. Wang, and H.-C. Chang, “Bacteria capture, concentration and detection by alternating current dielectrophoresis and self-assembly of dispersed single-wall carbon nanotubes.,” *Electrophoresis*, vol. 27, no. 7, pp. 1376–85, Apr. 2006.

[63] C. H. Chou and F. Zenhausern, “Electrodeless Dielectrophoresis for Micro Total Analysis Systems.”, *Micro- & Nanoelectrokinetics*, pp. 62–67, Dec. 2003.

[64] M. P. Hughes, H. Morgan, F. J. Rixon, J. P. Burt, and R. Pethig, “Manipulation of herpes simplex virus type 1 by dielectrophoresis.,” *Biochimica et biophysica acta*, vol. 1425, no. 1, pp. 119–26, Sep. 1998.

[65] H. Maruyama, K. Kotani, T. Masuda, A. Honda, T. Takahata, and F. Arai, “Nanomanipulation of single influenza virus using dielectrophoretic concentration and optical tweezers for single virus infection to a specific cell on a microfluidic chip,” *Microfluidics and Nanofluidics*, vol. 10, no. 5, pp. 1109–1117, Dec. 2010.

[66] M. P. Hughes, H. Morgan, and F. J. Rixon, “Dielectrophoretic manipulation and characterization of herpes simplex virus-1 capsids,” *European Biophysics Journal*, vol. 30, no. 4, pp. 268–272, Aug. 2001.

[67] P. R. C. Gascoyne, J. Noshari, T. J. Anderson, and F. F. Becker, “Isolation of rare cells from cell mixtures by dielectrophoresis.,” *Electrophoresis*, vol. 30, no. 8, pp. 1388–98, Apr. 2009.

[68] A. C. Sabuncu, J. a Liu, S. J. Beebe, and A. Beskok, “Dielectrophoretic separation of mouse melanoma clones.,” *Biomicrofluidics*, vol. 4, no. 2, pp. 1–7, Jan. 2010.

[69] L. Altomare, M. Borgatti, G. Medoro, N. Manaresi, M. Tartagni, R. Guerrieri, and R. Gambari, “Levitation and movement of human tumor cells using a printed circuit board device based on software-controlled dielectrophoresis.,” *Biotechnology and bioengineering*, vol. 82, no. 4, pp. 474–9, May 2003.

[70] J. Yang, Y. Huang, X. B. Wang, F. F. Becker, and P. R. Gascoyne, “Differential analysis of human leukocytes by dielectrophoretic field-flow-fractionation.,” *Biophysical journal*, vol. 78, no. 5, pp. 2680–9, May 2000.

[71] H. Imasato and T. Yamakawa, "Separation of leukemia cells from blood by employing dielectrophoresis.", *World Automation Congress*, 2010. .

[72] E. Henslee, M. B. Sano, A. D. Rojas, E. M. Schmelz, and R. V Davalos, “Selective concentration of human cancer cells using contactless dielectrophoresis.,” *Electrophoresis*, vol. 32, no. 18, pp. 2523–9, Sep. 2011.

[73] J. Lee and Y. Kim, “Negative - dielectrophoresis separation modules based high throughput and high efficient cell sorting platform for leukemia cell,” pp. 3–6, 2011.

[74] L. M. Broche, N. Bhadal, M. P. Lewis, S. Porter, M. P. Hughes, and F. H. Labeed, “Early detection of oral cancer - Is dielectrophoresis the answer?,” *Oral oncology*, vol. 43, no. 2, pp. 199–203, Feb. 2007.

[75] F. F. Becker, X. B. Wang, Y. Huang, R. Pethig, J. Vykoukal, and P. R. Gascoyne, “Separation of human breast cancer cells from blood by differential dielectric affinity.,” *Proceedings of the National Academy of Sciences of the United States of America*, vol. 92, no. 3, pp. 860–4, Jan. 1995.

[76] K.-H. Han, A. Han, and B. Frazier, “Microsystems for isolation and electrophysiological analysis of breast cancer cells from blood.,” *Biosensors & bioelectronics*, vol. 21, no. 10, pp. 1907–14, Apr. 2006.

[77] J. An, J. Lee, S. H. Lee, J. Park, and B. Kim, “Separation of malignant human breast cancer epithelial cells from healthy epithelial cells using an advanced dielectrophoresis-activated cell sorter (DACS).,” *Analytical and bioanalytical chemistry*, vol. 394, no. 3, pp. 801–9, Jun. 2009.

[78] Y. J. Lo, U. Lei, and P. C. Yang, “Selective separation and isolation of particles/cells of similar sizes using dielectrophoresis.", *15th International conference on Miniaturized Systems for chemistry and Life Sciences*, pp. 532–534, 2011.

[79] A. Salmanzadeh, H. Kittur, M. B. Sano, P. C Roberts, E. M. Schmelz, and R. V Davalos, “Dielectrophoretic differentiation of mouse ovarian surface epithelial cells, macrophages, and fibroblasts using contactless dielectrophoresis.,” *Biomicrofluidics*, vol. 6, no. 2, pp. 24104–2410413, Jun. 2012.

[80] C.-P. Jen, H.-H. Chang, C.-T. Huang, and K.-H. Chen, “A microfabricated module for isolating cervical carcinoma cells from peripheral blood utilizing dielectrophoresis in stepping electric fields,” *Microsystem Technologies*, vol. 18, no. 11, pp. 1887–1896, Apr. 2012.

[81] A. Salmanzadeh, L. Romero, H. Shafiee, R. C. Gallo-Villanueva, M. Stremler, S. D. Cramer, and R. V Davalos, “Isolation of prostate tumor initiating cells (TICs) through their dielectrophoretic signature.,” *Lab on a chip*, vol. 12, no. 1, pp. 182–9, Jan. 2012.

[82] R. Pethig, L. M. Jakubek, R. H. Sanger, E. Heart, E. D. Corson, and P. J. S. Smith, “Electrokinetic measurements of membrane capacitance and conductance for pancreatic b-cells.”, *IEEE Proc. Nanobiotechnology*, vol. 152, pp. 189–193, 1801.

[83] L. Flanagan, J. Lu, L. Wang, S. Marchenko, N. L. Jeon, A. P. Lee, and E. S. Monuki, “Unique dielectric properties distinguish stem cells and their differentiated progeny.,” *Stem cells (Dayton, Ohio)*, vol. 26, no. 3, pp. 656–65, Mar. 2008.

[84] M. S. Talary, K. I. Mills, T. Hoy, K. Burnett, and R. Pethig, “Dielectrophoretic separation and enrichment of $CD34^+$ cell subpopulation from bone marrow and peripheral blood stem cells.,” *Medical & biological engineering & computing*, vol. 33, no. 2, pp. 235–7, Mar. 1995.

[85] S. Agarwal, A. Sebastian, L. M. Forrester, and G. H. Markx, “Formation of embryoid bodies using dielectrophoresis.,” *Biomicrofluidics*, vol. 6, no. 2, pp. 24101–2410111, Jun. 2012.

[86] K. Ratanachoo, P. R. C. Gascoyne, and M. Ruchirawat, “Detection of cellular responses to toxicants by dielectrophoresis.,” *Biochimica et biophysica acta*, vol. 1564, no. 2, pp. 449–58, Aug. 2002.

[87] Y. Huang, J. Yang, X. Wang, F. F. Becker and P. R. C. Gascoyne, " The removal of human breast cancer cells from hematopoietic $CD34^{+}$ stem cells by dielectrophoretic field flow fractionation. ", *J. Hematother Stem Cell Research*, vol. 8, no. 5, pp. 481–490, 2009.

[88] H. Shafiee, J. L. Caldwell, M. B. Sano, and R. V Davalos, “Contactless dielectrophoresis: a new technique for cell manipulation.,” *Biomedical microdevices*, vol. 11, no. 5, pp. 997–1006, Oct. 2009.

[89] H. Moncada-Hernández and B. H. Lapizco-Encinas, “Simultaneous concentration and separation of microorganisms: insulator-based dielectrophoretic approach.,” *Analytical and bioanalytical chemistry*, vol. 396, no. 5, pp. 1805–1816, Mar. 2010.

[90] H. Moncada-Hernandez, J. L. Baylon-Cardiel, V. H. Pérez-González, and B. H. Lapizco-Encinas, “Insulator-based dielectrophoresis of microorganisms: theoretical and experimental results.,” *Electrophoresis*, vol. 32, no. 18, pp. 2502–2511, Sep. 2011.

[91] M. A. Miled, S. Member, and M. Sawan, “Dielectrophoresis-Based Integrated Lab-on-Chip for Nano and Micro-Particles Manipulation and Capacitive Detection,” vol. 6, no. 2, pp. 120–132, 2012.

[92] W. Qiao, G. Cho, and Y.-H. Lo, “Wirelessly powered microfluidic dielectrophoresis devices using printable RF circuits.,” *Lab on a chip*, vol. 11, no. 6, pp. 1074–80, Mar. 2011.

[93] J. M. Yang, J. Bell, Y. Huang, M. Tirado, D. Thomas, A. H. Forster, R. W. Haigis, P. D. Swanson, R. B. Wallace, B. Martinsons, and M. Krihak, “An integrated, stacked microlaboratory for biological agent detection with DNA and immunoassays.,” *Biosensors & Bioelectronics*, vol. 17, no. 6–7, pp. 605–18, Jun. 2002.

[94] I.-F. Cheng, C.-C. Lin, D.-Y. Lin, and H.-C. Chang, “A dielectrophoretic chip with a roughened metal surface for on-chip surface-enhanced Raman scattering analysis of bacteria.,” *Biomicrofluidics*, vol. 4, no. 3, Jan. 2010.

[95] P. Gascoyne, C. Mahidol, M. Ruchirawat, J. Satayavivad, P. Watcharasit, and F. F. Becker, “Microsample preparation by dielectrophoresis: isolation of malaria.,” *Lab on a chip*, vol. 2, no. 2, pp. 70–75, May 2002.

[96] A. Salmanzadeh, H. Kittur, M. B. Sano, P. C Roberts, E. M. Schmelz, and R. V Davalos, “Dielectrophoretic differentiation of mouse ovarian surface epithelial cells, macrophages, and fibroblasts using contactless dielectrophoresis.,” *Biomicrofluidics*, vol. 6, no. 2, pp. 24104–2410413, Jun. 2012.

[97] F. H. Labeed, H. M. Coley, H. Thomas, and M. P. Hughes, “Assessment of multidrug resistance reversal using dielectrophoresis and flow cytometry.,” *Biophysical journal*, vol. 85, no. 3, pp. 2028–34, Sep. 2003.

[98] J. Vykoukal, D. M. Vykoukal, S. Freyberg, E. U. Alt and P. R. C. Gascoyne, "Enrichment of putative stem cells from adipose tissue using dielectrophoretic field flow fractionation.", *Lab chip*, vol. 8, no. 8, pp. 1386–1393, 2009.

[99] J. Zhou (Ed.), "Multi-Drug resistance in cancer", *Humana Press*, 2010.

[100] Solvo Biotech., from “http://www.solvobiotech.com/”, retrieved on May 2013 .

[101] S. Chin, M. P. Hughes, H. M. Coley, and F. H. Labeed, “Rapid assessment of early biophysical changes in K562 cells during apoptosis determined using dielectrophoresis,” *International journal of nanomedicine*, vol. 1, no. 3, pp. 333–337, 2006.

[102] L. Duncan, H. Shelmerdine, M. P. Hughes, H. M. Coley, Y. Hübner, and F. H. Labeed, “Dielectrophoretic analysis of changes in cytoplasmic ion levels due to ion channel blocker action reveals underlying differences between drug-sensitive and multidrug-resistant leukaemic cells.,” *Physics in medicine and biology*, vol. 53, no. 2, pp. N1–7, Jan. 2008.

[103] A. Ogbi, L. Nicolas, R. Perrussel, S. J. Salon, D. Voyer, L. Ampère, C. Umr, U. De Lyon, and É. C. De Lyon, “Numerical Identification of Effective Multipole Moments of Polarizable Particles,” vol. 48, no. 2, pp. 675–678, 2012.

[104] T. B. Jones., "Basic Theory of dielectrophoresis and electrorotation.", *Micro- & Nanoelectrokinetics*, pp. 33–42, Dec. 2003.

[105] Y. Demircan, A. Koyuncuoğlu, M. Erdem, E. Özgür, U. Gündüz, and H. Külah, "Detection of imatinib resistance in K562 leukemia cells by 3D-electrode contactless dielectrophoresis", *Solid-State Sensors, Actuators and Microsystems Conference: Transducers 2013* (In press).

[106] S. S. Saliterman, "BioMEMS and medical microdevices.",SPIE Press, Bellingham, Washington, USA, 2006

[107] B. J. Kirby, "Micro- and nanoscale fluid mechanics", *Cambridge University Press*, 2010.

[108] B. Cetin and D. Li, “Dielectrophoresis in microfluidics technology.,” *Electrophoresis*, vol. 32, no. 18, pp. 2410–27, Sep. 2011.

[109] A. Kumar, Z. Qiu, A. Acrivos, B. Khusid, and D. Jacqmin, “Combined negative dielectrophoresis and phase separation in nondilute suspensions subject to a high-gradient ac electric field,” *Physical Review E*, vol. 69, no. 2, p. 021402, Feb. 2004.

[110] J. Wood and A. Docoslis, “AC electrokinetic templating of colloidal particle assemblies: effect of electrohydrodynamic flows.,” *Langmuir : the ACS journal of surfaces and colloids*, vol. 28, no. 9, pp. 4586–97, Mar. 2012.

[111] K. Khoshmanesh, S. Nahavandi, S. Baratchi, A. Mitchell, and K. Kalantar-zadeh, “Dielectrophoretic platforms for bio-microfluidic systems.,” *Biosensors & Bioelectronics*, vol. 26, no. 5, pp. 1800–14, Jan. 2011.

[112] D. A. Borkholder, "Cell based biosensors using microelectrodes", Stanford, 1998.

[113] G. Karp, "Cell and molecular biology", *Wiley& Sons Inc.*, USA, 2008.

[114] Y. Huang, R. Hölzel, R. Pethig, and X. B. Wang, “Differences in the AC electrodynamics of viable and non-viable yeast cells determined through combined dielectrophoresis and electrorotation studies.,” *Physics in medicine and biology*, vol. 37, no. 7, pp. 1499–517, Jul. 1992.

[115] Y. Demircan and H. Külah, " A Parylene Based Contactless 3D Dielectrophoresis Chip for Continuous Cell Separation, Trapping, and Manipulation Applications,” *Microfluidics 2012*, p. 109, Heidelberg, Germany, 2012.

[116] F. H. Labeed, H. M. Coley, H. Thomas, and M. P. Hughes, “Assessment of multidrug resistance reversal using dielectrophoresis and flow cytometry.,” *Biophysical journal*, vol. 85, no. 3, pp. 2028–34, Sep. 2003.

[117] C. Iliescu, G. Tresset, L. Yu, and G. Xu, “3D Dielectrophoretic Chips : Trapping and Separation of Cell Populations,” vol. 13, no. 1, pp. 49–64, 2010.

[118] G. Yılmaz, "Design and implementation of a MEMS based spiral channel dielectrophoretic separator for cytometry applications.", METU, 2010.

[119] LabSmith, " http://labsmith.com/", May 2013.

[120] M. B. Sano, J. L. Caldwell, and R. V Davalos, “Modeling and development of a low frequency contactless dielectrophoresis (cDEP) platform to sort cancer cells from dilute whole blood samples.,” *Biosensors & bioelectronics*, vol. 30, no. 1, pp. 13–20, Dec. 2011.

APPENDIX A

MATLAB CODES FOR CELL MODELING

MATLAB function utilized for the triple shell cell modeling of viable and nonviable yeast cell is the following:

```
function
out=CM_with_effective_multiple(a_wall,a_memb,a_cyto,eps_wall,eps_me
mb,eps_cyto,s_wall,s_memb,s_cyto,eps_m,s_m)

r1=(a_memb/a_cyto)^3;
r2=(a_wall/a_memb)^3;

f=logspace(0,10,10000);
w=2*pi*f;

for k=1:10000

    eps_cyto_comp=(eps_cyto-(i*(s_cyto/w(1,k))));
    eps_memb_comp=(eps_memb-(i*(s_memb/w(1,k))));
    eps_wall_comp=(eps_wall-(i*(s_wall/w(1,k))));

    eps_med_comp=(eps_m-(i*(s_m/w(1,k))));

    num_1=(eps_cyto_comp-eps_memb_comp);
    den_1=(eps_cyto_comp+(2*eps_memb_comp));

    par_1=(num_1/den_1);

    eps_eff_1=eps_memb_comp*((r1+(2*par_1))/(r1-par_1));

    num_2=(eps_eff_1-eps_wall_comp);
    den_2=(eps_eff_1+(2*eps_wall_comp));

    par_2=(num_2/den_2);

    eps_eff_2=eps_wall_comp*((r2+(2*par_2))/(r2-par_2));

    CM=real((eps_eff_2-eps_med_comp)/(eps_eff_2+(2*eps_med_comp)));

    out(1,k)=CM;
end

plot(log10(f(1,:)),out(1,:));
xlabel('Frequency 10^x (Hz)');
ylabel('Re(f_C_M)');
```

```
title('Frequency vs Re(f_C_M)');
grid on;
end
```

MATLAB function utilized for the double shell cell modeling of doxorubicin and imatinib resistant K562 cells is the following:

```
function
out=CM_with_effective_final(a_long,a_short,eps_i,eps_o,s_i,s_o,eps_
m,s_m)

r=(a_long/a_short)^3;

f=logspace(0,9,100000);
w=2*pi*f;

for k=1:100000

    eps_1_comp=(eps_i-(i*(s_i/w(1,k))));
    eps_2_comp=(eps_o-(i*(s_o/w(1,k))));
    eps_med_comp=(eps_m-(i*(s_m/w(1,k))));

    num=(eps_1_comp-eps_2_comp);
    den=(eps_1_comp+(2*eps_2_comp));

    par=(num/den);

    eps_eff_p=(eps_2_comp)*((r+(2*par))/(r-par));


    CM=real((eps_eff_p-eps_med_comp)/(eps_eff_p+(2*eps_med_comp)));

    out(1,k)=CM;
end

p=plot(log10(f(1,:)),out(1,:));
xlabel('Frequency 10^x (Hz)');
ylabel('Re(f_C_M)');
title('Frequency vs Re(f_C_M)');
set(p,'Color','blue');
end
```

APPENDIX B

SIMULATIONS IN MATLAB

Re(F_{CM}) vs. frequency characteristics of doxorubicin resistant K562 cells in various media with different conductivities: 0.25, 2.5 and 25 mS/m focusing on the high frequency region is presented in the following figure.

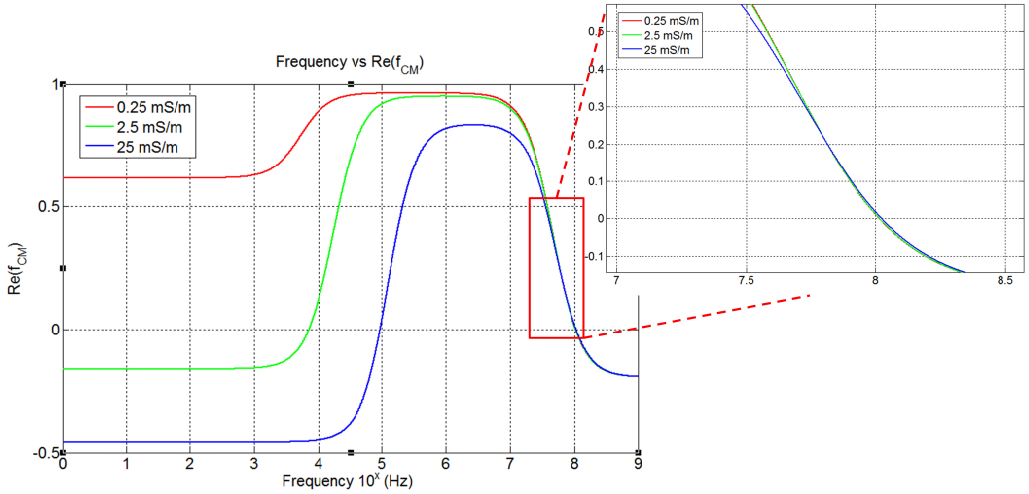


Figure B. 1: *Re(F_{CM})* vs. frequency characteristics of doxorubicin resistant K562 cells in various media with different conductivities: 0.25, 2.5 and 25 mS/m.

Figure B.2 and B.3 present the *Re(F_{CM})* vs. frequency characteristics of doxorubicin resistant and sensitive K562 cells in two media with different conductivities: 25 mS/m and 0.25 mS/m, respectively.

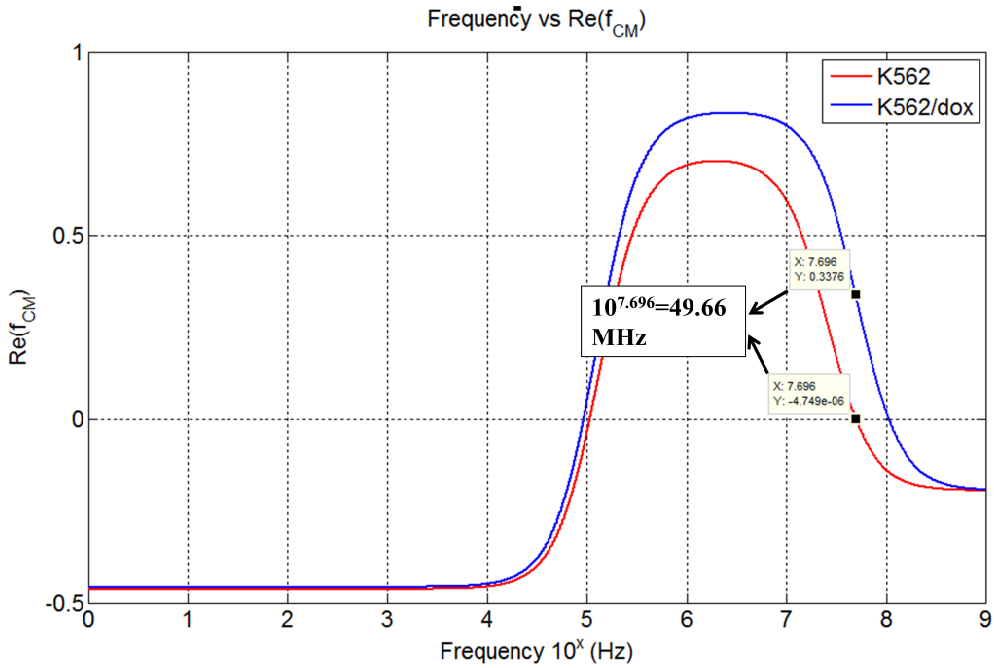


Figure B.2: *Re(F_{CM})* vs. frequency characteristics of doxorubicin resistant and sensitive K562 cells in the medium with a conductivity of 25 mS/m.

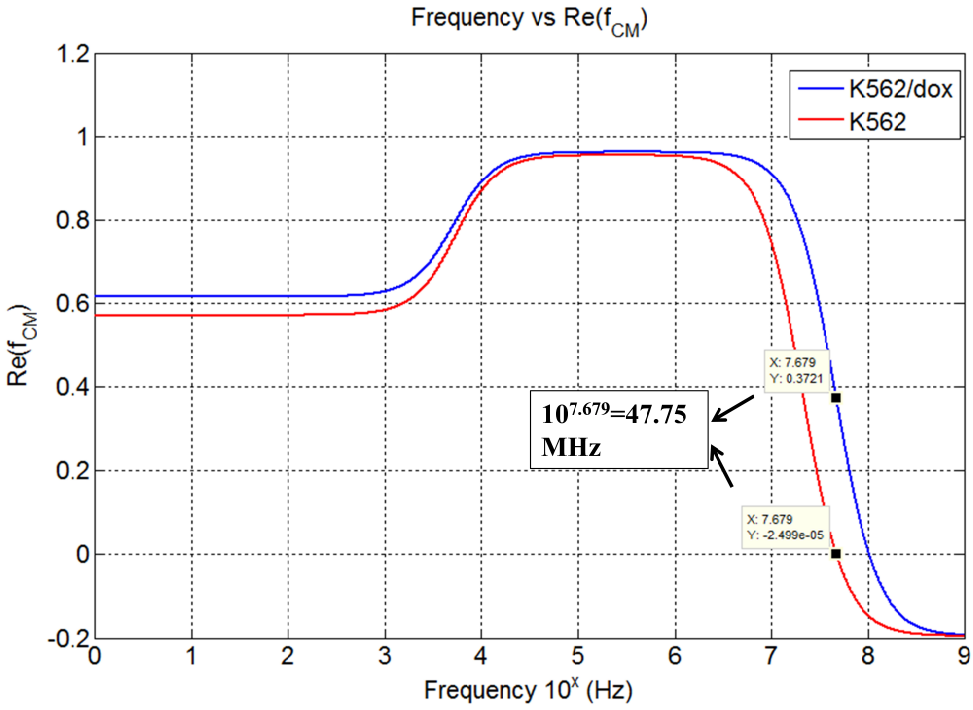


Figure B.3: *Re(F_{CM})* vs. frequency characteristics of doxorubicin resistant and sensitive K562 cells in the medium with a conductivity of 0.25 mS/m.

APPENDIX C

PROCESS FLOW

Fabrication flow of 1st generation devices is presented in Table C.1.

Table C.1: Detailed fabrication flow of the 1st generation devices.

	1st generation devices fabrication flow
1	***Glass wafer (4")***
2	***Dehydration at oven at 110°C for 10 min***
3	***Parylene coating***
	with silane
	4 g for 2 μm parylene thickness
4	***Dehydration at oven at 95°C for 10 min***
5	***Ti sputtering as adhesion layer (~20nm) (BESTEC)***
	300 W T1:120s T2:70s Distance:135mm Flow:2.5sccm
6	***Au sputtering layer (~400 nm) (BESTEC)***
	300 W T1:120s T2:400s Distance:130mm Flow:6.2sccm
7	***Dehydration at oven at 95°C for 10 min***
8	***Lithography for Au & Ti etch***
Mask 1	HDMS coating 500 rpm 7s + 3000 rpm 30s
	S1813 500 rpm 7s + 4000 rpm 30s
	Softbake @ 95°C for 70 s hotplate
	Expose UV for 6s vacuum+hard contact
	Develop in MF 319 for 1min
	DI water rinse 1.5min+1.5min
	Dry by N_2
	Inspection
	Hardbake at oven @ 95°C for 20 min
	Desicator for 5 min
9	***Au etch***
	Commercial Au etchant for 1.5 min
	DI water rinse 3 cycles
	Dry by N_2
	Inspection
10	***Ti etch***
	10ml HF+10ml H_2O_2+80ml DI water as Ti etchant

Table C1 (continued).

	Ti etchant for 30s
11	***Strip photoresist***
	Acetone for 30min
	DI water rinse 3 cycles
	Dry by N_2
	Inspection
12	***Dehydration at oven at 95°C for 10 min***
13	***Lithography for Cu-electroplating and microchannel formation***
Mask 2	HDMS coating 500 rpm 7s + 3000 rpm 30s
	AZ9260 300 rpm 10s + 800 rpm 30s
	Edge bead removal
	Wait for 15min
	Hardbake at oven from room temperature to 95°C and 50min @ 95°C
	Cooling at oven from 95°C to 70°C
	Rehydration (3 pipettes of DI water in blue box, overnight)
	Expose UV for 50s vacuum+hard contact
	Develop in AZ 826MIF for 15min
	DI water rinse 1.5min+1.5min
	Dry by N_2
	Inspection
14	***Cu electroplating***
	50 mA 0.3-0.7 duty cycle 90min for 15 μm Cu thickness
15	***Parylene coating***
	without silane
	40 g for 20 μm parylene thickness
16	***Opening lithography***
Mask 3	HDMS coating 500 rpm 7s + 3000 rpm 30s
	AZ9260 500 rpm 10 s + 750 rpm 20s
	Edge bead removal
	Wait for 15min
	Prebake @ 95°C for 3min at hotplate
	AZ9260 500 rpm 10 s + 750 rpm 20s
	Edge bead removal
	Wait for 15min
	Hardbake at oven from room temperature to 95°C and 50min @ 95°C
	Cooling at oven from 95°C to 70°C
	Rehydration (3 pipettes of DI water in blue box, overnight)
	Expose UV for 55s vacuum+hard contact
	Develop in AZ 826MIF for 30min
	DI water rinse 1.5min+1.5min

Table C1 (continued).

	Dry by N_2
	Expose UV for 55s vacuum+hard contact
	Develop in AZ 826MIF for 20min
	Dry by N_2
	Inspection
17	***Parylene etching with RIE***
	In RIE (20min+20min+20min)
	Inspection
18	***Dicing***
19	***Strip photoresist***
	Acetone for 2 days
20	***Parylene coating for insulation***
	with silane
	0.6 g for ~0.3 μm

Fabrication flow of 1st generation devices is presented in Table C.2.

Table C.2: Detailed fabrication flow of the 2nd generation devices.

	2nd generation devices fabrication flow
1	***Glass wafer (4")***
2	***Dehydration at oven at 110°C for 10 min***
3	***Parylene coating***
	with silane
	4 g for 2 μm parylene thickness
4	***Dehydration at oven at 95°C for 10 min***
5	***Ti sputtering as adhesion layer (~20nm) (BESTEC)***
	300 W T1:120s T2:70s Distance:135mm Flow:2.5sccm
6	***Au sputtering layer (~400 nm) (BESTEC)***
	300 W T1:120s T2:400s Distance:130mm Flow:6.2sccm
7	***Dehydration at oven at 95°C for 10 min***
8	***Lithography for Au & Ti etch***
Mask 1	HDMS coating 500 rpm 7s + 3000 rpm 30s
	S1813 500 rpm 7s + 4000 rpm 30s
	Softbake @ 95°C for 70 s hotplate
	Expose UV for 6s vacuum+hard contact
	Develop in MF 319 for 1min
	DI water rinse 1.5min+1.5min
	Dry by N_2
	Inspection
	Hardbake at oven @ 95°C for 20 min

Table C2 (continued).

	Desicator for 5 min
9	***Au etch***
	Commercial Au etchant for 1.5 min
	DI water rinse 3 cycles
	Dry by N_2
	Inspection
10	***Ti etch***
	10ml HF+10ml H_2O_2+80ml DI water as Ti etchant
	Ti etchant for 30s
11	***Strip photoresist***
	Acetone for 30min
	DI water rinse 3 cycles
	Dry by N_2
	Inspection
12	***Dehydration at oven at 95°C for 10 min***
13	***Parylene coating to prevent parasitic capacitance***
	with silane
	10 g for 5 μm parylene thickness
14	***Dehydration at oven at 95°C for 10 min***
15	***Lithography for forming of electrode well***
Mask 2 as dark field	HDMS coating 300 rpm 10s + 2000 rpm 30s
	AZ9260 300 rpm 10s + 800 rpm 30s
	Edge bead removal
	Wait for 15min
	Hardbake at oven from room temperature to 95°C and 50min @ 95°C
	Cooling at oven from 95°C to 70°C
	Rehydration (3 pipettes of DI water in blue box, overnight)
	Expose UV for 30s vacuum+hard contact
	Develop in AZ 826MIF for 8min
	DI water rinse 1.5min+1.5min
	Dry by N_2
	Inspection
16	***Parylene etching with RIE***
	In RIE (15min)
	Inspection
17	***Dehydration at oven at 95°C for 10 min***
18	***Lithography for Cu-electroplating***
Mask 2 as clear field	HDMS coating 500 rpm 7s + 1000 rpm 30s
	AZ9260 500 rpm 7 s + 1000 rpm 30s
	Edge bead removal

Table C2 (continued).

	Wait for 15min
	Prebake @ 95°C for 3min at hotplate
	AZ9260 500 rpm 7 s + 1000 rpm 30s
	Edge bead removal
	Wait for 15min
	Hardbake at oven from room temperature to 95°C and 50min @ 95°C
	Cooling at oven from 95°C to 70°C
	Rehydration (3 pipettes of DI water in blue box, overnight)
	Expose UV for 40s vacuum+hard contact
	Develop in AZ 826MIF for 10min
	DI water rinse 1.5min+1.5min
	Dry by N_2
	Expose UV for 20s vacuum+hard contact
	Develop in AZ 826MIF for 10min
	Dry by N_2
	Inspection
19	***Cu electroplating***
	100 mA 0.3-0.7 duty cycle 90min for 25 μm Cu thickness
20	***Strip photoresist***
	Acetone for 60min
	DI water rinse 3 cycles
	Dry by N_2
	Inspection
	O_2 plasma for 5min
	Inspection
21	***Dehydration at oven at 95°C for 10 min***
22	***Lithography for microchannel***
Mask 3	HDMS coating 500 rpm 7s + 1000 rpm 30s
	AZ9260 500 rpm 7 s + 1000 rpm 30s
	Edge bead removal
	Wait for 15min
	Prebake @ 95°C for 3min at hotplate
	AZ9260 500 rpm 7 s + 1000 rpm 30s
	Edge bead removal
	Wait for 15min
	Hardbake at oven from room temperature to 95°C and 50min @ 95°C
	Cooling at oven from 95°C to 70°C
	Rehydration (3 pipettes of DI water in blue box, overnight)
	Expose UV for 40s vacuum+hard contact
	Develop in AZ 826MIF for 10min

Table C2 (continued).

	DI water rinse 1.5min+1.5min
	Dry by N_2
	Expose UV for 20s vacuum+hard contact
	Develop in AZ 826MIF for 10min
	Dry by N_2
	Inspection
23	***Parylene coating***
	without silane
	40 g for 20 μm parylene thickness
24	***Opening lithography***
Mask 4	HDMS coating 500 rpm 7s + 3000 rpm 30s
	AZ9260 500 rpm 10 s + 750 rpm 20s
	Edge bead removal
	Wait for 15min
	Prebake @ 95°C for 3min at hotplate
	AZ9260 500 rpm 10 s + 750 rpm 20s
	Edge bead removal
	Wait for 15min
	Hardbake at oven from room temperature to 95°C and 50min @ 95°C
	Cooling at oven from 95°C to 70°C
	Rehydration (3 pipettes of DI water in blue box, overnight)
	Expose UV for 55s vacuum+hard contact
	Develop in AZ 826MIF for 30min
	DI water rinse 1.5min+1.5min
	Dry by N_2
	Expose UV for 55s vacuum+hard contact
	Develop in AZ 826MIF for 20min
	Dry by N_2
	Inspection
25	***Parylene etching with RIE***
	In RIE (20min+20min+20min)
	Inspection
26	***Dicing***
27	***Strip photoresist***
	Acetone for 2 days
28	***Parylene coating for insulation***
	with silane
	0.6 g for ~0.3 μm